Model-based optimization and control of maize growth under water stress conditions through precision irrigation

Von der Fakultät für Ingenieurwissenschaften,
Abteilung Maschinenbau und Verfahrenstechnik
der
Universität Duisburg-Essen
zur Erlangung des akademischen Grades
einer
Doktorin der Ingenieurwissenschaften
Dr.-Ing.

genehmigte Dissertation

von

Lina Atieno Owino
aus
Nairobi, Kenia

Gutachter: Univ.-Prof. Dr.-Ing. Dirk Söffker
Prof. Dr. sc. agr. Hartmut Stützel

Tag der mündlichen Prüfung: 04. Juli 2023

No matter how slippery,
No matter how high,
No matter how fleeting,
No matter how far,
Hold onto your dream,
Pursue it, flesh it out,
Until it is no more a vision,
But a moment, a memory, a part of your history.

To my beloved daughter, Isabella
The world is yours for the taking.

Acknowledgements

The results presented herein are part of the findings from my doctoral research at the Chair of Dynamics and Control (SRS) at the University of Duisburg-Essen.

I take this opportunity to extend my sincerest gratitude to Prof. Dirk Söffker for his support, guidance, and supervision at the Chair of Dynamics and Control. From my initial arrival and throughout my work he has proven a great source of inspiration and has provided a significant measure of positive critique at every stage.

My gratitude extends as well to Prof. Hartmut Stützel, who has served as a valuable point of contact in the agronomical research world, and at the conclusion of my work willingly accepted to be my second examiner. I have benefited greatly from his keen insight in relation to the agronomy-related aspects of my work, as well as several memorable scientific discussions during the annual meetings of the *Gesellschaft für Pflanzenbauwissenschaften*.

I also wish to relay my thanks to Yvonne Vengels and Adnan Hasanovic for the technical and administrative support, which aided greatly in managing the tasks behind the scenes. Many thanks as well to colleagues within the Chair of Dynamics and Control, who have supplied encouragement, positive critique, warm camaraderie, and useful advice.

Funding is an integral part of research, and in this respect I wish to acknowledge the part played by the National Research Fund (NRF) of the Government of Kenya in collaboration with the German Academic Exchange Service (DAAD). I would also like to thank the administration of Jomo Kenyatta University of Agriculture and Technology (JKUAT) for granting me study leave for a significant period of my research. I am especially grateful to Prof. Mabel Imbuga and Dr. Rehema Ndeda for lighting up the path ahead of me.

To my mum, my siblings, my friends: you have continued to believe in me, and I am forever grateful.

Duisburg, September 2023 Lina Atieno Owino

Kurzfassung

Die rasche Verknappung der Süßwasserressourcen als Folge der steigenden Weltbevölkerung ist eine Herausforderung zur Deckung des weltweiten Nahrungsmittelbedarfs. Die Bewässerungslandwirtschaft ist der Hauptverbraucher von Süßwasser weltweit, und es wird erwartet, dass die Bewässerungsflächen in Zukunft weltweit zunehmen werden. Die Herausforderung, die Welt zu ernähren, ohne das verfügbare Süßwasser zu erschöpfen, erfordert eine Neubewertung der Anbaupraktiken im Hinblick auf die Optimierung der Erträge bei gleichzeitiger Verringerung des Bewässerungsbedarfs - ein Ansatz, der gemeinhin als "mehr Ertrag pro Tropfen" bezeichnet wird [GRS06].

Ansätze, die auf Defizitbewässerung beruhen, nutzen die physiologischen Reaktionen der Pflanzen auf Wasserstress in verschiedenen Wachstumsstadien, um eine Verringerung des zugeführten Bewässerungswassers zu erreichen und gleichzeitig die nachteiligen Auswirkungen auf die Wachstumsraten der Pflanzen zu minimieren. Eine genaue Charakterisierung der Pflanzenreaktion in Echtzeit ist der Schlüssel zur Gewährleistung einer minimalen Verringerung des Ernteertrags bei gleichzeitiger Reduzierung des Gesamtwasserverbrauchs. Aus praktischer Sicht bleibt die Erkennung von Stress mit Hilfe herkömmlicher Sensortechniken eine große Herausforderung, da es keine kostengünstigen Sensoren gibt, die pflanzen-basierte Stressreaktionen erkennen können, bevor der Schaden eintritt, was zu Ertragseinbußen führt. Die Verwendung von auf dem Wasserstatus basierenden Modellen für das Pflanzenwachstum und damit zusammenhängende physiologische Prozesse gilt daher als attraktive Alternative zur Echtzeit-Erfassung. Vom Standpunkt der Steuerung aus betrachtet, ermöglicht die Umsetzung von auf Präzisionsbewässerung basierenden Strategien das Erreichen der beiden Ziele der Optimierung des Pflanzenwachstums und der Reduzierung des Wasserverbrauchs.

In dieser Arbeit werden auf einem Zustandsautomaten basierende Modellierungsansätze für Pflanzenwachstumsparameter, insbesondere für die Blattexpansion, die Blatterscheinung und die Biomasseakkumulation, entwickelt und vorgestellt. Ein Evapotranspirationsmodell, das auf Maispflanzen im Gewächshaus unter Wasserstressbedingungen zugeschnitten ist, wird ebenfalls entwickelt. Die Wachstums- und Evapotranspirationsmodelle werden in einem Algorithmus zur präzisen Bewässerungssteuerung integriert und zur Optimierung und Steuerung des Pflanzenwachstums im geschlossenen Regelkreis eingesetzt, wobei ein Ausgleich zwischen der Maximierung der Gesamtblattlänge und der Minimierung des Wasserverbrauchs geschaffen wird.

Die Validierung und Prüfung der Pflanzenwachstumsmodelle und des Wachstumssteuerungsansatzes erfolgt in einem Gewächshaus mit Maispflanzen (*Zea mays*) als Kontrollobjekt. Die Ergebnisse zeigen, dass die vorgeschlagenen Modelle die Gesamtblattlänge, den Zeitpunkt des Blattaustriebs und die Evapotranspiration

unter verschiedenen Stressbedingungen genau vorhersagen können. Der Steuerungsalgorithmus ist auch in der Lage, die Wachstumsziele auf der Grundlage der generierten Bewässerungssequenzen zu erreichen und gleichzeitig den Wasserverbrauch innerhalb der gewünschten Grenzen zu halten. Chronologische Schwellenwerte für die Reaktion von Maispflanzen auf den Beginn von Wasserstress und die Erholung nach einer erneuten Bewässerung wurden ebenfalls anhand von Sensormessungen experimentell validiert. Die Grenzen statischer Wachstumsmodelle, die auf konstanten Übergangsschwellen beruhen, wurden ebenfalls festgestellt, was auf die Notwendigkeit der Implementierung dynamischer Stressschwellwerte in zukünftigen Arbeiten führt.

Abstract

Rapid dwindling of freshwater resources as a result of rising global population is a challenge that urgently requires to be addressed if global food demand is to be met. Irrigation-fed agriculture is the main consumer of global freshwater, with future expansion of land under irrigation expected globally. Meeting the challenge of feeding the world without exhausting available freshwater requires a re-evaluation of crop management practices with a view to optimize yield while reducing irrigation requirements, an approach commonly referred to as "more crop per drop" [GRS06].

Deficit irrigation-based approaches exploit physiological responses of plants on exposure to water stress at different stages of growth to achieve a reduction in irrigation water supplied while minimizing detrimental effects to the plant growth rate. Accurate characterization of plant response in real time is key to ensuring minimal reduction in crop yield while simultaneously reducing overall water consumption. From a practical point of view, detection of stress onset using conventional sensing techniques remains a key challenge due to unavailability of cost-effective sensors capable of detecting stress responses before onset of damage, which results in loss of yield. Use of water status-based models for plant growth and related physiological processes is therefore considered an attractive alternative to real-time sensing. From the control viewpoint, implementation of precision irrigation-based strategies allows achievement of the dual objectives of optimizing plant growth and reduction of water consumption.

In this thesis, water status-based modeling approaches for plant growth parameters, specifically leaf elongation, leaf appearance and biomass accumulation are developed based on a state machine approach and presented. An evapotranspiration model tailored to greenhouse-grown maize plants under water stress conditions is also developed. The growth and evapotranspiration models are integrated into a precision irrigation control algorithm and applied to closed loop optimization and control of plant growth, balancing between maximizing total leaf length and minimizing water consumption.

Validation and testing of the plant growth models and the growth control approach is performed in an indoor greenhouse using maize plants (*Zea mays*) as the control subject. Results demonstrate that the proposed models can accurately predict total leaf length, timing of leaf appearance and evapotranspiration under different stress conditions. The control algorithm is also able to match growth targets based on generated irrigation sequences, while maintaining water consumption within desired limits. Chronological thresholds related to response of maize plants to initiation of water stress and recovery after reirrigation have also been validated based on sensor measurements. The limitations of static growth models based on constant transition thresholds have also been observed, suggesting a need for implementation of dynamic stress thresholds in future work.

Contents

List of Figures

List of Tables

Nomenclature

Symbols

Abbreviations

ABE	Absolute Error
ALMANAC	Agricultural Land Management Alternative with Numerical Assessment Criteria
APSIM	Agricultural Production Systems simulator
DI	Deficit irrigation
DSSAT	Decision Support System for Agrotechnology Transfer
ET	Evapotranspiration
FAO	Food and Agriculture Organization
FI	Full irrigation
GDD	Growing degree days
HS	High (water) stress
IR	Infrared
KW	Kalendarwoche (calendar week)
LAI	Leaf area index
LAR	Leaf appearance rate
LER	Leaf elongation rate
LIDAR	Light Detection And Ranging
LSTR	Least squares with trust region (optimization algorithm)
MS	Mild (water) stress
NSGA	non-denominated sorting genetic algorithm
PET	Polyethylene terephthalate
RGB(D)	Red Green Blue (Depth) imaging
RMSE	Root mean squared error
RUL	Remaining useful lifetime
SDG	Sustainable development goals (of the United Nations)
STICS	Simulateur mulTIdisciplinaire pour les Cultures Standard (multidisciplinary simulator for standard crops)
SUCROS	Simple and Universal Crop growth Simulator
TLL	Total leaf length
VRI	Variable rate irrigation
WE	Wang and Engel model
WOFOST	World Food Studies simulation model

1 Introduction

The United Nations Sustainable Development Goals (SDGs) envision global food security through sustainable agriculture (SDG 2) and the availability and sustainable management of water (SDG 6) [UN 15]. Despite technological advances and global support towards agricultural food production, hunger continues to be a global threat, with reports projecting 670 million people facing world hunger in 2030, indicating no significant progress towards achievement of SDG 2 [FIU+22]. To mitigate this trend, it is imperative that food production be proportionally increased in response to population growth. Irrigation-based agriculture is currently responsible for 40 % of global agricultural output, utilizing 20 % of arable land but consuming 69 % of global freshwater withdrawals [FAO20]. Driven by a rising global population, available freshwater resources per person face increasing pressure, with a reported decline of more than 20 % in the last two decades. While water treatment and desalination provide alternatives to cover the freshwater need, existing techniques are costly and energy intensive, particularly at low to medium scale [AGd+17, AGM20, HORB+19, OPRW21, OSCA20]. Freshwater generation via atmospheric water harvesting [LSG+22,TWZW18] offers a novel, but energy intensive alternative which is currently limited to smaller production units under specific conditions [LZZ+21]. However optimization of crop irrigation appears to be the most suitable solution to achieve a sustainable compromise between increasing freshwater demand for food production and the associated energy and environmental costs to realize adequate global food supply [FAO18].

Precision irrigation approaches offer a solution for avoiding wastage of freshwater resources. Precision irrigation is described as the application of a precise amount of water at the right time to the right plant or in the right location. Traditional definitions of precision irrigation consider the "precise amount" of water to be applied to be the full amount of water required to meet the plant demand, which has commonly been determined based on the relationship between crop evapotranspiration and environmental factors [MMC+15,LMA+16]. Further water savings are feasible through the incorporation of deficit irrigation-based regimes, where plants are subjected to periods of water stress, generally timed to coincide with growth phases that are tolerant of reduced water supply. A balance is however required to avoid negatively impacting crop yield, which would negate the overall impact of water savings. To achieve this, a determination of water supplied to and demanded by the plant is required in real-time.

Identification of physiological signals indicative of the onset and progression of water stress is imperative in application of precision irrigation control under water deficit conditions. A comprehensive overview of common physiological responses to water stress in vegetables is presented by Nemeskëri and Helyes [NH19], presenting a basic guideline for selection of relevant sensing devices for the detection of plant stress.

Integral to the implementation of deficit irrigation approaches is the quantification of stress levels. A distinction between mild and severe or high stress is based on the growth behavior of the plant once the stress is withdrawn. Exposure to high stress results in irreversible damage, which is expressed as a retardation in the growth rate and eventual reduction in yield [LLT+19]. A recovery upon withdrawal of the stress event indicates mild stress levels, and in some cases results in accelerated growth, referred to as the "catch-up phenomenon" [Sla69].

1.1 Automation of precision irrigation

Irrigation has been an integral part of crop production since the introduction of agriculture. Early irrigation approaches involved intricate systems of canals, with later additions of reservoirs, dikes, and overflow canals to mitigate flooding [GHHM00, Wes19]. Irrigation control focused on direction of irrigation water to specific locations, regulation of irrigation duration and mitigation of flooding. Surface irrigation methods involving use of flooded basins, furrows, dykes, dams, and artificial reservoirs remain the predominant form of irrigation to date [JGH+15]. Control methods aimed at more efficient use of irrigation water have been targeted at regulating the timing, duration, and frequency of supply to the fields through control of gates, sluices, valves, and pumps. New methods of water application to plants in the field, namely through sprinklers and drip lines, have provided new opportunities for more accurate control of irrigation water supply, allowing regulation of water supply to individual plant level. These developments on the actuation side of irrigation have been accompanied by corresponding developments in sensing and control approaches.

The incorporation of spatial variability in the management of irrigation is a key concept in distinguishing between traditional irrigation and precision irrigation [SESC05,SB09]. In Smith et al. [SBM+10], a distinction is made between traditional definitions of precision irrigation, which focus on maximizing efficiency through precise determination of volume, location, and timing of irrigation, with uniform application over the entire system, and an updated definition that incorporates spatial and temporal variation in irrigation treatment. The focus is shifted from field level to management zones within the field [Fer17,GDGZTF14], or to individual plant level [KKMD+18,KHH+18]. Camp et al. describe precision irrigation as "site-specific water management, specifically the application of water to a given site in a volume and at a time needed for optimum crop production, profitability, or other management objectives at that specific site" [CSE06]. In this work, implementation of precision irrigation as a means of growth control is investigated with the help of water use-based crop growth modeling. Supporting technologies are considered with regard to their flexibility in allowing variable precision irrigation of individual plants, rather than achieving efficiency through generation of uniform irrigation schedules.

Integration of automation for achievement of specific goals related to monitoring of plant physiological responses, efficient use of water, and maximization of crop productivity is also described.

1.2 Motivation and research objectives

The aim of this thesis is to describe the development and testing of a model-based plant growth control system based on precision deficit irrigation, allowing simultaneous optimization of overall plant growth while minimizing total water consumption. Development of the system requires modeling of plant growth parameters and physiological processes based on water status. This informs the first set of research objectives, which are

- Validation and adaptation of a previously developed state machine-based leaf growth model with a focus on identifying quantitative and chronological water stress thresholds,
- Definition of water stress-related plant growth functions applicable to existing experimental conditions,
- Development and validation of a model describing timing of new leaf appearance, and
- Defining a water stress-based evapotranspiration model characterizing experimentally observed relations.

Application of the growth and physiological models to achievement of specific goals related to plant growth or water consumption forms the next significant part of the research work. A closed-loop model-based control approach is developed, tested, and implemented to produce optimal scheduling of irrigation and mild stress events. A secondary task involves automation of the irrigation system to achieve automated growth control. These tasks are defined by a second set of research objectives, namely

- Development of a control system with desired total plant growth and cumulative water consumption as control variables, and the required sequence of irrigation and mild stress events as control signal, and
- Automation of sensing and actuation requirements for real-time determination and supply of required irrigation quantity.

1.3 Thesis organization

Chapter 2 describes the current State-of-the-Art in modeling and prediction of relevant plant growth parameters, with a focus on leaf-related variables as well as overall plant growth. Models specifically characterizing maize growth are explored. Comparative remarks are made and existing research gaps are highlighted. In Chapter 3 the development of growth models used in this work are introduced. Leaf elongation is represented using a state machine model adapted from previous research work [Kög19], and a set of linear relationships characterizing individual stress states is developed. Inspiration is taken from linear degradation models to develop a linearized model to represent leaf appearance in maize plants as a function of the growth trajectories of older leaves. A regression model based on environmental variables, total leaf length and stress state is adopted for modeling of evapotranspiration within the greenhouse. Section 4 details the control approach, using a trellis-based representation to describe state trajectories required to achieve desired target outputs. A trellis path finding algorithm is developed to extract the optimal trajectory based on desired output and resource-based constraints, integrated into a model predictive controller to achieve irrigation-based growth control. Overall results and conclusions are summarized in Chapter 5. Major parts of this thesis have been published or are awaiting publication. Texts originate from [OS19a], [OS19b], [SKO19], [OS21a], [OS21b], [OS21c], [OS22a], [OS22b], and [OS23].

2 State-of-the-Art in modeling of plant growth and evapotranspiration

To identify existing research gaps in modeling and control of plant growth based on deficit irrigation strategies, it is important to examine existing approaches described in literature. For this purpose, an examination of various strategies employed in modeling and prediction of plant growth and evapotranspiration is presented in this chapter. Emerging trends likely to influence further development in the research field are discussed and evaluated.

2.1 Background

Overall growth and development of a plant involves incremental increase in the size and number of cells forming individual plant organs, such as leaves, stems, roots, fruit, and so on. This is dependent on a number of factors and processes influencing the growth rate, including genetics, temperature, water, nutrient concentration, and carbon dioxide. The plant can be considered to exist within a continuum in which it interacts with atmospheric and soil-based factors. This is illustrated in Figure 2.1.

Plant growth models aim to define the incremental growth of an entire plant or specific components as a function of relevant factors or processes.

Commonly modeled and measured plant growth parameters are classified into two categories

i) Morphological parameters relate to the physical form, shape and/or structure of a plant or its constituent organs. Common morphological parameters of interest in plant growth modeling include

   - Leaf length, width, area, number, angle, thickness
   - Stem thickness/diameter
   - Rooting depth, number of secondary roots, rooting area/density
   - Fruit number, size, mass
   - Plant height, elongation rate

ii) Physiological parameters relate to biological functions required for normal growth and development of a plant or its constituent organs. Common physiological parameters of interest in plant growth modeling include

   - Photosynthesis
   - Hormonal function

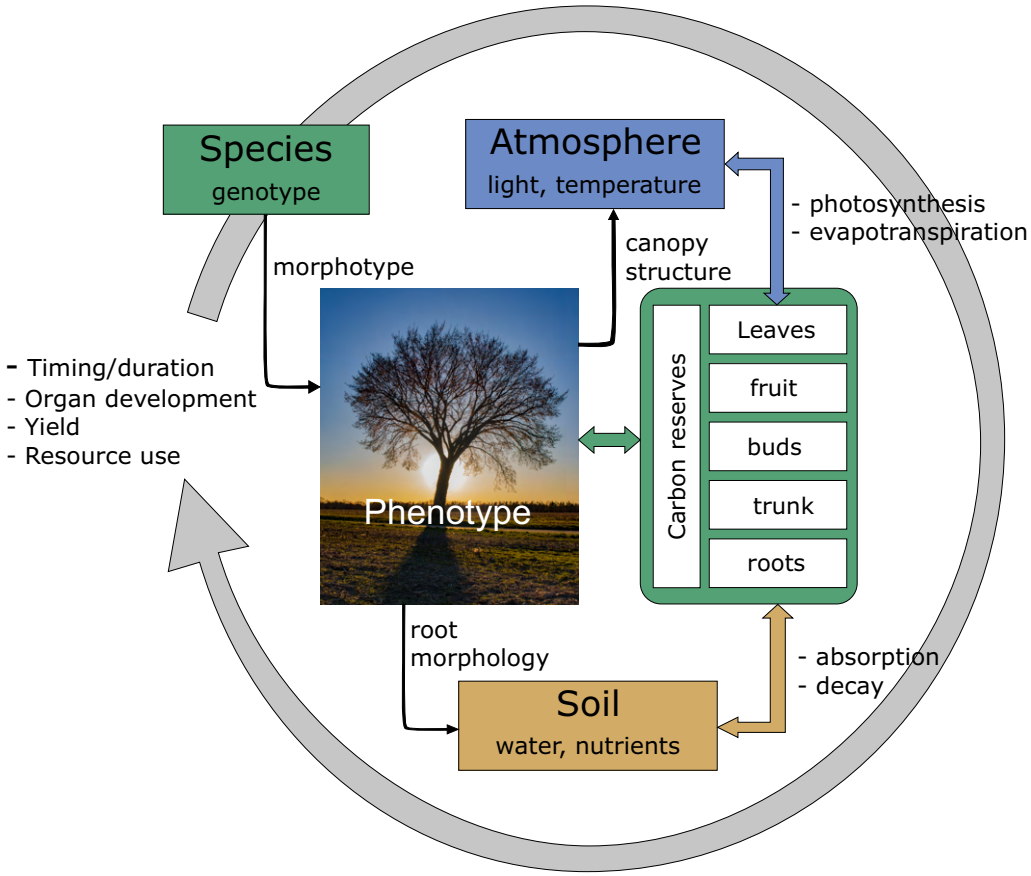

Figure 2.1: Schematic representation of interactions within the atmosphere-plant-soil continuum, based on [FZS+07]

- Respiration
- Evapotranspiration
- Dormancy
- Senescence
- Stress response

For optimal growth and development, it is important to ensure adequate and timely provision of such resources as the plant may need based on the developmental stages. In practice, assessment of growth stages is done by visual observation as well as use of predictive models to estimate timing and duration of individual growth phases. Common approaches for estimation and prediction of plant growth and development rely on temperature-based approaches ([JCR99], [DP03], [PO05]), as well as respiration-rate-based methods ([SLH93]). More recent predictive approaches have been implemented using 2D and 3D image processing with application of statistical methods ([SSPG18]), machine learning techniques ([NMW+19]), and

neural networks ([SUST19]). Fuzzy logic algorithms ([SPA17]) have also been employed in prediction of plant growth.

2.2 Leaf growth modeling approaches

The above-ground biomass of growing plants is partitioned betweeen leaves, stems/trunks, branches, and reproductive organs. Plant leaves are integral to the accumulation of biomass through photosynthetic processes, which convert carbon dioxide from the atmosphere to carbohydrates, mainly sucrose and starch [HB07], in the presence of solar energy and water. Leaves are also the main site of transpiration, which facilitates thermoregulation and transport processes. Additional roles served by leaves include rain interception and respiratory processes via the stomata. Modeling of morphological and physiological characteristics of leaves is therefore a significant aspect of plant growth modeling.

Leaf area index

Quantification of leaf material in a field is accomplished using a dimensionless ratio referred to as leaf area index (LAI), and described as half the total leaf area per unit ground surface area [JFN$^+$04]. The ground surface area is specifically defined as horizontal ground surface area to determine LAI on sloping surfaces [SCST07]. LAI defines the size of the plant-atmosphere interface, thus an accurate estimation is key in modeling of key physiological processes such as evapotranspiration and canopy photosynthesis.

Destructive measurement of leaf area index typically involves partial or complete defoliation of plants within the selected sample area. Non-destructive approaches include gap fraction-based methods [WBS$^+$04], use of imaging devices [CC12,LZW$^+$16], and LiDAR-based approaches [TBZ$^+$14].

Where direct or indirect measurement of LAI is impossible or impractical, modeling approaches allow relatively accurate estimation. Allometric methods rely on the derivaion of empirical relationships between LAI and other more easily measurable variables.

An estimate of LAI based on rainfall and temperature data (expressed in Growing Degree Days/GDD) is described by Davood et al. [DGBA17], where LAI is determined based on equation 2.1 as

$$LAI = aP^b e^{\frac{-(GDD-c)^2}{d}}, \tag{2.1}$$

where

a,b,c, and d are model parameters to be estimated via calibration,
P represents spatially interpolated rainfall / precipitation, and
GDD is a cumulative thermal-based measure of growing time
(growing degree days).

Using the thermal time, plant population, and canopy height as independent variables, Colaizzi et al. developed an allometric model for LAI estimation of different row crops (corn, sorghum, cotton and soybean) over multiple growing seasons [CEB+17].

$$LAI = f(P_{(x,crop)}, \theta) = Y_0 \exp\left[-0.5(\frac{\ln(\theta/\theta_0)^2}{\gamma})\right], \tag{2.2}$$

where

$f(P_{(x,crop)}, \theta)$ is a bell-shaped function,
P_x is a set of parameters specific to the allometric model version (x) and crop,
θ is the normalized thermal time (CGDD),
γ is a shape parameter ($0 < \gamma < 1$), and
Y_0 is the peak value of the function.

Allometric LAI models developed for forestry applications are described in various research works [JMC05,TAMG00,PBD22]. A summary of recent allometric approaches is presented in Table 2.1.

Table 2.1: Allometric approaches for leaf area index (LAI) modeling

Authors	**Dependent variables**	**Remarks**
Davoodi et al. [DGBA17]	Rainfall, thermal time (GDD)	Basin-scale LAI simulation
Colaizzi et al. [CEB+17]	GDD, plant population, canopy height	Multi-season estimation for multiple row crops
Jonckheere et al. [JMC05]	Diameter at breast height, basal trunk diameter	Projected needle area estimate at stand-level
Turner et al. [TAMG00]	Sapwood area at breast height, sapwood area at crown base	Sapwood area values derived from diameter at breast height
Paramanik [PBD22]	Diameter at breast height, tree density, canopy height	Symbolic regression-based model for mangrove forest LAI estimation

Leaf appearance

Plant growth during the vegetative phase can be quantitatively described using the quantity of biomass produced or the rate of generation of biomass. Growth

stages in the vegetative phase of several plants in the grass family are demarcated by emergence of specific leaves ([HI71], [ZCK74]). Tracking the appearance of successive leaves can therefore be used to characterize plant development over time. An integration of the leaf appearance rate over time allows estimation of canopy size, biomass production, and prediction of yield.

In [KRJH91], the leaf appearance rate and duration of leaf expansion are modeled based on incremental temperature during the growth period, expressed in Growing Degree Days (GDD). The effects of drought stress, photoperiod, and solar radiation are examined. The duration of leaf expansion is expressed as a function of leaf numbers and daily mean temperatures. A modified approach developed by Jame et al. introduces a non-linear temperature response function that allows the determination of leaf appearance rate under a wider range of temperatures by accumulating leaf appearance rates calculated hourly rather than daily [JCR99]. The equations are based on the assumption that leaf appearance rate is constant through the growing season and is fixed at the time of seedling emergence/germination.

The phyllochron concept is a commonly used approach in modeling leaf appearance. Phyllochron is defined as "the interval between similar growth stages of successive leaves on the same calm", and is assumed to be constant from emergence to flowering [BVK+98]. The leaf appearance rate (LAR) can be directly obtained as the inverse of phyllochron. In this approach, plant development is expressed as a function of thermal time, with crop-specific base temperatures applied for evaluating the accumulated thermal time (TT), as shown in equation 2.3 as

$$TT = \begin{cases} (T - T_{min}) & T_{min} < T < T_{opt} \\ -\frac{(T_{opt} - T_{min}) \times (T_{max} - T)}{(T_{max} - T_{opt})} & T_{opt} < T < T_{max}, \\ 0 & \text{otherwise} \end{cases} \tag{2.3}$$

where

T_min, T_{max} and T_{opt} are crop-specific minimum, maximum and optimal growing temperatures, and
T is the actual temperature averaged hourly and accumulated daily.

A linear regression of total emerged leaves against accumulated thermal time is generated, with phyllochron defined as the inverse of the slope of the regression curve. A modification of the phyllochron model to account for photoperiod and plant-specific temperature response results in the Wang and Engel (WE) model [WE98], with the general form

$$LAR = LAR_{max} f(T) f(P) \tag{2.4}$$

where

LAR is the daily leaf appearance rate, and
$f(T)$ and $f(P)$ are dimensionless temperature and photoperiod response functions.

The function $f(T)$ is defined in equation 2.5 as

$$f(T) = \frac{2(T - T_{min})^{\alpha}(T_{opt} - T_{min})^{\alpha} - (t - t_{min})^{2\alpha}}{(T_{opt} - T_{min})^{2\alpha}}, \tag{2.5}$$

with α defined as a shape factor that determines the skew direction of the function.

When the three base temperatures T_{max}, T_{min} and T_{opt} are known, α can be calculated as

$$\alpha = \frac{\ln 2}{\ln[(T_{max} - T_{min})/(T_{opt} - T_{min})]}. \tag{2.6}$$

The function $f(P)$ is defined in equation 2.7 as

$$f(P) = 1 - \exp(-\omega(P - P_c)), \tag{2.7}$$

where

P is the actual photoperiod,
P_c is the critical photoperiod below which no development occurs, and
ω is a crop-specific photoperiod sensitivity coefficient.

Further modification of the WE model to account for nonlinear temperature and age effects on the LAR introduces a chronology response function $f(C)$, defined in [Str03] as

$$f(C) = \begin{cases} 1 & \text{if } HS < 2 \text{ and} \\ (\frac{HS}{2})^b & \text{if } HS \geq 2, \end{cases} \tag{2.8}$$

where

HS is the Haun stage, which is a numerical designation for cereal growth staging based on appearance of consecutive leaves on the main stem, and
b is a sensitivity coefficient.

Studies on effect of water stress on leaf appearance in maize indicate a delay in appearance of new leaves resulting from periods of water deficit [SJH19, NR92, TCPR00]. When periods of water deficit are followed by periods of full irrigation, the growth of previously water stressed plants temporarily exhibits a recovery phenomenon, with leaf appearance rates greater than control plants that have not experienced water stress [MC89,KS18]. Further research is however needed to establish a causative

link between the increased elongation rate experienced during recovery from water stress and the accelerated leaf appearance observed in recovered plants, with the possibility of introducing optimal water management strategies for control of biomass production and timing of leaf appearance. Additionally, determination of the duration of recovery is necessary to establish optimal timing of renewed exposure to stress in order to reactivate the accelerated growth response without adversely affecting overall yield.

The contribution of genotypic factors [BAF02, PO05], photoperiod sensitivity [ZBZ$^+$22], plant density [AHB06], and water stress [BLB$^+$04] to the timing and rate of leaf appearance have been additional areas of research focus, albeit with the main focus primarily on the relationship between thermal time and maize leaf development. Modification of thermal time calculations and use of bilinear phyllochron functions [dAC$^+$22], has allowed application of leaf appearance models independent of crop variety and management practices, expressed in equation 2.9 as

$$GDD(T_{ave}, C) = \begin{cases} 0 & T_{ave} \leq 0, \\ \frac{T_{ave}}{1.8}) & 0 < T_{ave} \leq 18, \\ T_{ave} - 8 & 18 < T_{ave} \leq 34, \\ 26 - [(T_{ave} - 34) \times 2.6] & 34 < T_{ave} \leq 44, \text{ and} \\ 0 & 44 < T_{ave}, \end{cases} \tag{2.9}$$

with T_{ave} representing the average daily temperature.

Application of dynamic nonlinear functions in modeling leaf appearance has been applied, with chronological coefficients integrated in the modified WE models accounting for the effect of seed reserves for initial leaves, and decrease in LAR as plants progress towards maturity. Existing models perform well over a wide range of meteorological conditions, for different crop management approaches, and with different genotypes.

A summary of existing models is presented in Table 2.2. Two-stage phyllochron models provide more reliable prediction of leaf appearance timing, but are less accurate than WE and modified WE models, which integrate interaction of multiple environmental and chronological factors that play a role in the rate of leaf appearance.

Limitations of existing leaf appearance models include variation in calculation of thermal time, and a focus on field-grown crops, making them unreliable for approximation of crop development in indoor growth conditions. Additionally, variations due to biotic and abiotic stress factors are not integrated, thus pointing to a need for further modification if they are to be integrated into precision deficit irrigation-based agriculture.

Table 2.2: Comparative summary of leaf appearance models

Authors	**Findings**	**Research gaps**
Kiniry et al., [KRJH91]	Relationship between phyllochron and thermal time	Limited consideration of non-thermal effects
Jame et al., [JCR99]	Integration of temperature response function	Restricted to thermal factors
Bennouna et al., [BLB$^+$04]	Internode elongation correlated to leaf collar emergence under water stress conditions	Response during recovery not evaluated
Padilla & Otegui, [PO05]	Genotypic variations in leaf initiation and appearance in response to temperature	Restricted to well irrigated conditions
Fournier et al., [FDL$^+$05]	Causative link between leaf elongation and collar emergence	Directionality of causal effect not considered
Kögler & Söffker, [KS18]	Response of leaf appearance to water stress and recovery	Link between elongation rate and leaf appearance
Song et al., [SJH19]	Growth response during recovery	Application to growth control

2.3 Plant height modeling

During plant growth, significant energy reserves are invested towards increasing total height. This allows the plant to compete for light. Correlations also exist between plant height and life span, seed mass and time to maturity [MWW$^+$09]. Plant height has also been shown to be directly linked to yield potential [AMM$^+$19, MN20], flowering [AMB$^+$21] and above ground biomass [HYD$^+$19], enabling early intervention for optimal yield.

A study of the factors contributing to increase in plant height allows for modeling using allometric functions. Relationships between plant height and stem diameter have been found to produce reliable growth estimates [dSV$^+$18, ZSC$^+$20]. Existing studies describe plant height models based on environmental factors such as light intensity and temperature [RHT18, JLG$^+$20, SKA$^+$20], or physiological processes such as evapotranspiration [WBB95] and sapwood-specific hydraulic conductivity [LGH$^+$19]. Crop management practices have also been found to play a role, with correlations planting date, water content and nutrient application emerging as reliable indicators of expected terminal height [LYL$^+$22, LY21]. More generalized models for predicting of expected final height exist, with growing latitude and altitude employed as independent variables in a number of studies [MWW$^+$09, XMJL17, MCZZ16].

Integration of measurements from unmanned aerial vehicles has allowed development

of crop surface models (CSM), from which plant height can be accurately estimated [VAP+17, WGA+17]. Early stage measurements are used to generate predictive models from which terminal height can be estimated, allowing biomass and yield prediction. Through the use of multitemporal imagery, three-dimensional models of plant height can be generated, though accuracy is limited by change of reflectance during successive developmental stages [MPM+18, AMC+20].

Recent developments in plant height modeling involve the implementation of machine learning-based algorithms in prediction of plant height, allowing prediction of potential plant height based on genomic factors [VK22] and identification of the most significant environmental factors contributing to plant height [LdO+22]. An additional field of research interest lies in modeling the height of specific plant organs (such as leaves, flowers or fruit) to facilitate automation of specific management processes, as described in Wong et al. [WSA+20], where deep learning is applied for prediction of corn ear height based on video input for automation of harvesting. Similar approaches could be applied in future to enable automation of in-season site-specific application of agricultural chemicals.

2.4 Evapotranspiration modeling

Water supplied to plants is lost either through evaporation from the soil surface or transpiration from the stomatal interface. During the early stages of plant development, water losses are primarily due to evaporation. As the plant develops and forms a canopy, the exposes soil surface area decreases, leading to an increased contribution of transpiration to overall water losses (Figure 2.2). Due to the difficulty in distinguishing between the two processes, losses from evaporation and transpiration are frequently combined as evapotranspiration (ET).

Approaches used in measurement of evapotranspiration are based on concepts from hydrology, micrometeorology, and plant physiology. Micrometeorological approaches involve instrumentation based on the Bowen ratio integrated into energy balance functions, aerodynamic equations and eddy covariance-based methods. Hydrological approaches include use of weighing lysimeters, which directly determine the amount of water lost or gained over time in an enclosed mass of soil, and water balance equations (equation 2.10), where incoming and outgoing water flux into the root zone are assessed to calculate evapotranspiration as

$$ET = I + P - RO - DP + CR \pm \Delta SF \pm \Delta SW, \tag{2.10}$$

where
I represents irrigation,
P is the precipitation / rainfall,

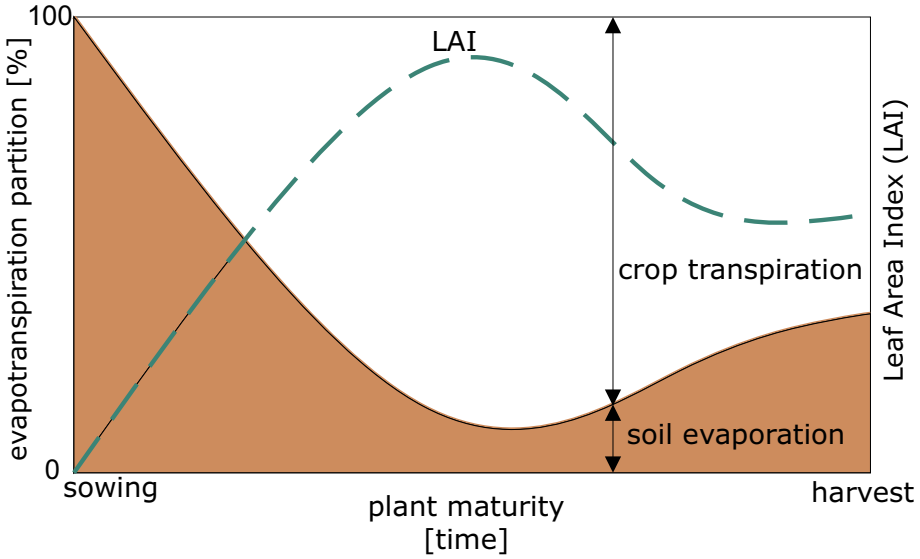

Figure 2.2: Partition of evapotranspiration over crop growth season, based on [FAO98]

RO represents surface runoff,
DP is deep percolation, which goes towards recharging the water table,
CR is capillary rise from shallow water tables,
SF represents horizontal subsurface flow, and
SW is the soil water content.

Modeling of evapotranspiration is commonly based on combination models that use equations based on aerodynamic theory and energy balance. A well-known combination model for estimation of crop evapotranspiration is the Penman-Monteith equation

$$\lambda ET = \frac{\Delta(R_n - G) + \rho_a c_p \frac{e_s - e_a}{r_a}}{\Delta + \gamma(1 + \frac{r_s}{r_a})}, \tag{2.11}$$

where

R_n is the net radiation,
G is the soil heat flux,
$e_s - e_a$ represents the vapor pressure deficit,
ρ_a is the mean air density at constant pressure,
c_p is the specific heat of the air,
Δ represents the slope of the saturation vapor pressure/temperature relationship,
γ is the psychrometric constant, and
r_s and r_a are the surface and aerodynamic resistances.

A modification of the Penman-Monteith equation is introduced in [FAO98] to account

for crop-specific differences. A single crop coefficient approach combines the effects of crop transpiration and evapotranspiration into a single constant K_c, and is typically used for resource planning and long-term irrigation management. For real time and/or high frequency irrigation scheduling applications, a dual crop coefficient approach is employed, where a basal crop coefficient K_{cb} describing plant transpiration is added to a soil water evaporation coefficient K_e representing evaporation from the soil surface to obtain the overall crop coefficient K_c [RPR+12]. The actual evapotranspiration is then determined as

$$ET = K_c ET_0 \tag{2.12}$$

where ET_0 is the maximum evapotranspiration evaluated either on a reference crop or on free water in a pan.

Recent developments in evapotranspiration modeling based on the Penman-Monteith equation integrate the effects of planting density [JKT+14], soil texture [AMER+21], and water deficit [PSM+17, GQS+20]. Current research investigates estimation of crop coefficients based on data from ground sensors or unmanned aerial vehicles, with leaf area index, multispectral vegetation indices, fraction of ground cover and canopy height as some of the reported variables of interest [SHZ+21, PPM+20, ZKL+18, ZHNL19]. Greater accuracy could be achieved through implementation of dynamic crop coefficients using daily calculations and historical thresholds to modify predicted values of ET [HZZ+22].

A simpler approach for estimating evapotranspiration on large scale from well watered vegetation was developed by Priestley and Taylor [PT72], focusing on radiation variables to simplify estimation. The regional evaporation rate is expressed as

$$\lambda ET = \alpha \lambda ET_{eq} = \alpha[\varepsilon A/(\varepsilon + 1)], \tag{2.13}$$

where

λET_{eq} is the equilibrium evaporation rate,
α is an empirical constant, and
ε is defined as the ratio of latent to sensible heat as air is warmed to saturation.

Recent developments applying the Priestley-Taylor approach include modifications to integrate spatial distribution of soil moisture [XWS+21] and soil water index measurements [HBC19]. For further simplification, the Hargreaves-Samani approach has been developed as an evapotranspiration model requiring only temperature and latitude as input variables [HS85]. Evapotranspiration is calculated as

$$ET_0 = HCR_a(\Delta T)^{HE}(T_C + HT), \tag{2.14}$$

where

$HC = 0.0023$ is an empirical coefficient,
R_a is extraterrestrial radiation (in mm/day),
$\Delta T = T_{max} - T_{min}$,
$HE = 0.5$ is an empirical exponent,
T_C is the average daily temperature, and
$HT = 17.8$ is a conversion factor from farenheit to celcius

For greater accuracy, spatio-temporal calibration is integrated to the Hargreaves-Samani model to allow incorporation of wind speed [CCHK16, GEA+18] and long-term site-specific meteorological data [KIWO20, OEE+21].

A summary of evapotranspiration modeling approaches is presented in Table 2.3, describing major limitations inherent in each model. Significant gaps exist in modeling evapotranspiration under artificial lighting conditions, particularly accounting for the distribution curve of incident radiation resulting from switching conditions between day and night. Factors relating to air flow in enclosed conditions are also neglected.

Table 2.3: Comparison of evapotranspiration models

Model	**Key features**	**Limitations**
Dalton [Dal98]	Mass transfer equation based on saturation vapor pressure and wind speed	Requires assumption of uniform leaf temperature and vapor-saturated air
Cummings [CR27]	Energy balance-based model	Sensitive to advection
Thornthwaite [Tho48]	Based on mean air temperature	Underestimation of incident solar radiation
Blaney-Criddle [BC62]	Based on mean daily temperature and daylength	Monthly variations neglected
Penman [Pen48]	Combination of energy balance and mass transfer equations	Plant-specific variations not incorporated
Penman-Monteith [Mon65]	Expansion of Penman equation with canopy and atmospheric resistance values	Complex model with many input variables
Priestley-Taylor [PT72]	Based on radiation parameters	Sensitive to wind speed and saturation deficit
Hargreaves-Samani [HS82]	Temperature-based equation with minimal climatological data	Requires calibration to local conditions

2.5 Modeling of maize growth and development

Maize (*Zea mays*), is a cereal plant of the grass family grown both as a staple food crop and as an energy crop. The plant possesses a simple stem of nodes and internodes, with leaves developing in pairs on each internode, with leaf number at maturity ranging between 8 and 21 leaves, based on genetic and environmental factors.

Growth of maize is typically divided into three main phases, with subsidiary stages:

i) the vegetative phase, characterized by development of leaves, which facilitate the conversion of sunlight and water into carbon reserves under the influence of chlorophyll and in the presence of various nutrients.

ii) the reproductive phase, during which the focus is on production of carbohydrate reserves, which eventually form the harvest. This phase is characterized by development of tassels, silking, and kernel production.

iii) the maturity phase, during which the developed kernels experience conversion of sugars into starches, accompanied by an overall loss of water weight as the stalk and ears dry out.

Plant growth during the vegetative phase can be quantitatively described using the quantity of biomass produced or the rate of generation of biomass. The growth stages in the vegetative phase of maize plants are demarcated by emergence of specific leaves ([HI71], [ZCK74]).

Using existing models, leaf appearance, and rate of biomass accumulation can be predicted. The reliance of thermal time as a predictor however neglects the physiological responses exhibited by plants during water stress and recovery, expressed as variations in growth rate. Implementation of deficit irrigation-based growth control requires accurate modeling of maize growth during stress and recovery, integrating the effects of severity and duration of water stress on the growth trajectory.

The program DSSAT-CERES, developed by the Decision Support System for Agritechnology Transfer (DSSAT) models plant growth, focusing on the correlation between dynamic conditions in the soil-plant-atmosphere continuum and plant growth, development and yield [HPB$^+$19]. Individually parametrized models exist, allowing crop-specific modeling of plant growth with the integration of climatic variations, genomic differences, irrigation management, and nutrient availability.The maize-specific version CERES-Maize was developed for simulation of yield under different management strategies, and provides a flexible platform that allows optimization of yield through variation of farm inputs [JK86]. Responses to biotic stresses such as parasites and disease can also be integrated, allowing an analysis of risk factors. Crops are

evaluated as a complete unit, allowing a closer representation of field conditions, where complementary and competitive effects arise from neighboring plants. CERES-Maize is freely available from the developers. However simulation requires precise formatting of a complex set of input variables, making it challenging to implement.

The WOFOST simulation model explains daily crop growth as a function of underlying physiological processes such as photosynthesis and respiration, under the influence of environmental variables [vWvR89]. Crop production, biomass accumulation, and water consumption can be progressively modeled over the growth cycle with required inputs including cultivar-specific values of thermal time, assimilate conversion coefficients, maximum rooting depth, daily root development rate, and shoot/root partitioning ratio. The model assumes uniform distribution of water within the root zone and runoff values proportional to amount of precipitation. A key limitation of WOFOST lies in the evaluation of stress effects on plant growth and development. When nutrient stresses occur concurrently with water stress, the strongest factor is selected to represent the overall stress experienced by the crop, which neglects interactions between physiological responses to combined stresses as compared to individual stress responses [dBF+19].

The ALMANAC model is a temperature-driven model which simulates crop growth and development in a competitive environment, with integration of effects from water stress, thermal stresses, and nutrient limitation [KWGD92]. Accurate simulation of yield requires input of precipitation and runoff curves, and soil characteristics. The model also exhibits sensitivity to variations in solar radiation, documented for sorghum and maize [XKW03].

The SUCROS model [vGv97a] simulates dry matter accumulation in a crop both under water-adequate and water-stressed conditions, with biomass partitioning dependent on thermal time. A light response curve is used for modeling leaf photosynthesis, with photosynthetic activity over differing canopy depths integrated over the day. Comparatively good results for prediction of leaf area index and above ground biomass have been observed, with lower accuracy in prediction of soil moisture content [XGF96].

The crop model STICS is comprised of seven submodules, modeling plant growth in terms of development, shoot growth, yield components, root growth, water balance, thermal environment, and nitrogen balance [BMR+98]. The model uses generic parameters relevant for most crops relating to physiology and management, with customization options allowing for calibration to particular species to improve performance accuracy. A distinct feature of the STICS ecosystem is the continued evolution of the platform through improvements integrated by users of the platform. Main limitations of the model relate to environment/management combinations excluded from the range of applications, for instance physiological responses to phosphorus or potassium deficiencies.

The simulation model Hybrid-Maize [YDL+04] was developed through a combination of crop-specific modeling approaches employed in CERES-Maize for representation of growth and development, and generic formulation of physiological processes as employed in the WOFOST model. The simplified model displays greater responsiveness to environmental variations while requiring fewer genotype-related parameters. Model limitations include in prediction of LAI, biomass partitioning, and plant response under various abiotic stresses.

Aquacrop is a crop model developed by the FAO, focusing on modeling growth, development, and yield formation under water deficit conditions [SRH+08]. Yield is defined based on evapotranspiration as

$$\frac{Y_x - Y_a}{Y_x} = K_y * \frac{ET_x - ET}{ET_x}, \tag{2.15}$$

where

Y_x and Y_a are maximum and actual yield respectively,
K_y is a proportionality factor representing the ratio between relative yield reduction and relative decrease in evapotranspiration, and
ET_x and ET_a are the maximum and actual evapotranspiration.

The evapotranspiration is partitioned into evaporation from the soil, E_s, and transpiration Tr. Biomass accumulation is described in relation to transpiration as

$$B = WP * \sum(Tr), \tag{2.16}$$

where WP is a coefficient representing water productivity.

Key limitations of Aqua-crop lie in the complexity of partitioning evapotranspiration values, and the exclusion of stress-mitigation responses exhibited by plants undergoing repeated exposure to water stress.

The APSIM model presents a comprehensive framework for modeling biophysical processes in agricultural systems, with species-based parametrization required to configure it to specific plants or animals. The biophysical modules are supported by a set of management modules that allow variation of scenarios under simulation, allowing predictive optimization of resource management decisions [BHH+14]. Limitations have however been observed in maize yield simulation at high latitudes, attributed to variation in light interception efficiency, radiation use efficiency and day length observed at higher latitudes [MPH+20].

A comparative summary of commonly used maize growth models is presented in table 2.4. A common characteristic of the aforementioned plant growth models is a focus on yield, making them unsuitable for projecting or tracking growth trajectories during early vegetative growth stages. Application of static plant-related parameters

Table 2.4: Common maize growth models

Model	**Authors**	**Key features**
Ceres Maize	Kiniry et al., [JK86]	Cumulative leaf area, with appearance based on thermal time
WOFOST	Van Diepen et al., [vWvR89]	Yield simulation for varying water availability
ALMANAC	Kiniry et al., [KWGD92]	Based on thermal time, light interception, and competition
SUCROS	van Laar et al., [vGv97b]	Based on irradiation, temperature, crop characteristics, and water supply
STICS	Brisson et al., [BMR+98]	Thermal-driven growth integrating nitrogen and water stresses
Hybrid-Maize	Yang et al., [YDL+04]	Adaptation of CERES-Maize integrating respiration and biomass partitioning
Aquacrop	FAO, [SRH+08]	Growth and yield response under water stress conditions
APSIM	Brown et al., [BHH+14]	Thermal driven model integrating phenology and architecture

to adapt the models to different crop varieties does not allow consideration of dynamic phenological responses caused by abiotic stresses, such as are induced by deficit irrigation. For the development of irrigation-based growth control applicable from early vegetative stages, it is necessary to develop more suitable growth models.

State machine model overview

The dynamical behavior of plants under water deficit conditions has been explored in various studies, with incorporation of yield reduction functions to integrate effects of water stress [BWB06], or description of stress-related dynamical behavior [KPKS12, LIS+16]. Plant water status can be related directly to growth factors, with plant available water used to describe plant water status as 'full irrigation', 'mild stress', and 'high stress'. The distinction of different states is mainly defined by the underlying models and related parameters and thresholds. Most stress-related thresholds for plant-based output variables described in literature refer to stress incipience, i.e. transition from a 'no stress' state to initial observation of stress symptoms [WA02, Jon07]. Plant-based thresholds for the transition of a 'mild stress' state to a 'high stress' state, or a response-driven distinction between mild and high stress states, are described in few cases as in [BKA+10].

A state machine model as established in [KS18, KS20] combines a set of different parameterized equations describing plant growth. Each equation is related to different

growth states linked by conditional transitions, described as combinations of specific stress thresholds. Data-driven optimization is applied to define the stress thresholds based on gravimetric water content and duration within specific states. This approach is first described in [BS17] for application in machine wear processes. The use of a state machine model allows the representation of the event-discrete nature of plant growth, and enables integration of structural variability in the system description, such as in the case of deficit irrigation-based crop management.

In Figure 2.3 the state machine model describing plant growth as a function of water status over time is shown. Transition conditions govern the switching of the plant from an initial state S_i to a final state S_j. Transition conditions are defined as

L	=	Stress level with:
		L = 0 (L_0; no stress),
		L = 1 (L_1; mild stress),
		L = 2 (L_2; high stress),
t_M	=	Memory retention time,
t_D	=	Chronological damage threshold,
t_{L1}	=	Time duration of stress level L=1 (L_1), and
$t_{L_{1i}-L_{1j}}$	=	Time between the successive stress levels L_{1i} to L_{1j}.

A response threshold is defined by the onset of observable physiological symptoms

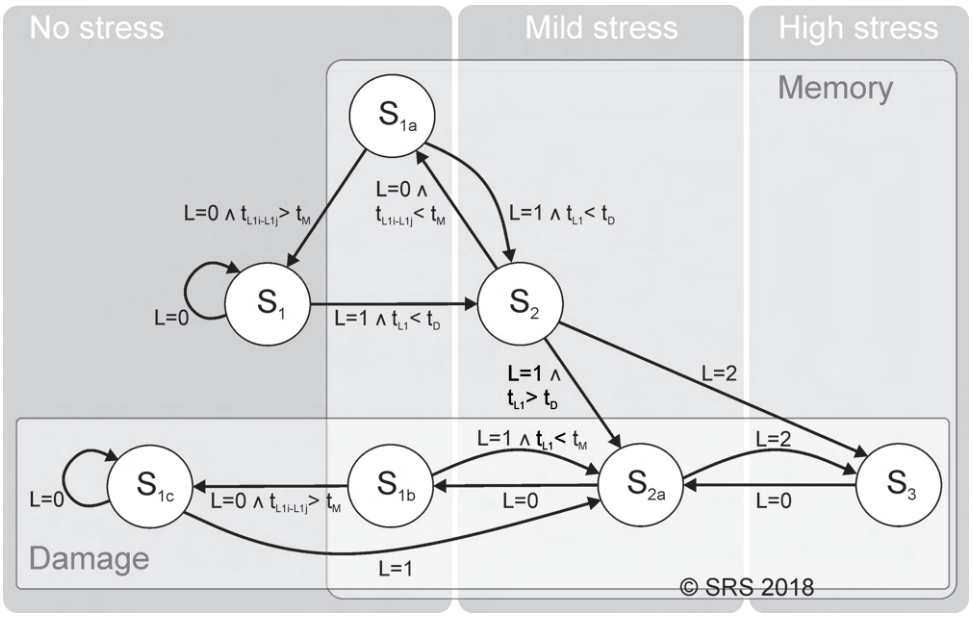

Figure 2.3: State machine model of plant behavior due to water stress [KS20]

in response to a water deficit, in this case based on leaf elongation rate. The

threshold is experimentally determined by comparing growth of plants subjected to water deficit to a reference group maintained under continuous full irrigation. Recuperation threshold is defined as point of no return, at which the progressed water deficit leads to irreversible growth because of damage.

The thresholds divide the water content scale into three ranges, defined as stress level L=0 (L0) for no stress, stress level L=1 (L_1) for mild stress, and stress level L=2 (L_2) for high stress. Identification of the described thresholds requires training of the model using experimental data to determine the levels and durations associated with onset of both mild stress and high stress conditions, or use of expert knowledge relating to different water deficit levels associated with different crops.

Additional descriptors are included to represent memory due to stress exposure and damage as a result of severe or prolonged water deficit. Hence, the plant states S are described by the vector

$$S = [L, M, D]^T, \tag{2.17}$$

with

L	=	Stress level as a function of plant available water content,
M	=	Memory as a function of stress occurrence and duration of recovery, and
D	=	Damage as a function of high stress occurence and mild stress duration.

Within the state-machine-model context the states S_i are denoted as

S_1	:	Vector [0/0/0];	reference growth behavior (full irrigation)
S_2	:	Vector [1/1/0];	reversibly reduced growth,
S_3	:	Vector [2/1/1];	irreversibly reduced growth,
S_{1a}	:	Vector [0/1/0];	increased growth,
S_{1b}	:	Vector [0/1/1];	irreversibly reduced growth,
S_{1c}	:	Vector [0/0/1];	irreversibly reduced growth, and
S_{2a}	:	Vector [1/1/1];	irreversibly reduced growth.

Here, the states S_1, S_2, and S_{1a} are the desirable states for deficit irrigation purposes, as growth is not irreversibly affected due to water stress.

Use of a state machine model allows integration of water status in modeling of plant growth, allowing implementation of water stress-based approaches in plant growth control [Kög19]. The stepwise incremental generation of growth variables allows estimation of growth from very early stages of vegetative growth, allowing for timely intervention and early planning of water use. Challenges exist in the establishment of transition thresholds, leading to a reliance on expert knowledge and experimental observation. Demarcation of thresholds based on plant physiological response would

provide greater accuracy in water stress-based control, allowing a transition from a deficit-based to a stress-based control paradigm. The static definition of thresholds as presented does not take into account variation in the physiological responses of plants as they acclimatize to stress conditions, or as increase in rooting depth and density extends access to available water within the growth substrate. Further work is required in development of dynamic thresholds, and consideration of the effects of substrate depth and volume on the relationship between water deficit and physiological responses to water stress.

2.6 Summary and discussion

A review of modeling approaches for various plant growth parameters of interest and physiological processes is presented. A survey of existing research reveals a significant focus on thermal time-based functions for description of plant growth, characterized by leaf area, leaf length and plant height. Models describing progressive development through different stages in the vegetative phase of maize growth are examined, with current research indicating a shift from static leaf appearance models to dual-phase models consisting of two static functions. The development of evapotranspiration models over time is also described, with research focus moving towards simplification and generalization of existing models to allow greater ease of implementation and reduction of measurement requirements.

The evaluation of growth and evapotranspiration models addressed in this chapter focuses on integration of plant physiological responses to water deficit, allowing an insight into research gaps that need to be addressed for comprehensive modeling of plant growth and development from a water status-based perspective. Based on suitability for integration into precision irrigation-based growth control applications, the described state machine-based growth model is selected for use in the development of the control approach described in this work.

3 Modeling and prediction of maize growth and evapotranspiration

In this chapter a description of the key models used to characterize growth and development of maize plants during the vegetative state is presented. Plant growth and development is defined by leaf elongation, appearance of new leaves and biomass accumulation. A data-driven evapotranspiration model configured for application in an indoor greenhouse is also developed. All models described integrate plant water status as an independent variable, allowing the inclusion of water stress-related variations in plant response to environmental conditions. Leaf elongation is modeled based on a reduced state machine model, operating entirely within 'mild stress' and 'no stress' regions. Individual linearized equations are generated to represent different stress states, and a discussion of limitations encountered in evaluation of threshold values is presented. Biomass accumulation is modeled using allometric relationships relating total plant biomass to measured leaf dimensions. A novel approach for prediction of new leaf appearance based on growth trajectories of individual leaves is developed and tested, with a discussion of observed results. A linear regression function relating evapotranspiration to environmental conditions within the greenhouse, plant dimensions and water status is developed and validated.

Part of the material in this chapter has been published in various research publications [OS19b, OHKS19, SKO19, OS22c].

3.1 Modeling and prediction of leaf elongation

With the steadily increasing world population, a sustained pressure to expand agricultural production in the face of limited natural resources such as freshwater can be observed. Incorporation of automation technologies in agricultural practice is a logical next step if the world is to meet the needs of its expanding populace. Optimization of irrigation practices has been identified as a significant area of interest in exploration of agricultural automation ([JDPS19]). A key element in automation and optimization of irrigation is modeling of crop growth, with recent research exploring a variety of methods to reliably estimate the growth trajectory of plants.

Plant growth is dependent on availability of multiple resources such as light, heat, water, and nutrients. For optimal growth and development, it is important to ensure adequate and timely provision of such resources as the plant may need based on the developmental stages. In practice, assessment of growth stages is done by visual observation as well as use of predictive models to estimate timing and duration of individual growth phases.

Experimental setup

Experimental data for training and validation of the models described in this section was obtained from an indoor greenhouse situated in the Chair of Dynamics and Control at the University of Duisburg-Essen in 2019 (KW 44 to 50). The greenhouse is located in a climate-controlled room with temperature maintained between 18° C and 29° C. Artificial lighting was supplied by a set of eight 75W 9500K fluorescent grow lights at each of four tables set up, with the illuminated area under each lighting set covering approximately 0.5 m by 0.5 m (Figure 3.1). The height of the lamps above the growing plants is manually adjustable, and was maintained as close as possible to the leaf canopy without making contact with the leaves. The windows in the room are blacked out and sealed with silicone for prevention of air currents from outside, and there is a single point of entry into the room, which was kept closed except for access to the plants for measurements. The maize seed used

Figure 3.1: Indoor greenhouse test rig with potted maize plants equipped with artificial lighting, Chair SRS, University of Duisburg-Essen, Germany.

in the experiments was KWS Ronaldinio variant. The seed was sowed in 500 ml PET tumblers filled with 175 g of Seramis® clay granulate as the growth substrate. “Seramis Vitalnahrung” liquid fertilizer for green plants was mixed into the irrigation water for fertigation. The plants received 14 hours of illumination daily.

Daily minimum and maximum temperature and relative humidity were recorded

using a digital temperature and humidity sensor, and leaf length and width measurements were performed using a flexible meter rule.

State machine description of maize growth

A state machine description of maize growth under different irrigation conditions has been described in section 2.5, as developed in [KS20], with daily total leaf elongation for each state described by the equations 3.1 as

$$\Delta LT_{HS} = a_{m0} + \frac{a_{m1}}{1 + e^{a_{m2}(TLL - a_{m3})}} + a_{m4}TLL + a_{m5}TLL^{a_m6} + \frac{a_{m7}}{1 + e^{a_{m8}TLL}}, \tag{3.1a}$$

$$\Delta LT_{MS} = a_{n0} + \frac{a_{n1}}{1 + e^{a_{n2}(TLL - a_{n3})}} + \frac{a_{n4}}{1 + e^{a_{n5}(TLL - a_{n6})}} + a_{n7}e^{a_{n8}(1 - TLL)}, \text{ and} \tag{3.1b}$$

$$\Delta LT_{FI} = a_{p0} + \frac{a_{p1}}{1 + e^{a_{p2}(TLL - a_{p3})}} + \frac{a_{p4}}{1 + e^{a_{p5}(TLL - a_{p6})}} + \frac{a_{p7}}{1 + e^{a_{p8}TLL}}. \tag{3.1c}$$

The result from the equations, ΔLT, defined in [Kög19] as lifetime increment, represents an incremental projection of the time it would take the plants in the test data set to achieve the measured increase in elongation. Parametrization of the model requires determination of the coefficients a_{xx} for each of the three main equations describing leaf elongation under high stress (HS), mild stress (MS) and no stress / full irrigation (FI), with the total leaf length (TLL) defined as the sum of the individual lengths of all visible leaves.

To obtain an elongation rate, the inverse of the calculated value was used, such that the total leaf length computed daily was expressed as

$$TLL_{k+1} = TLL + \frac{1}{\Delta LT}. \tag{3.2}$$

A visual representation of the state machine model is shown in Figure 2.3. Each of the seven states defined in the state machine-based growth model is described by one of the equations in 3.1, resulting in a system description with a total of 56 variables for optimization. The plant growth model is described by defining three level-related thresholds, representing the initialization of plant response to water deficit, transition into a mild stress state, and transition into a high stress state. Two chronological thresholds are also defined, representing the maximum duration under mild stress permissible before transition into a damaged state, and the minimum duration under full irrigation levels required for a previously stressed plant to lose its memory (and thus the physiological response related to priming), transitioning out of the recovery state.

Model parametrization using NSGA-II optimization

A non-denominated sorting genetic algorithm (NSGA-II) based on [BS17] and [JKS19] is applied to historical growth data from growth experiments conducted in May 2019, for determination of stress thresholds. As described in the state machine model, five state thresholds are defined: three based on stress level and two based on stress duration.

Experimental data from 14 plants were selected and evaluated over two successive growth periods, each of 10-day duration. During the first 10-day growth period, two irrigation strategies were employed, with six plants (individuals 1 and 2, and 11 to 14) being fully irrigated throughout and eight plants (individuals 3 to 10) cycling through the entire range of stress levels, beginning at no stress, then progressing naturally due to withholding of water to mild stress and high stress. For the second 10-day cycle, additional variations of mild stress and high stress periods were introduced, resulting in a total of seven unique treatments, covering six of the seven states described in the state machine model, with the omitted state representing loss of memory after continuous reirrigation of a previously mild-stressed individual.

The stress sequences are presented in Figure 3.2, with each header S_n representing the stress state on day n. Tuning of the data-driven NSGA-II algorithm is primarily

Plant No	S_0	S_1	S_2	S_3	S_4	S_5	S_6	S_7	S_8	S_9	S_10	S_11	S_12	S_13	S_14	S_15	S_16	S_17	S_18	S_19	S_20
1	S1	S1	S1	S1	S1	S1	S1	S1	S1	S1	S1	S1	S1	S1	S1	S1	S1	S1	S1	S1	S1
2	S1	S1	S1	S1	S1	S1	S1	S1	S1	S1	S1	S1	S1	S1	S1	S1	S1	S1	S1	S1	S1
3	S1	S1	S1	S1	S2	S2	S2	S3	S3	S3	S3	S1b	S1b	S1b	S1b	S1b	S2a	S2a	S2a	S3	S3
4	S1	S1	S1	S1	S2	S2	S2	S3	S3	S3	S3	S1b	S1b	S1b	S1b	S1b	S2a	S2a	S2a	S3	S3
5	S1	S1	S1	S2	S2	S2	S2	S3	S3	S3	S3	S1b	S1b	S1b	S1b	S1b	S1b	S1b	S1b	S1b	S1b
6	S1	S1	S1	S2	S2	S2	S2	S3	S3	S3	S3	S1b	S1b	S1b	S1b	S1b	S1b	S1b	S1b	S1b	S1b
7	S1	S1	S1	S2	S2	S2	S2	S3	S3	S3	S3	S2a	S2a	S2a	S1b	S1b	S1b	S1b	S2a	S2a	S2a
8	S1	S1	S1	S2	S2	S2	S2	S3	S3	S3	S3	S2a	S2a	S2a	S1b	S1b	S1b	S1b	S2a	S2a	S2a
9	S1	S1	S1	S1	S2	S2	S2	S3	S3	S3	S3	S3	S3	S3	S3	S3	S3	S3	S3	S3	S3
10	S1	S1	S1	S2	S3	S2	S2	S3	S3	S3	S3	S3	S3	S3	S3	S3	S3	S3	S3	S3	S3
11	S1	S1	S1	S1	S1	S1	S1	S1	S1	S1	S1	S1	S2	S2	S1a	S1a	S1a	S1a	S2	S2	S1a
12	S1	S1	S1	S1	S1	S1	S1	S1	S1	S1	S1	S1	S2	S2	S1a	S1a	S1a	S1a	S2	S2	S1a
13	S1	S1	S1	S1	S1	S1	S1	S1	S1	S1	S1	S1	S2	S2	S2	S2	S2	S2	S2	S2	S2
14	S1	S1	S1	S1	S1	S1	S1	S1	S1	S1	S1	S1	S2	S2	S2	S2	S2	S2	S2	S2	S2

Figure 3.2: Sequence of stress states of sample plants for testing of state machine-based maize growth model

through variation of population size and maximum number of generations, with the total number of iterations obtained from the product of the two parameters. Default values set in previously reported work [JKS19,Kög19], at 50 and 200 respectively, are implemented for prediction of leaf growth trajectory and compared with measured values. A set of 63 coefficients are obtained to describe the seven states of the plant growth model as applied to the selected experimental data. The coefficients used

are shown in Table 3.1.

Table 3.1: Model coefficients from NSGA-II optimization algorithm after training using experimental growth data

State	a_{x0}	a_{x1}	a_{x2}	a_{x3}	a_{x4}	a_{x5}	a_{x6}	a_{x7}	a_{x8}
S1	0.01394	0.00814	0.01508	-0.00301	0.00889	-0.00655	0.01349	0.02418	-0.00488
S1a	0.00132	0.00949	-0.00051	0.00468	-0.00847	-0.01386	-0.00472	0.01076	-0.02129
S1b	-0.02433	-0.01241	0.03178	0.02948	-0.03757	-0.02865	0.02521	0.00143	-0.03174
S1c	-0.00479	-0.01316	-0.00644	0.04333	0.02035	-0.01131	-0.00561	0.03519	-0.01521
S2	0.00054	-0.00869	-0.00342	0.00237	0.01029	0.03020	0.00547	0.01617	-0.01018
S2a	0.02151	0.02334	0.00504	0.02087	-0.01591	0.01550	0.00628	-0.02567	0.00789
S3	0.02990	-0.03819	-0.00583	0.00764	-0.01612	0.01042	0.02003	-0.00565	-0.02562

Initial results using the coefficients generated by the NSGA-II optimization model applied to prediction of leaf elongation over two success-ive growth periods, each of 10-day duration. For each measurement, a set of ten predictions were made, allowing for projection into the future. The actual leaf length was updated from manual measurement at each step.

The prediction error observed for the first observation cycle is presented in Figure 3.3, with the shown results representing only the first order prediction (made from the actual measurement of the previous day). Higher order predictions were not considered at this point, due to the significant magnitude of the error values obtained from the prediction model.

It can be observed in Figure 3.3 that a distinct separation into two categories occurs, with prediction error from individuals subjected to full irrigation treatment showing increasingly worsening performance when compared to measurement values. An additional observation involving the individuals subjected to both mild and high stress treatment during the initial 10 day cycle is the directiona-lity of error, with all obtained predictions trending negative.

The obtained results suggest a significant modeling error possibly arising either from the equation used to represent elongation under full irrigation, or from the optimization algorithm, based on previous work by [BS17] and [Kög19]. Additional plausible sources of the observed error could arise from differences in pre-processing of growth data (as compared to the machine lifetime data used in the original model), or a general unsuitability of the selected model for representation of plant growth processes.

The same plant growth dataset was used to train a trust-region-reflexive least squares algorithm from the MATLAB curve fitting toolbox, with the equations defining the individual states in the growth model identical to those used for the NSGA-II optimization, but applied to calculate a direct daily elongation rate instead of an elongation time. Coefficients describing the new model are shown in Table 3.2.

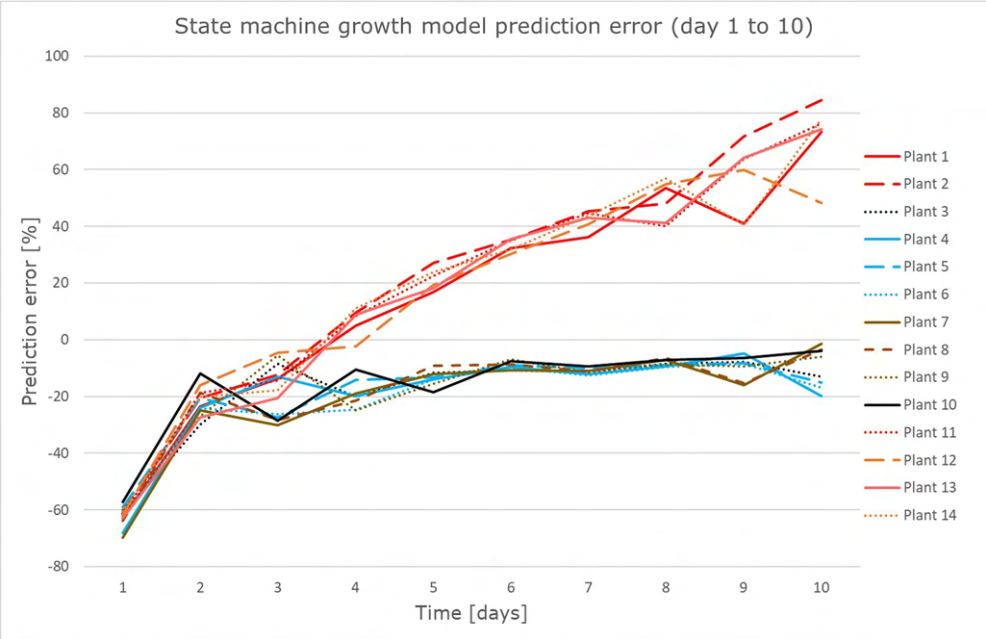

Figure 3.3: Percentage error in total leaf length estimates for first 10-day experimental cycle based on state machine model with NSGA-II optimization-based parameters for coefficient determination

Table 3.2: Model coefficients from trust-region-reflexive least squares optimization algorithm

State	a_{x0}	a_{x1}	a_{x2}	a_{x3}	a_{x4}	a_{x5}	a_{x6}	a_{x7}	a_{x8}
S1	0.2523	0.3141	0.1876	36.33	-1.062	1.058	1.001	-4.806	1.806
S1a	0.1133	0.04677	29.71	160.3	0.4984	0.9597	0.3404	79.29	0.9889
S1b	-0.1892	0.2806	-2.289	0.2638	25.34	0.2028	35.72	0.2435	0.9293
S1c									
S2	0.0662	0.4524	0.2978	0.7997	1.266	0.02128	-64.33	2.352	1.405
S2a	0.08575	0.4733	0.3517	0.8308	0.5853	0.5497	0.9172	0.2858	0.7572
S3	0.01378	0.1109	0.2566	91.82	0.9572	0.4854	0.8003	0.1419	0.4218

The percentage error obtained is illustrated in Figure 3.4. An improvement in prediction accuracy is observed as compared to the NSGA-II based growth model, with individuals subjected to full irrigation throughout the experimental period displaying marginally higher error values than individuals cycling through no stress, mild stress and hih stress. Additionally, error values for individuals in the control group (experiencing no stress) are predominantly positive after the initial prediction, while individuals experiencing stress have varying levels of prediction error, both positive and negative.

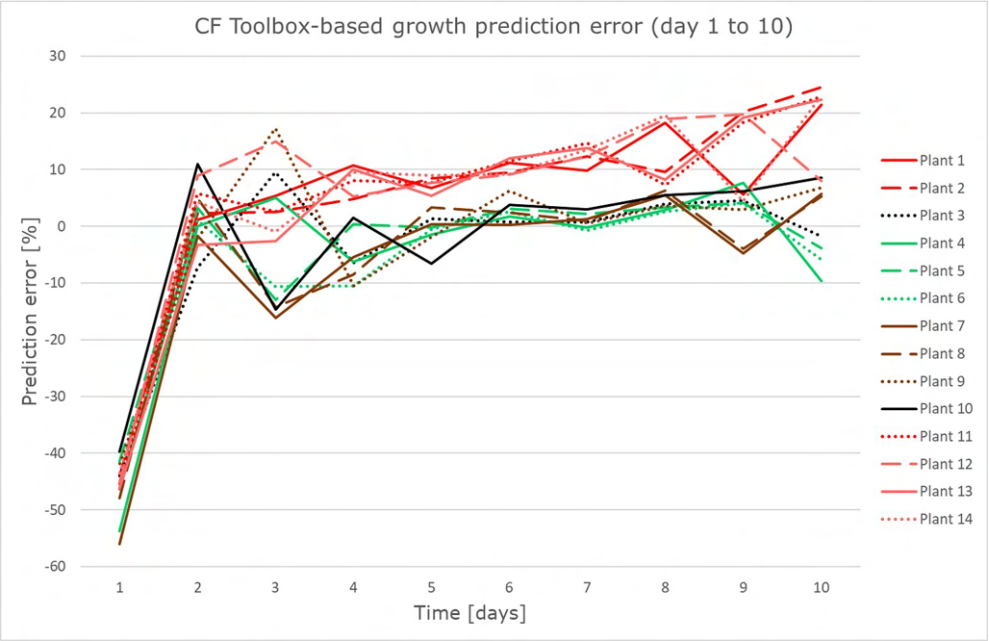

Figure 3.4: Percentage error in total leaf length estimates for first 10-day experimental cycle based on trust-region-reflexive least squares algorithm

An additional observation is related to appearance of new leaves, which register as sudden steep reversals in directionality of observed error, as seen in the results for days 3, 5 and 9. The daily measurement update however allows for rapid correction of the error brought about by the new leaf appearances.

A direct comparison of the prediction results for the two approaches as at day 10 is shown in Figure 3.5. An overall overestimation of total leaf length is observed for both approaches in the test plants selected from the control group (plants 1, 2, and 11 to 14), however the estimates from the curve fitting toolbox-based approach are closer to the measured values. Estimates involving mild stress and high stress states show good agreement with measured values for both approaches.

The improved exponential model was then applied to prediction of total leaf length for a second 10-day interval immediately following the first experimental cycle, producing the results displayed in Figure 3.6. An analysis of the results reveals three distinct groupings:

i) Two individuals with significantly larger prediction error, with an observable rise in error percentage with time. These represent the fully irrigated control group, and the obtained results imply that, even with application of an alternate approach for determination of the coefficients related to the described state

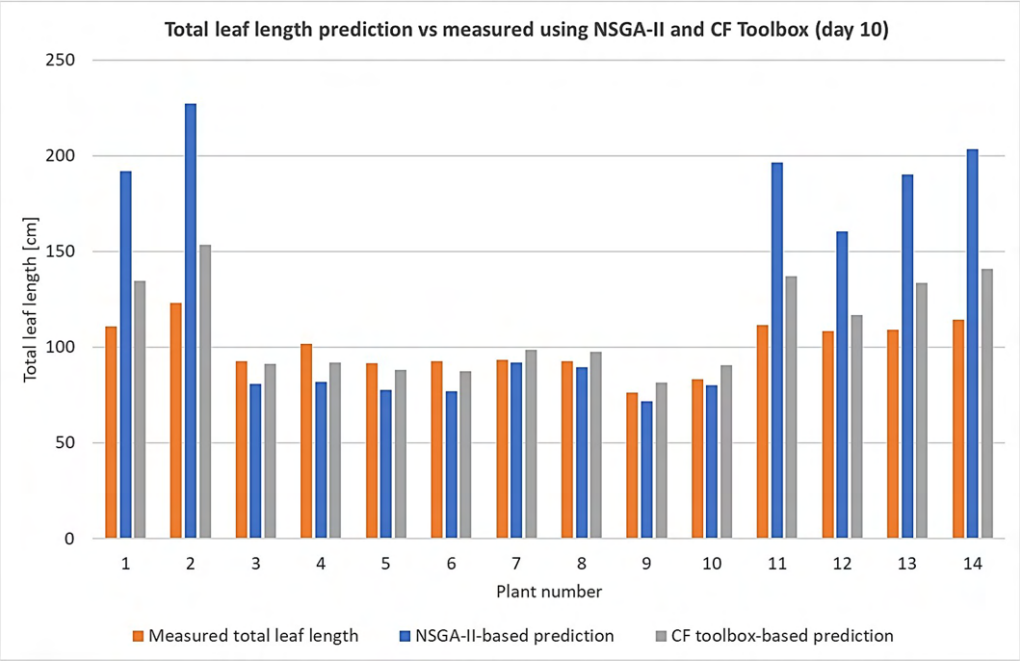

Figure 3.5: Comparison of total leaf length estimates using exponential growth model with parametrization based on NSGA-II optimization and trust-region-reflexive least squares algorithms

machine model, significant prediction errors arise in the implementation of the equation representing significant change (here used to represent plants under full irrigation and plants experiencing recovery after mild stress). This indicates that a reevaluation of the representative equations is necessary, with particular focus on the selected equation for no stress.

ii) Two individuals demonstrate some variation in observed error during the first two days before finally settling at a terminal prediction error. These represent high stress treatment without subsequent reirrigation, resulting in extended damage and death. An adjustment of the prediction algorithm to recognize terminal total leaf length during measurement update could possibly result in the error value converging to zero, but this was not implemented in this case because further research would not involve extended damage and death of plants.

iii) The remaining ten individuals, subjected to varied stress sequences are closely clustered together, with variations in error value observable upon appearance of new leaves. An observable drift towards the negative with passage of time is also observed, implying that the applied equations for modeling of leaf elongation might require updating as total leaf length values increased.

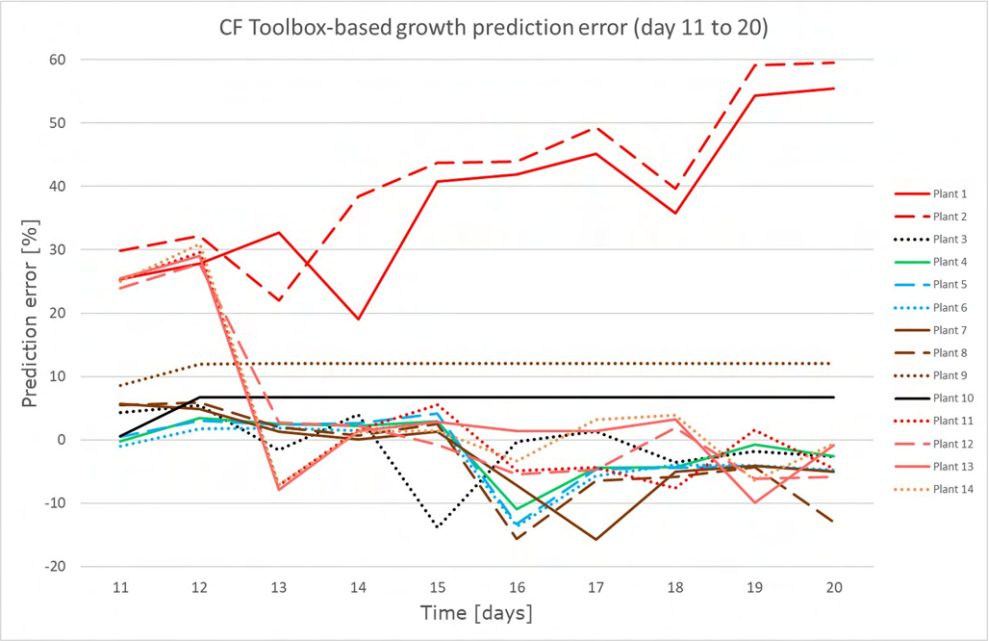

Figure 3.6: Percentage error in total leaf length estimates for second 10-day experimental cycle based on trust-region-reflexive least squares algorithm with 1-day prediction horizon

A comparison of results obtained from the two optimization approaches is presented in Figure 3.7, with Plant 1 representing the control group and Plant 8 representing the test group. An increasing divergence between measurement and prediction is discernible for the plant under no stress, whereas the predicted trajectory of the stressed plant consistently tracks the recorded observations over time.

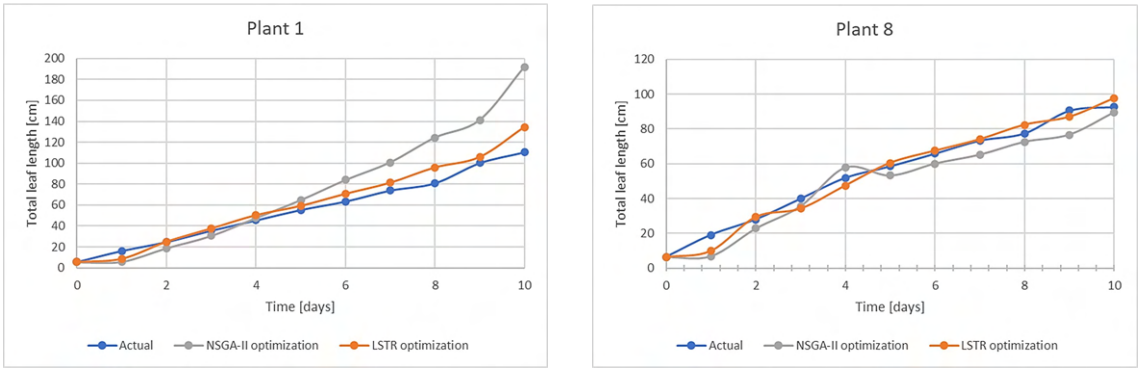

Figure 3.7: Comparison of leaf length modeling results for NSGA-II and trust-region-reflexive least squares optimization algorithms applied to state machine model of leaf elongation.

Linear regression-based parametrization of state machine model

A linear regression equation was selected to generate a model describing six of the seven states for which experimental data was available. The growth data was pre-processed by generating corresponding pairs of values of total leaf length based on the membership rule

$$X_k \in State_m \iff S_{n-1}(X_k) = S_n(X_k), \tag{3.3}$$

where

X_k is a pair of total leaf length measurements for the same individual taken on two consecutive days,
$State_m$ refers to one of the seven defined states in the maize growth model, and
S_{n-1} and S_n describe the stress states of the plant on the two days sampled.

The sizes of the training sets available for each state after pre-processing are shown in Table 3.3.

Table 3.3: Linear regresssion model training dataset sizes

State	Number of plants	Data points
S1	60	783
S1a	100	270
S1b	60	270
S1c	0	0
S2	120	249
S2a	40	53
S3	80	206

The linear model is described by the coefficients shown in Table 3.4, with the total leaf length being predicted, TLL_{k+1} related to the current total leaf length TLL_k as

$$TLL_{k+1} = TLL_k + p_1 TLL_k + p_2, \tag{3.4}$$

where p_1 and p_2 are coefficients obtained from training data, and are assumed to be variety-specific.

Implementation of the linearized leaf length prediction model resulted in more accurate projections with an RMSE value of 17.09 cm obtained over a prediction period of 20 days with a test group of 14 individuals. The percentage error value over the evaluated period remained within a stable range for all plants, as shown in Figure 3.8.

Table 3.4: Model coefficients used for linear model parametrization

State	p_1	p_2
S1	1.02	8.915
S1a	1.051	10.01
S1b	1.067	1.175
S1c	–	–
S2	1.025	6.619
S2a	1.053	1.845
S3	0.9407	12.02

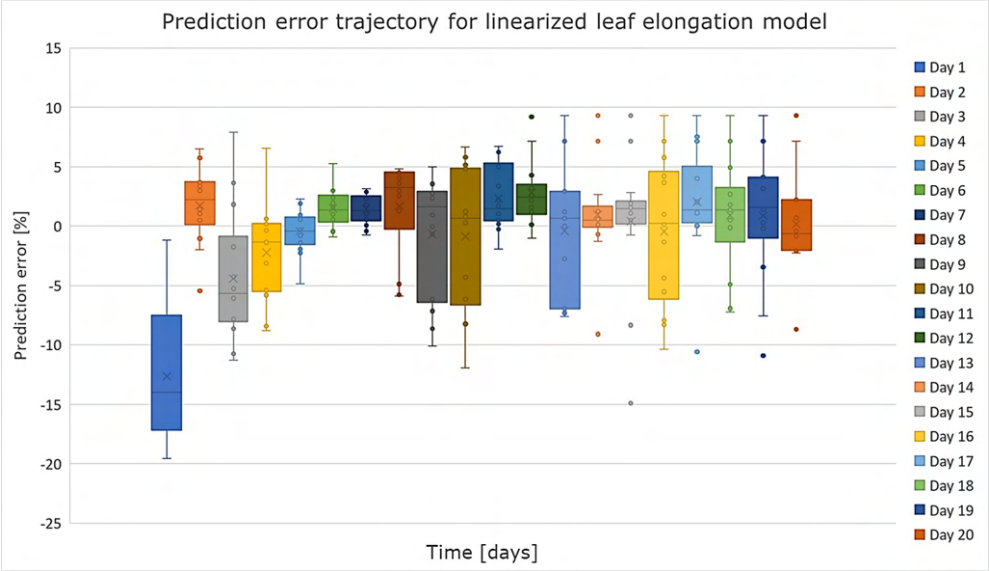

Figure 3.8: Prediction error distribution over time

The anomalous results observable on the first day of prediction are attributable to the nonlinearity associated with the initial period of active leaf elongation immediately after the appearance of new leaves, in this case leaf 3. Similar outliers are visible throughout the experimental period whenever new leaf appearance occurs, for instance on days 10, 13, and 16.

Based on existing predictions, the prediction horizon was expanded to three days, based on the chronological thresholds previously observed in previous work [Kög19]. The error distribution for the three-day prediction horizon is presented in Figure 3.9. A larger range of values is obtained, with mean prediction error predominantly negative for the initial predictions, then trending upwards over time. More outliers are observed, indicating a need to perform periodic measurement updates (using a one-step prediction) for any prediction scheme primarily employing a three-day

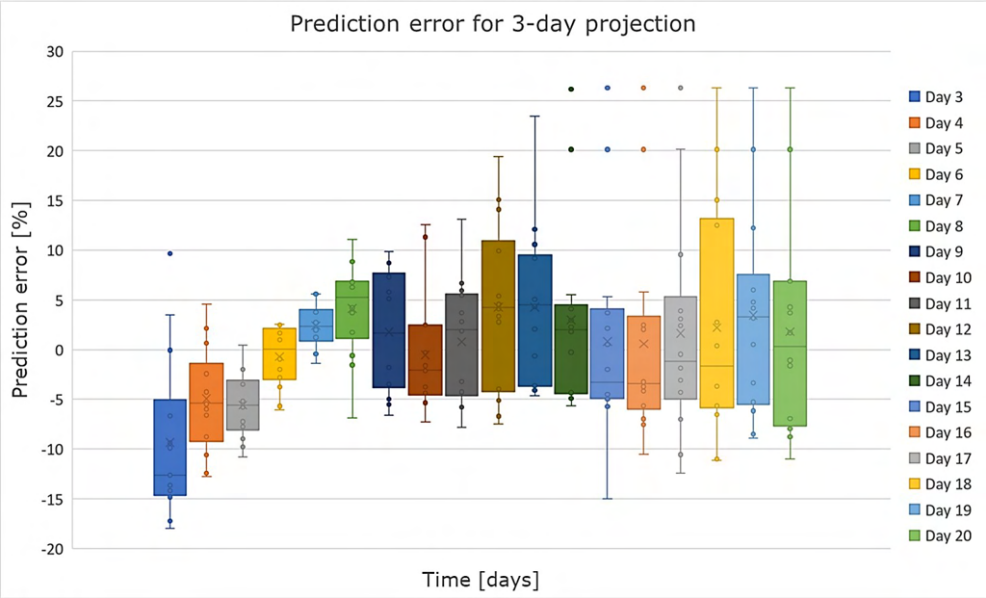

Figure 3.9: Prediction error distribution for three-day prediction horizon

prediction horizon.

To observe the prediction error trend with variation in prediction horizon, the deviation from measurements taken on day 10 were compared with predictions obtained with prediction horizons varying from one-step to 10-step, with the measurement update in each case occuring 10-n days earlier (where n is the length of the prediction horizon). The results are presented in Figure 3.10.

A shorter prediction horizon is seen to lead to lower mean error values and fewer outliers. A drift towards more negative error values is also observed over time, beginning from a 7-step prediction horizon. An additional observation is a reduction in the range of observed errors, accompanied by the presence of a few outliers as the prediction horizon increases.

3.2 Prediction of above ground biomass

Biomass is one of the key indicators used by maize producers to assess the growth and development of the growing crop throughout its growth stages. The growth and development of maize had been described by a number of growth models, with the most commonly used such as described in section 2.5, and their variants such as APSIM [KCH+03], CSM-IXIM [LBJ+11] requiring comprehensive data on the climate, soil, genotypes, and management to simulate crop growth during an entire growth cycle. Further developments have seen rise to simplified models, primarily

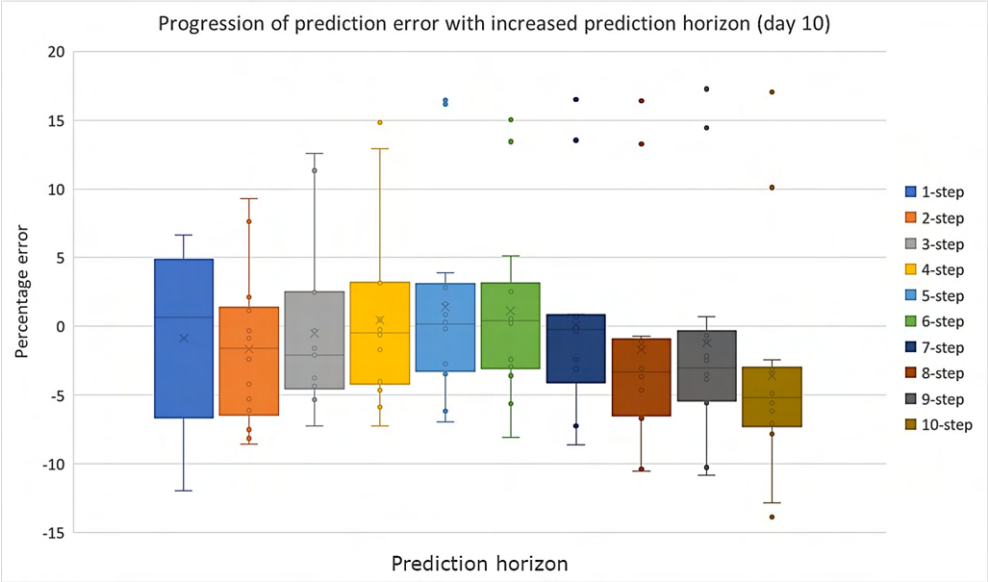

Figure 3.10: Variation of prediction error with length of prediction horizon

relying on characterization of maize growth and development as a function of thermal time [YDL+04, KYT+12].

The effect of climatic variations on the reliability of maize growth models has also been explored [BBD+14], with an emerging concern that changes in temperature and CO2 levels have a significantly high impact on the performance of crop growth models so as to necessitate further research in how to adapt the models to varying conditions. Additionally, constraints to freshwater resources and the accompanying extensive adoption of deficit irrigation require a shift in growth modeling approaches to account for the effect of water stress and recovery on biomass accumulation in C4 plants such as maize [MQS+17].

Estimation approaches based on imaging are also a key area of research interest, with studies involving use of RGB and infrared photographs [SGW+11, CTM+19], LIDAR [LNW+15, WNX+16, JSS+20]. Prediction of biomass on a larger scale is achieved by use of satellite imagery [MF16, BAM+16]. While certainly advantageous for extensive fields, application on small scale, and particularly indoors is at the moment still an open area of study.

To exploit the advantages of precision irrigation and its potential for facilitating not just the monitoring and management, but also the control of growth and development in plants, it is necessary to explore growth models that give adequate weight to the role of water consumption in the growth and development of maize. This plays an even more pivotal role in the case of possibly fully controlled environments such as smart greenhouses, or in environments where the dynamics of water availability play

a more dominant role than thermal variations, which tend to be the most common foundation for crop growth modeling.

In the course of this work, the potential of applying a state machine model with optimized deficit irrigation parameters developed for the prediction of leaf length [JKS19] to the estimation of leaf area and biomass in maize plants at the early vegetative stage was examined. The obtained results were compared to the FAO Aquacrop model [SRH$^+$08], which is one of the most widely used crop growth models focusing on the effect of water deficit on growth and development in plants. Aquacrop was also selected because the model allows for stepwise calculation of parameters of interest, thus allowing for comparison with values obtained in the early vegetative stage as opposed to yield at harvest.

Experimental setup

Experiments were conducted within an indoor greenhouse setup as described in section 3.1. Daily individual leaf length and width measurements were manually performed using both flexible and rigid linear rules, as appropriate. Fresh above ground biomass was determined at the end of the growth experiment through the use of a precision weighing balance with a sensitivity of 0.01 g.

A control group of fully irrigated plants was maintained at the experimentally predetermined full holding capacity of the substrate. Training of the state-machine model was carried out using a sample of data from the two experiments for which leaf width measurements (twenty plants in total) were available throughout the growth period. Test data was sampled from the remaining 260 plants. To investigate the accuracy of the proposed prediction model, data from two growth experiments carried out from October to December 2019 was used.

For each experiment, plants were divided into four groups each containing 35 plants, equally distributed on the four growing tables within the greenhouse. The control group was supplied with enough irrigation water daily to replenish evapotranspiration losses, bringing the substrate to full capacity, which was determined to be 145 g of water. Mild stress and severe stress states were determined based on threshold values obtained from an NSGA-II algorithm that was trained with data from previous growth experiments under identical conditions. Plants were considered to be under no stress (hence fully irrigated) for water content above 115 g and 113.42 g respectively for the first and second set of experiments. The lower boundary for the mild stress region for the two experiments was similarly determined to be 67 g and 62.97 g respectively. Plants required to be maintained at mild stress were reirrigated to achieve water content of 100 g.

Irrigation was manually performed once daily using syringes, with the total weight of the potted plants (pot + substrate + water + plant) measured using a precision

balance. During the later stages of the experiment where expanded leaf area resulted in daily evapotranspiration values high enough to trigger initiation of mild stress in the control group, or severe stress in the test groups, additional water was supplied to the plants with the quantities calculated based on projected evaporation rate and predetermined stress boundary values.

All plants were maintained under no stress until the appearance of the third leaf, after which irrigation was carried out as per the predetermined sequences. For the first growth experiment, the test duration started 10 days after planting and ran for 12 days. During the second growth experiment, the testing phase began 6 days after planting and ran for 16 days. The plants were harvested upon reaching the maximum height achievable within the growing space.

The irrigation sequences for the two growth experiments are shown in Table 3.5, with 0 representing no stress and 1 representing mild stress. For the first experiment, each digit represents three consecutive days, while for the second experiment each digit represents a 2-day period.

Table 3.5: Irrigation sequences during maize growth experiments for biomass prediction.

Group	**Experiment 1**	**Experiment 2**
A	0 - 0 - 0 - 0 - 0	0 - 1 - 0 - 1 - 0 - 1 - 0
B	0 - 1 - 1 - 0 - 1	0 - 1 - 1 - 0 - 0 - 1 - 1
C	0 - 0 - 1 - 0 - 0	0 - 1 - 1 - 1 - 0 - 0 - 0
D	0 - 1 - 0 - 1 - 1	0 - 0 - 0 - 0 - 0 - 0 - 0

Aquacrop modeling parameters

The Aquacrop model [SRH+08] was developed to allow the modeling of plant growth and yield with a focus on the relationships between supplied water and evapotranspiration losses. Biomass calculations are accomplished stepwise, with the relationship between biomass and water consumption expressed as

$$B = WP * \sum Tr, \tag{3.5}$$

where

B is the calculated plant biomass,
WP is the water productivity, and
Tr is the transpiration from the plant.

Due to the direct linking of biomass production to the water supplied to the plant,

the model is able to effectively factor in effects of deficit irrigation strategies, allowing for prediction of in-season plant growth, which provides a source of valuable information for allocation and management of water supply to the crop.

For the configuration of the growth simulation using Aquacrop, the irrigation water supplied was converted to irrigation depth by division of the supplied volume by the cross-sectional area of the pots used in the greenhouse. The substrate was represented as a clay-loam granulate, and groundwater level was set to zero, because the only source of water to the growing plants was irrigation water supplied from above.

State machine-based modeling of biomass

The growth of a maize plant was described using a state machine model as described in [JKS19]. Optimization of the model parameters was carried out using an NSGA-II algorithm, resulting in the determination of level and temporal thresholds describing the stress condition of the growing plants. Level thresholds defined the demarcation between the three different water stress levels described in the plant growth model-no stress, mild stress and high (or severe) stress. The temporal thresholds consist of a maximum mild stress duration threshold, which leads to a transition into high stress, and a recovery threshold, which leads to loss of memory acquired during previous periods of stress.

Biomass was estimated directly by training of the state machine model using intermediate biomass values calculated from leaf length and width, expressed by [MTS$^+$10] as

$$\ln(B) = \sum_{1}^{n} a + b\ln(L)_n + c\ln(W)_n, \tag{3.6}$$

where

B is the calculated plant biomass,
L is the leaf length,
W is the leaf width,
a, b, and c are crop-related constants, and
n is the leaf number.

The model was additionally applied for determination of total leaf area based on the relationship developed by [Mon11] as

$$LA = kL * W, \tag{3.7}$$

with a value of 0.79 used for k, following [BVK$^+$98],

where

LA is the leaf area,
k is a crop-specific constant,
L is the length of the leaf from the base to the tip, and
W is the width at the broadest part of the leaf.

Results and discussion

Leaf area estimation by the state machine was able to follow the trajectory of observed leaf area for the test group. Absolute error and root mean squared error values were calculated for the entire set of generated values, as reported in Table 3.6.

Table 3.6: Sample error metrics for leaf area estimation using a state-machine based model (all values in cm^2)

Parameter	**Test 1**	**Test 2**	**Test 3**	**Test 4**	**Test 5**
Absolute error	6.543	2.685	2.977	0.325	1.158
RMSE	2.334	0.958	1.062	0.116	0.413

For the range of leaf areas represented, the error values are small enough to be insignificant, indicating that this model can be applied in projection and estimation of leaf area under deficit irrigation conditions, with minimal input requirements, and at very early stages of vegetative growth. The growth trajectory of individual leaves for a sample of the test individuals in the group is shown in Figure 3.11.

It has however to be noted that since the calculated leaf area is reliant on existing theoretical models, the accuracy of the results is closely tied to the equation selected for calculation of training values. Further improvement of the model could be achieved by employing more accurate destructive or optical-based techniques for generation of more reliable training data, which would improve the accuracy of the prediction.

Biomass estimation

Estimation of biomass directly using the state machine model showed significant deviations from measured values, with the time axis exhibiting a contraction of up to 50 %, resulting in biomass estimates that were up to 100 % larger than measured values (Figure 3.12). This result may be due to the limited number of training values for which accurate biomass values were available, or could also be an indication of systemic errors with the approach selected. For this reason, this approach was abandoned, and an estimation approach based on the generated total leaf length was applied instead. A linear model was trained using measured total

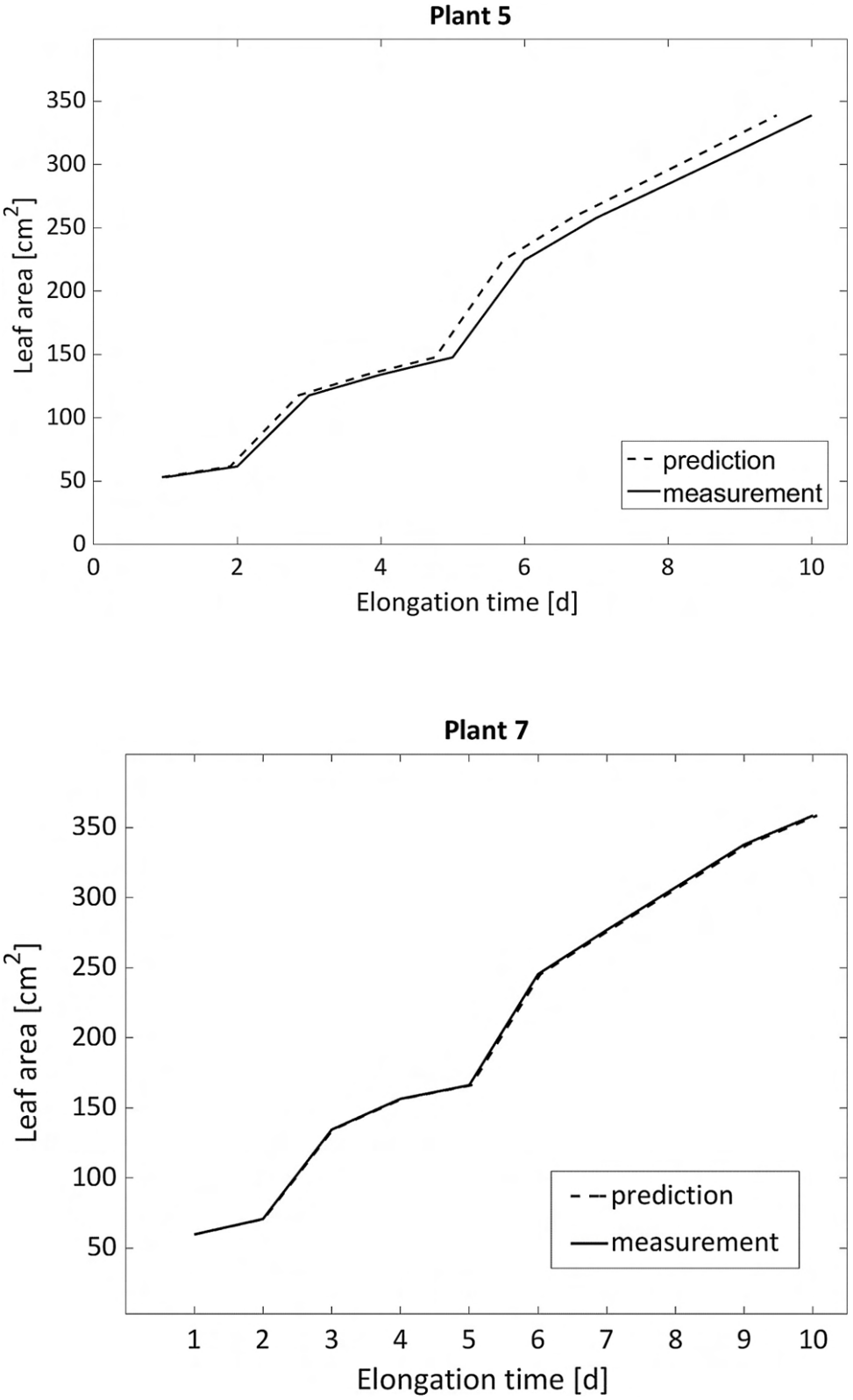

Figure 3.11: Leaf area growth trajectories predicted by the modified state machine model compared to leaf surface area calculated from direct length and width measurements

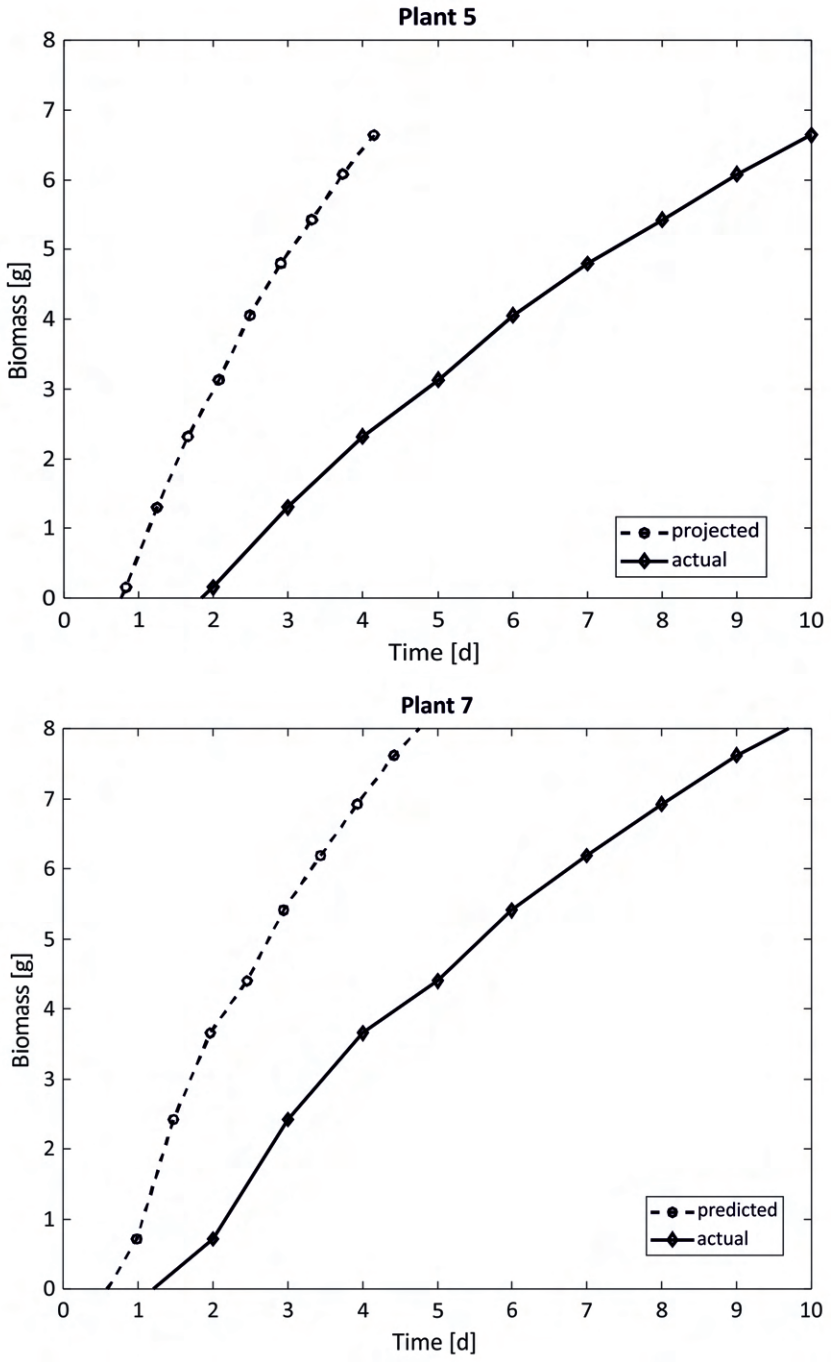

Figure 3.12: Direct biomass estimation using modified state machine model.

leaf length and biomass values obtained at the end of the two experiments. The resultant equation took the form

$$B = k_1 TLL + k_2, \tag{3.8}$$

where k_1 and k_2 are constants obtained by fitting leaf length and biomass data.

The linear model was trained with two sets of data- one including samples from six different sets of experiments conducted between 2017 and 2019, and a second set of data restricted to the two experimental periods from which the test data was also obtained. The model and associated error metrics are presented in Table 3.7.

Table 3.7: Linearized biomass prediction model based on total leaf length

Parameter	k_1	k_2	R^2	**RMSE [cm^2]**
Dataset 1 (2017-2019)	0.09179	-8.311	0.8002	1.389
Dataset 2 (May 2019)	0.079	-5.38	0.9462	0.6026

The distribution of error values obtained is illustrated in Figure 3.13, with 5-I and 5-II using test data from the first experiment and training data from the expanded and restricted sets respectively. The variables 6-I and 6-II similarly represent the test data from the second experiment evaluated using parameters obtained from the two respective sets of training data.

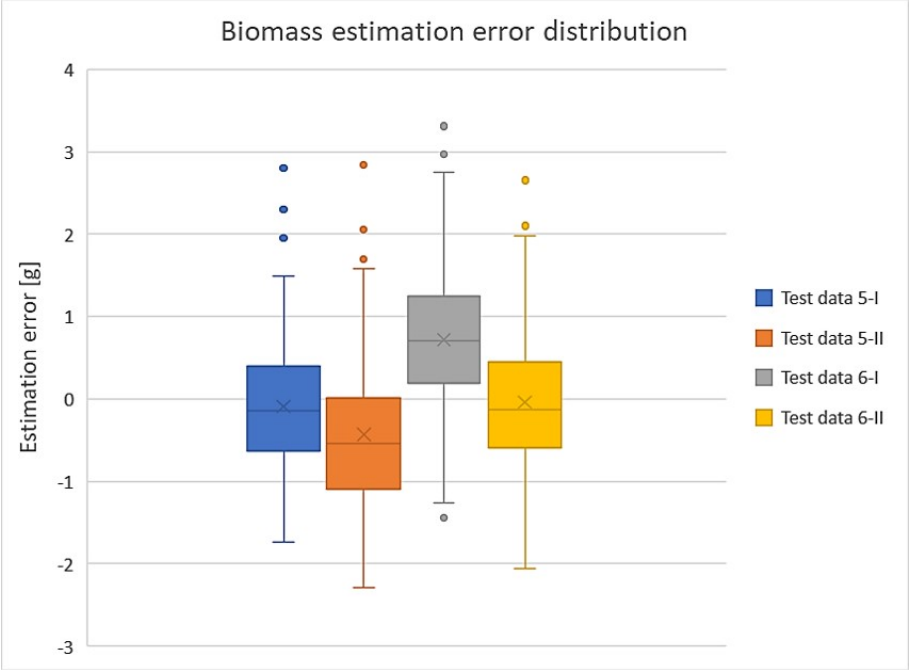

Figure 3.13: Error distribution for biomass estimation using linearized allometric model

It can be observed that the median values of the estimated biomass are relatively close to zero, and the distribution of the data between the 25th and the 75th

percentile is uniform for all combinations of test and training data. Although it can be seen estimates for test data from the first experiment tended towards under-estimation while test data from the second experiment tends towards over-estimation, the absolute error values in both cases are relatively small.

The next step involved applying the linearized estimation of biomass to total leaf length values generated by the state machine model. In Figure 3.14 a comparison between the obtained results and values obtained from the Aquacrop model is shown, with both models displaying a tendency towards underestimation of the biomass value, as seen by the position of the median line. The modified state-machine generated for this set of data a median error value closer to zero as compared to Aquacrop, but produced a larger number of outliers, suggesting a need for additional refinement of the model to enable its application to plants in earlier growth stages, where total biomass is relatively small. Values of above ground biomass were seen

Figure 3.14: Comparison between linearized allometric biomass model and Aquacrop

to vary even in plants grown from the same cultivar, under identical conditions, during the same growth period. This leads to a reduced reliability of prediction accuracy for models that rely on common variables such as temperature, day length and available radiation, particularly in controlled environments or for purposes of research.

The implemented state machine-based growth prediction model has been applied to successfully predict leaf area by training the model using leaf length and width

data. Significant drawbacks were however experienced in direct application of the model for use in estimation of biomass, indicating a need to examine the underlying equations used to generate incremental biomass values in response to plant water status with a view to building a link between the leaf length, leaf area and above ground biomass.

The simplicity of the linearized relationship between total leaf length and biomass observed during the early vegetative stage in this case allows for accurate estimation of biomass during the early stages of development with low computational demands, and, coupled with a predictive algorithm, enables for forecasting of expected biomass based on irrigation quantities and sequencing.

3.3 Prediction of leaf appearance

Growth of plants during the vegetative phase can be quantitatively described using the quantity of biomass produced or the rate of generation of biomass.

The growth cycle of maize can be divided into two major phases- the vegetative stage, covering the period from seedling emergence to tasselling, and the reproductive stage, covering the development of kernels up to maturity. The growth stages in the vegetative phase of maize plants are demarcated by emergence of specific leaves ([HI71], [ZCK74]). Tracking the appearance of successive leaves can therefore be used to track the successive progression of the plant through different growth stages.

Cereal plants have been observed to exhibit a distinct pattern during vegetative growth, with resources concentrated on a fixed number of growing leaves at different stages of development [Ett51, HWRZ88]. Studies on the timing and rate of leaf appearance in maize plants have primarily focused on the influence of temperature, with observations indicating that the duration between appearance of successive leaf tips for a specific maize cultivar can be represented as a fixed thermal time, referred to as phyllochron, with modifications to the determination of thermal time to account for different temperatures during the growing period [KRJH91, GBB95, BVK$^+$98]. A causal link is suggested between the emergence of the collar in maize leaves and the end of active elongation [FA00, FDL$^+$05].

A link can be made between the decreasing rate of leaf elongation as the older leaves approach maturity, and the appearance of new leaves, marked by the visual observation of leaf tips. Experimental data is used to determine threshold values of leaf elongation rate that serve as markers to predict appearance of new leaves. The estimated values of leaf appearance time and duration of leaf elongation are compared to experimentally observed values as well as to calculated values present in literature [KRJH91].

Using existing models, leaf appearance and duration of elongation can be predicted. However, due to the variation of elongation rate as the leaf progresses from initiation

to maturity, the growth trajectory of the leaf is inadequately described based on these two parameters. A different approach is therefore developed, tracking the growth of the leaf over the duration of its active expansion cycle which combines the forecast of leaf appearance and the prediction of the subsequent leaf elongation rate of the leaf to maturity. By aggregating the results obtained for individual leaves, the developed approach can be used to estimate the overall growth trajectory of the plant and therefore allow forecasting of expected biomass at different stages of plant growth.

Experimental setup

The data used in this work was obtained from maize plants grown in an indoor greenhouse in the Chair of Dynamics and Control at the University of Duisburg-Essen, whose setup is described in subsection 3.1. A total of 241 individual plants are used to generate the data. Irrigation treatments used for generation of experimental data were as follows:

1. 70 plants maintained under fully irrigated condition (FI), with gravimetric moisture content maintained constantly above 0.65 g/g.
2. 93 plants exposed to at least one mild water stress (MS) period during the growth period, with mild stress defined as occurring when the gravimetric moisture content of the growth substrate was between 0.29 g/g and 0.65 g/g. All plants exposed to mild stress were reirrigated after each mild stress episode to moisture content levels equivalent to the fully irrigated group.
3. 78 plants exposed to at least one episode of high water stress (HS) during the growth period, with high stress defined as occurring when the gravimetric moisture content of the growth substrate was below 0.29 g/g.

Thermal time is used for result analysis, expressed in growing degree days (GDD), using a base temperature of 10° C. Growth data from 241 individual plants are used for training and testing the linear prediction models. Training and test data sets are obtained by randomly splitting the data in a 4:1 ratio for 5-fold validation and in a 9:1 ration for the 10-fold validation.

Comparative analysis of leaf appearance and individual leaf elongation

The timing between the appearance of successive leaf tips was calculated in growing degree days using a base temperature of 10° C [KRJH91] for all data from seven growth experiments conducted between February 2018 and November 2019 (Figure 3.15) and separately for data from an experiment in May 2019 (Figure 3.16).

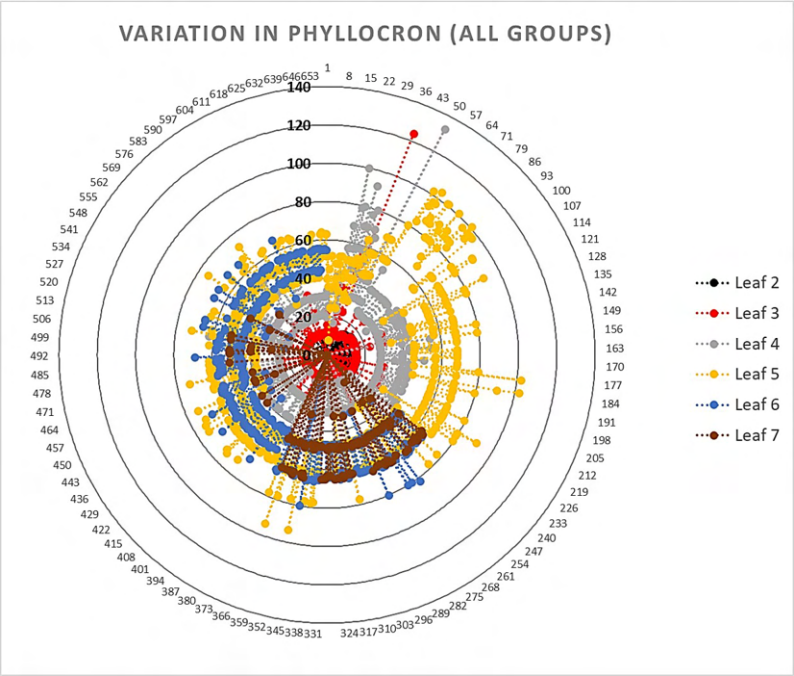

Figure 3.15: Distribution of phyllochron by leaf in test plants. All values are in GDD, with each point representing the time difference between successive leaf appearances on an individual plant.

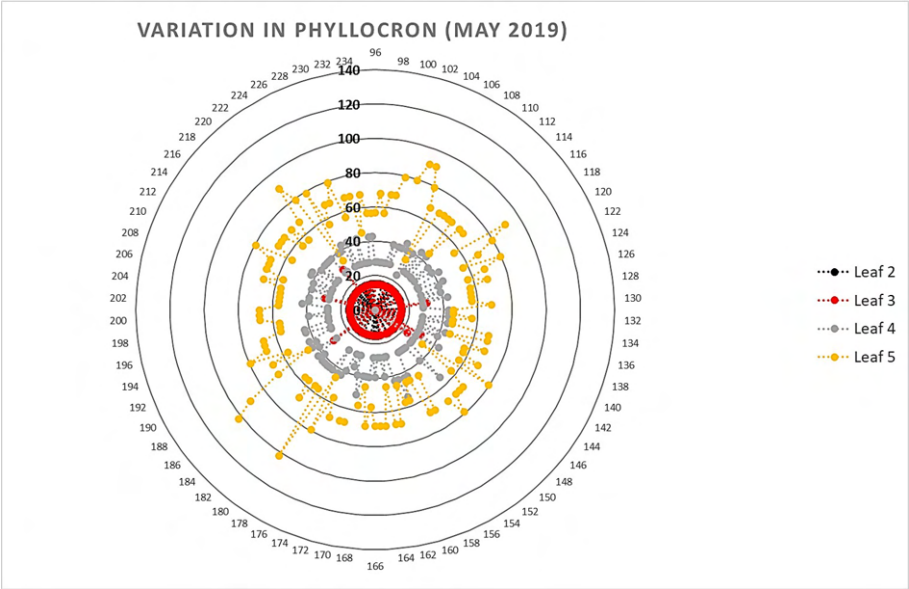

Figure 3.16: Phyllochron values for May 2019 growth experiment (combined results for control and test groups)

Significant variation was observed in the duration of the interval between appearance of successive leaves, despite the plants being grown under nearly identical environmental and nutritional conditions as well as being the same cultivar. This illustrates the challenge of using a statically calculated value of phyllochron based on thermal time for prediction of leaf appearance, and is hypothesized that environmental conditions other than temperature may play a more significant role in the appearance of new leaves than proposed by existing research.

Segmentation of phyllochron data by stress treatment shows similar variations in leaf appearance (Figure 3.17). Values of phyllochron in the control group are observed to be comparable to values obtained in the mild stressed group, with more outliers observed in the control group as compared to the mild stressed group. This confirms observations in literature [MC89, KS18], indicating a catch-up phenomenon in leaf growth and appearance rate during recovery periods after water stress, resulting in a neutralization of the delay effects witnessed during the period of stress. The recorded observations emphasize the need to integrate irrigation management data in determination of leaf appearance, and suggesting the possibility of controlling new leaf appearance by subjecting plants to targeted levels of water stress at a predetermined time.

Based on leaf length measurements, the elongation rate of the individual leaves is calculated. The leaf elongation rate (LER) of maize exhibits an initial high growth phase followed by a decline in growth rate to zero (Figure 3.18), as also described in Muller et al. [MRT01]. As the elongation rate of previously appeared leaves slows down and eventually stops, new leaves appear, suggesting a causal relationship between emergence / appearance of new leaves and elongation of existing leaves [FDL$^+$05, EDB$^+$15]. Monitoring of the growth rate of individual leaves can thus be employed in the prediction of appearance of new leaves.

The individual leaves in the maize plant show a growth trajectory similar to the lifetime evolution of the state of health of mechanical systems (as shown in Figure 3.18), and thus leads to the assumption that similar modeling techniques can be applied here. Determination of cut-off thresholds signifying the end of the linear elongation phase is required in order to implement prediction approaches similar to those employed in estimating the useful life of mechanical systems.

The relationship between elongation rate of the earliest appearing leaves is compared to the leaf lengths of newly appearing leaves as illustrated in Figure 3.19. The progressive evolution of the elongation rate as successive leaves appear is illustrated by the envelopes enclosing measured values. As it can be seen, the decrease in elongation rate shrinks to an observable threshold for measurements taken during the growth of leaf 4, and by the appearance of leaf 5, the elongation rate of leaf 1 is reduced to zero. A similar pattern is observed for other leaves during the vegetative growth phase. The trajectory of elongation rate of a leaf numbered N in order of appearance is proposed for use as a signal to predict the appearance of leaf number

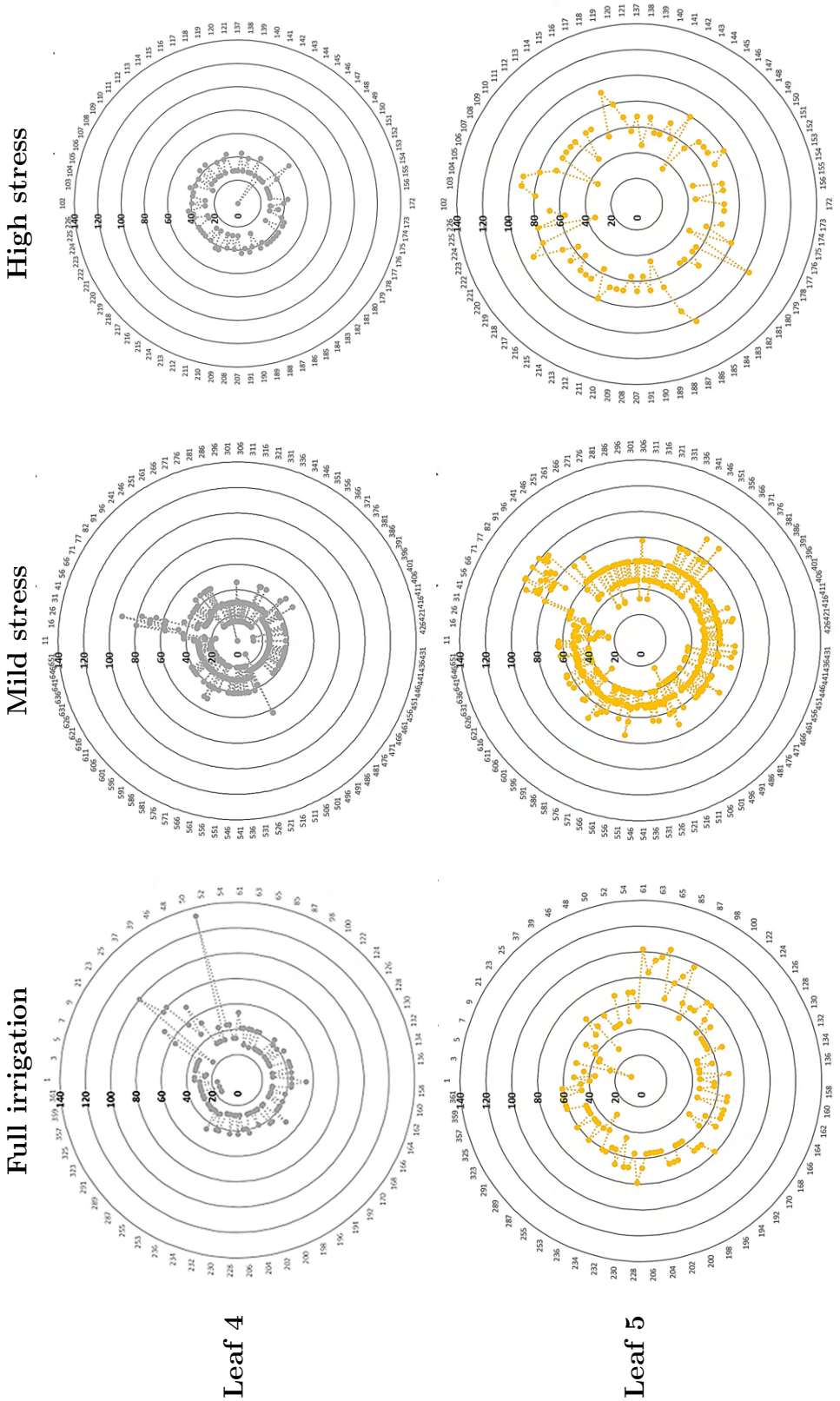

Figure 3.17: Comparison of phyllochron values for leaves 4 and 5 by water stress levels.

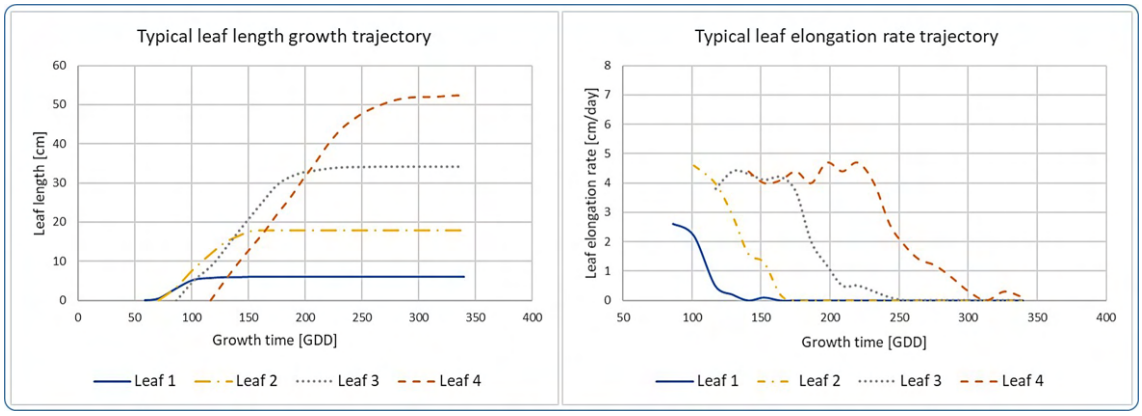

Figure 3.18: Typical leaf growth trajectories. A significant section of the elongation rate curve lends itself to a linear approximation.

N+3 based on identifying the time at which the elongation rate of the former crosses a threshold defined using experimental data.

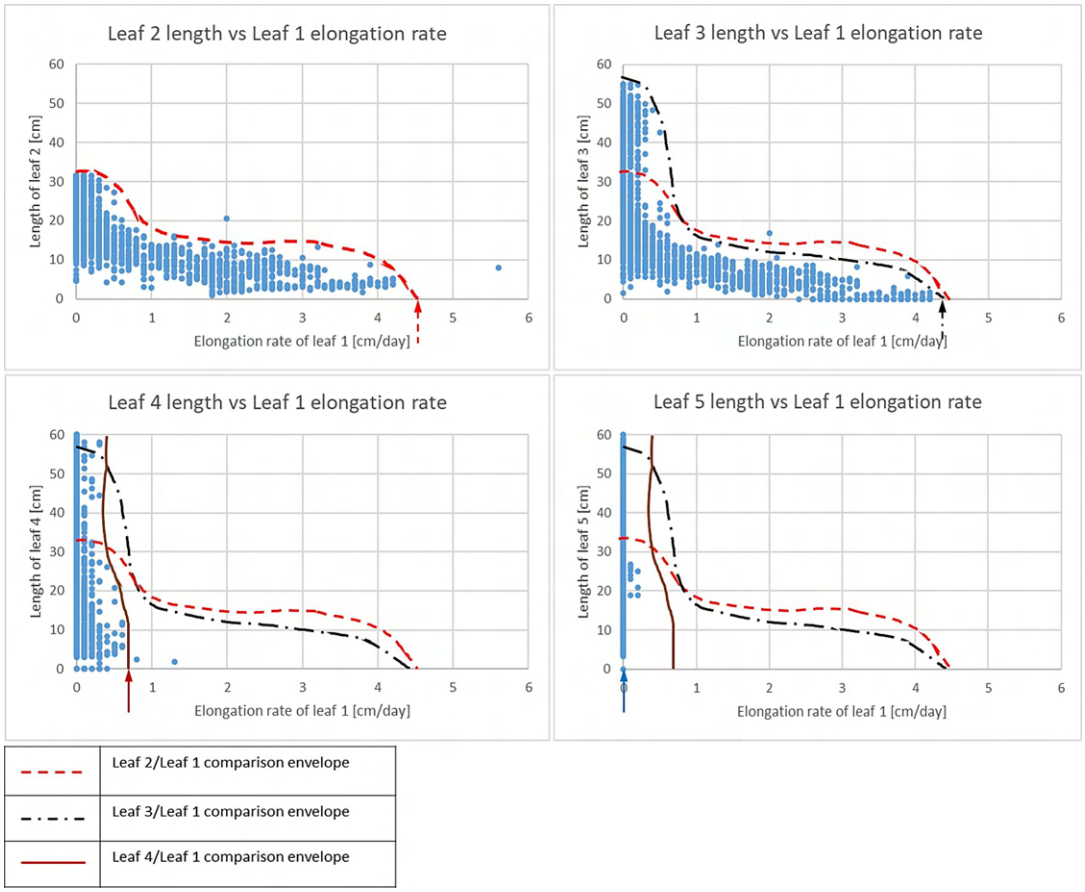

Figure 3.19: Comparison of growth of individual leaves

Modeling of leaf appearance using linear degradation-based approach

Degradation modeling is applied in industry for condition monitoring and prediction of time to failure of machinery and components. A data-based linear degradation model for residual lifetime prediction is described in [ZSG11] as applied to crack growth data. The model is used to forecast the evolution of sensed damage indicative signals over the lifetime of the system in operation. A linear degradation model for prediction of remaining useful lifetime (RUL) has also been applied by [Zhe19] in monitoring of the state of health of bearings based on vibration signals, providing an effective monitoring tool for bearing degradation and predicting the RUL of the machinery. Remaining lifetime modeling has also been applied in [BS17] in estimating the state of health of systems with constant load but stochastically occuring damage. A state machine model is used to describe the system behavior under different operating conditions.

In agricultural applications, a state machine-based RUL estimation model has been applied in [JKS19] and [KS20] in estimating the growth trajectory of entire maize plants and estimating irrigation requirements, allowing the determination of irrigation values to be used in application of different irrigation treatments (mild stress and high stress), as well as estimating the growth trajectory of individual maize plants based on the irrigation treatment received.

In this work, a linear MATLAB©-based degradation model, described by

$$S(t) = \phi + \theta(t)t + \epsilon(t), \tag{3.9}$$

with

$S(t)$	:	: Degradation signal,
ϕ	:	Model intercept,
θ	:	Model slope, a random variable with normal distribution with mean Θ and variance Θ_{var}, and
ϵ	:	Model additive noise, modeled as a normal distribution with zero mean and variance ϵ_{var},

is used to perform the prediction of the end of the growth phase of the individual plant leaves. Based on training data, the model estimates when the leaf elongation rate of the selected leaf reduces below a set threshold, signaling appearance of a new leaf.

The model parameters are obtained after training as

Θ	:	-0.0370,
Θ_{var}	:	9.964 e-05,

ϵ_{var} : 0.9298, and
ϕ : 6.8763.

For application to prediction beyond the 5th leaf, these parameters are assumed to change. It can be assumed that for different growth phases suitable assumptions (different constant parameters for different phases, as variables for the whole period etc.) have to be made.

The linear degradation model was selected particularly due to its suitability for applications in which the degradation signal is non-cumulative. Based on observation of the behavioral trend of LER over time, thresholds of 0.5 cm/day and 1 cm/day elongation rates were selected to indicate the termination of elongation for the first and second leaves respectively.

Results

The linear model is used to generate a projection of the time until the LER of the selected leaf would cross the set threshold. This is compared to the date of appearance of leaves 4 and 5. The absolute error (ABE) and mean squared error (MSE) are used to quantify the performance of the model against experimental data. The upper and lower boundaries of the box represent the 75th and 25th percentile values of the data respectively, with the median represented by a horizontal line within the box. The maximum and minimum values are also represented by horizontal lines located above and below the box respectively, with outliers appearing as crosses above or below the designated maximum and/or minimum. For prediction based on a 10-fold cross validation, the test group comprises 6, 7, and 11 representatives from the FI, MS, and HS treatments respectively. In the 5-fold cross validation, the test group comprises 13, 16, and 19 representatives from the FI, MS, and HS treatments respectively.

From the linear estimation, the projected remaining leaf elongation time is calculated, indicating when the LER crosses the thresholds for appearance of a new leaf (0.5 cm/day for leaf 1 and 1 cm/day for leaf 2). The ABE is plotted for the entire test group, as well as differentiated by irrigation treatment, as shown in Figure 3.20.

The prediction accuracy evaluated using root mean squared error (RMSE) for the prediction of end of active leaf elongation (corresponding to end of life in the model) is given in Table 3.8.

The predicted end of elongation time values for leaves 1 and 2 are compared to the appearance of leaf 4 and 5 respectively, as illustrated in Figure 3.21. Prediction accuracy evaluated based on RMSE is presented in Table 3.9.

Application of the linear model to the prediction of appearance of leaf 4 and 5 results in prediction accuracies to within 2 calendar days, with prediction of leaf 5

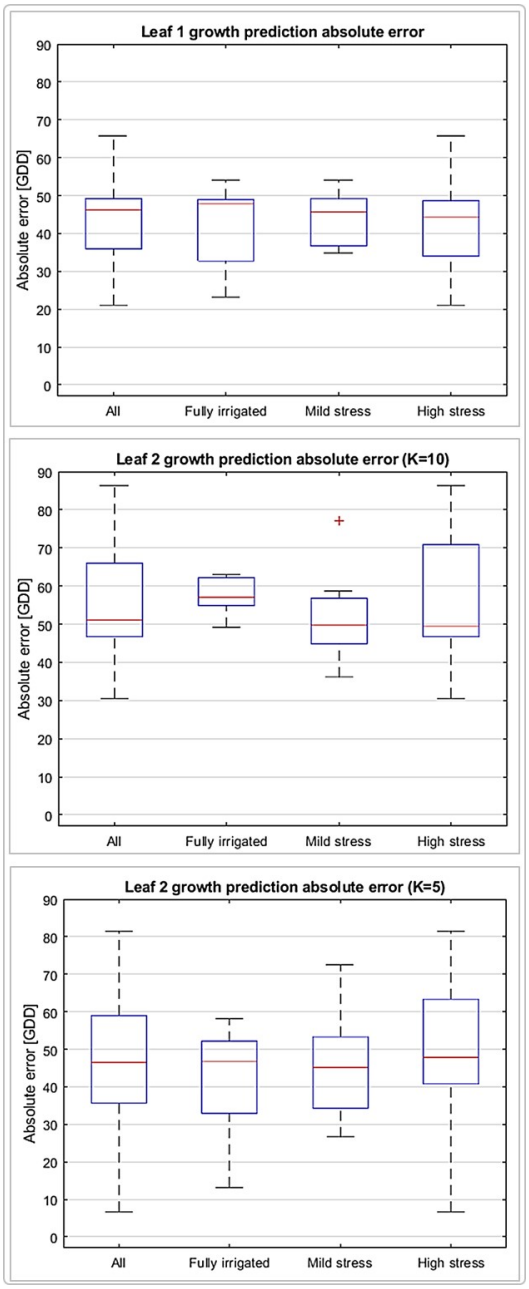

Figure 3.20: Performance of linear degradation model for prediction of end of active leaf elongation

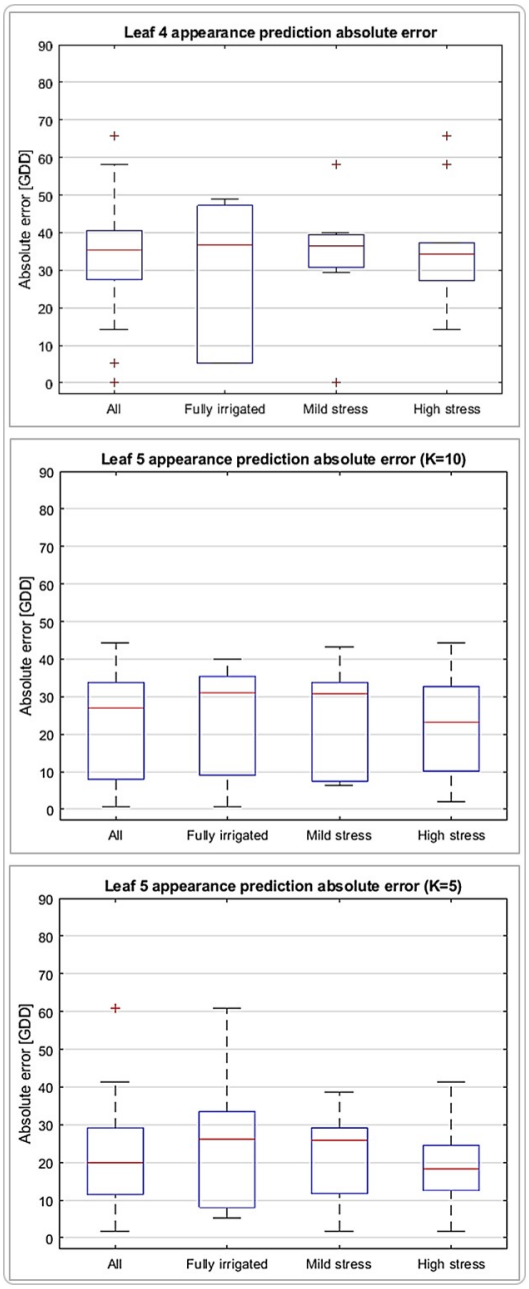

Figure 3.21: Performance of linear degradation model for prediction of new leaf appearance

Table 3.8: End of active leaf elongation prediction accuracy evaluated based on root mean squared error (RMSE)

Leaf No.	**Plant group**	**RMSE [GDD]**
Leaf 1	All	44.00
	Fully irrigated	43.85
	Mild stress	45.68
	High stress	41.28
Leaf 2 (K=10)	All	58.47
	Fully irrigated	61.81
	Mild stress	45.68
	High stress	57.60
Leaf 2 (K=5)	All	51.28
	Fully irrigated	47.46
	Mild stress	52.97
	High stress	52.35

Table 3.9: Accuracy of timing of leaf appearance evaluated based on RMSE

Leaf No.	**Plant group**	**RMSE [GDD]**
Leaf 4	All	37.38
	Fully irrigated	35.13
	Mild stress	37.43
	High stress	38.53
Leaf 5 (K=10)	All	33.35
	Fully irrigated	48.38
	Mild stress	27.51
	High stress	25.85
Leaf 5 (K=5)	All	40.46
	Fully irrigated	71.50
	Mild stress	23.97
	High stress	21.53

appearance consistently yielding a closer result to observed times as compared to predictions for appearance of leaf 4. Analysis of the observations by stress levels shows greatest consistency in prediction of leaf 4 (Figure 3.22) appearance for plants that were subjected to high (severe) stress, followed by reirrigation. The control group shows the greatest variability, with predictions both lower and greater than the observations occurring within the data set.

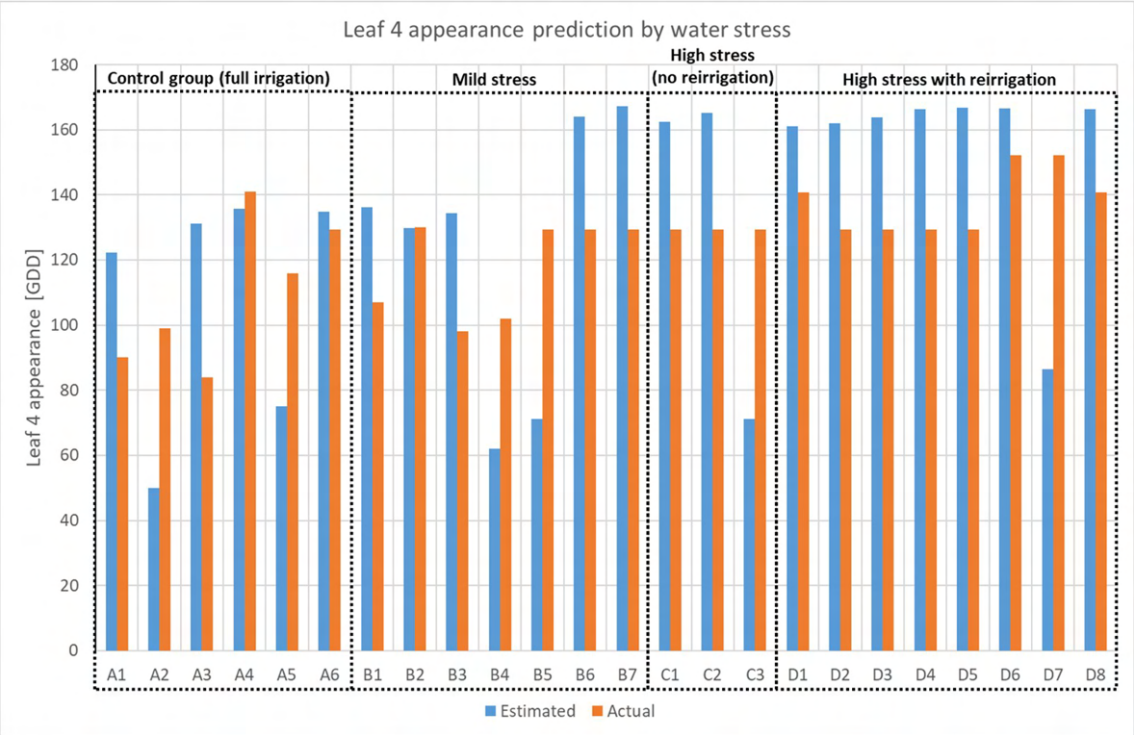

Figure 3.22: Results of leaf appearance prediction model for leaf 4 appearance estimation segmented by irrigation treatment, comparing estimated timing of leaf appearance and actual (observed) timing of leaf appearance

A similar segmentation of leaf 5 appearance predictions by stress treatments shows relatively good performance for all groups with the exception of a few outliers within the data set (Figure 3.23). There is a tendency towards overestimation of the appearance date of the new leaf. The improvement in accuracy is likely due to the availability of more data for leaf 2 growth, as well as the relative ease in accurately measuring the length (and hence determining the elongation rate) of the leaf, due to the sharpness of the leaf tip, as opposed to the more rounded tip observed for the first maize leaf.

Discussion

A linear modeling approach is developed to define suitable life growth parameters based on measurements. Applying the assumed approach and the defined parameters the approach is used to predict the timing of the end of the growth phase of the first and second leaves of individual maize plants as well as the appearance of the fourth and fifth leaves. Training and test data sets are generated using both 10-fold and 5-fold cross validation.

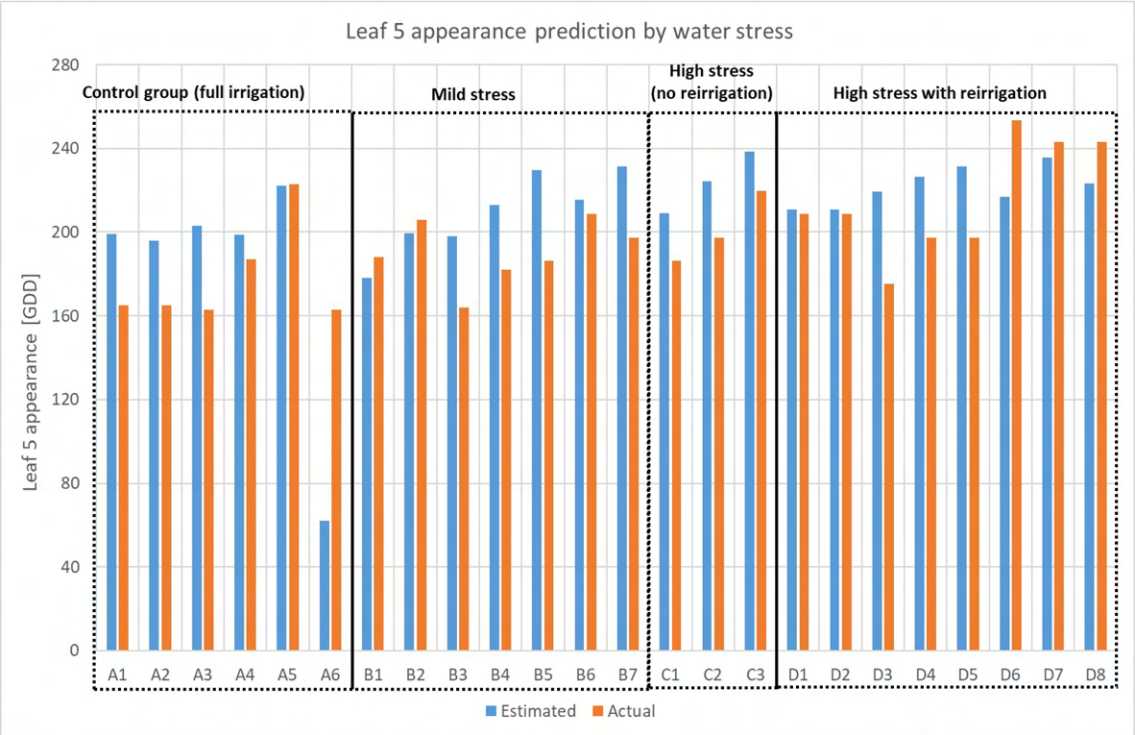

Figure 3.23: Results of leaf appearance prediction model for leaf 5 appearance estimation segmented by irrigation treatment, comparing estimated timing of leaf appearance and actual (observed) timing of leaf appearance

Prediction of the end of the growth phase for leaf 1 and leaf 2 using the linear model yielded results which are accurate to within 46 and 54 GDD respectively, with better results obtained using 5-fold cross validation during training of the model as compared to 10-fold cross validation. This has been presented in Table 3.8. Application of the results to leaf appearance prediction (presented in Table 2.2)is accurate to within 39 and 49 GDD for leaf 4 and 5 respectively, with outliers observed in th efully irrigated sample for leaf 5.

Evaluation of the performance of the model across different irrigation treatments based on absolute error revealed insignificant differences across irrigation treatments, as can be seen in Figures 3.20 and 3.21, with the exception of a marginal improvement in the prediction of leaf 5 appearance in one case. Comparison of the root square of error and mean square of error however points to a better performance in prediction of leaf appearance in plants exposed to either mild stress or high stress.

The estimates based on leaf 2 elongation rate values are more accurate than estimates based on leaf 1 elongation rate values. The reason for the differences were not established, and should be explored in future work. An initial hypothesis is that measurement error could arise due to the rounded tip of the first leaf in maize

plants, as compared to pointed tips in all later leaves, making manually measured leaf length less reliable for the first leaf as compared to all other leaves.

3.4 Prediction of evapotranspiration

The quantity of water lost to evapotranspiration within the indoor greenhouse can be modeled using multivariate least squares fitting, which is a multiple linear regression model allowing determination of the relationship between a selected dependent variable Y, and multiple predictors (independent variables) x_i. The resultant equation takes the form

$$Y = \beta_0 + \sum \beta_i x_i, \tag{3.10}$$

where β_i are coefficients.

Evapotranspiration is affected by a variety of factors, such as temperature, light intensity, daylength, humidity, wind, stomatal density, and stress level. To model evapotranspiration under different water stress conditions, it is assumed that lighting, day length, wind, and stomatal density are uniform for all plants, and can therefore be excluded from the list of predictors. Daily maxima and minima for temperature and relative humidity are measured, and the leaf length is used to represent the exposed surface area of the leaf.

Linear regression model

A linear regression model was developed, expressing the evapotranspiration ET as a function of the minimum and maximum daily temperature T and relative humidity H, the leaf length L and the stress state, represented by an additional coefficient β_{stress} that corresponds to the water stress level.

$$ET = \beta_0 + \beta_1 T_{max} + \beta_2 T_{min} + \beta_3 H_{max} + \beta_4 H_m in + \beta_5 L + \beta_{stress} \tag{3.11}$$

The predicted response was graphically compared to the true response (Figure 3.24), with the resultant coefficients and their p-values presented in Table 3.10. The p-value indicates the probability that the given variable has a coefficient of zero, with a boundary value of 0.05 (corresponding to a 5 % significance level) generally considered as a critical threshold for determining relevance of variables included in a linear regression model. An analysis of the p-values indicates that maximum daily relative humidity is not statistically significant at a 5% significance level given the other terms in the model, and may be eliminated without significantly altering the prediction outcomes.

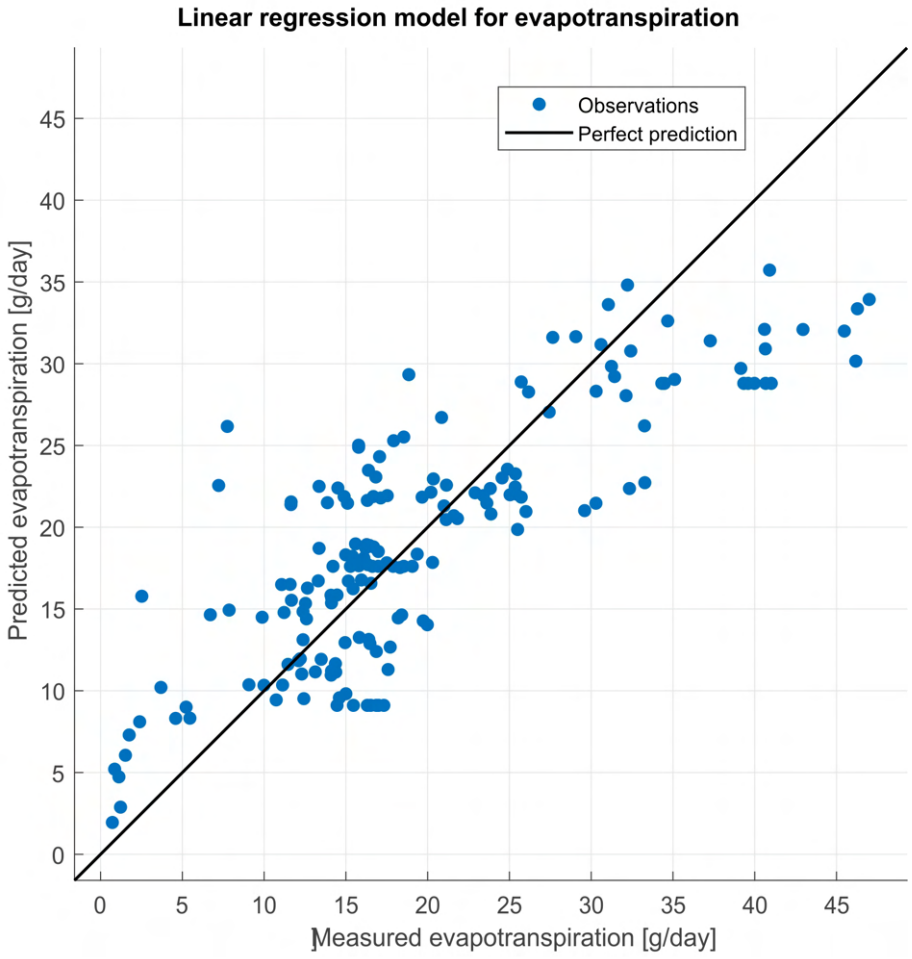

Figure 3.24: Predicted evapotranspiration based on linear regression model with 5-fold cross-validation. Accuracy metrics: $R^2 = 0.71$; $RMSE = 5.551$ g

3.5 Summary

The description of leaf elongation using a state machine model is confirmed to allow for better projection of plant growth based on water status. Challenges related to determination of stress thresholds are however observed, with the NSGA-II optimization algorithm producing large estimation errors in the case of plants under full irrigation. Implementation of a least squares optimization algorithm improves prediction accuracy, however there are still significant errors for estimation of growth under full irrigation. A linearized model trained using experimental data is employed for estimation of leaf elongation, producing good prediction accuracy and reliable estimations over a prediction horizon of up to ten steps.

Table 3.10: Linear regression evapotranspiration model coefficients

Coefficient	**Associated variable**	**Estimate**	**Standard error**	**p-value**
β_0	Constant	14.215	4.421	0.0014
β_1	T_{max}	-2.388	0.380	5.681 e-10
β_2	T_{min}	2.294	0.282	1.738 e-15
β_3	H_{min}	-0.527	0.0577	6.946 e-19
β_4	H_{max}	-0.0145	0.0443	0.744
β_5	L	0.1139	0.380	8.225 e-112
β_6 (MS)	Mild stress	3.3404	0.522	2.839 e-10
β_6 (HS)	High stress	-9.325	0.581	1.717 e-49

Experimental observations of maize cultivated under controlled greenhouse conditions, both under well-watered and water stressed conditions indicate that the application of static values of phyllochron based purely on thermal time (or on thermal time and levels of illumination) are insufficient to accurately predict appearance of leaves, with significant variations observed in plants grown under identical thermal and lighting conditions. It is proposed that other environmental conditions, in particular, exposure to water stress, may play a role in the appearance of new leaves in growing plants, hence an approach that is applicable to a variety of different growing conditions due to sole reliance on the growth characteristics of the plant itself offers significant improvement in prediction of development of new leaves in maize plants.

The link between growth of different leaves on the same plant has been conclusively observed. Further exploration of effects of mild stress as well as severe stress with and without recovery periods would be vital in determining the possibility of realizing targeted leaf appearance through strategical sequencing of stress and recovery periods. This would allow control of both the actual growth of maize plants and the timing of developmental stages, resulting in a fully controllable plant growth by precision deficit irrigation. Additionally, the simplicity of the linear prediction function lends itself to ease of automation, which is one of the main goals of precision irrigation approaches.

4 Control of maize growth

Based on a state machine description, it is possible to model growth of maize plants as a function of the water stress status. This section describes a model based control algorithm developed for control and optimization of maize growth under indoor greenhouse conditions, with maximization of total leaf elongation and minimization of water consumption as control targets. The section begins with an overview of automation tasks carried out to allow fully automated operation within the indoor greenhouse setup. A brief introduction to the state of the art in precision irrigation control follows, categorized based on the atmosphere-plant-soil continuum and with an additional focus on application level: field, zone and individual plant level. The development of a model predictive controller incorporating a trellis decoding approach for generation of optimal precision deficit irrigation sequences is described, and experimental results are presented.

A significant part of the material in this chapter has been published in various research publications [OHKS19, OS19a, OS22a, OS22b, OS22c, OS23].

4.1 Greenhouse automation

Growing of plants in a greenhouse setup requires a replication of conditions necessary for optimal plant growth within a controlled environment. In an indoor greenhouse, factors requiring monitoring and control include lighting, temperature, relative humidity, irrigation, supply of nutrients, among others. Special growth substrates may also be required in the case of pot-grown plants to ensure adequate aeration and moisture distribution within the rooting zone.

The experimental work described in this thesis took place in an indoor greenhouse located within the Chair of Dynamics and Control at the University of Duisburg-Essen, described in Section 3.1.

Automation tasks in the greenhouse were closely related to the variables that required monitoring and control, with a focus on the following:

i) Soil moisture content, manually obtained using a precision weighing scale.

ii) Total leaf length, manually measured using a flexible rule.

iii) Number of appeared leaves, manually determined by visual observation.

iv) Above ground biomass, which was manually measured at the end of each growth experiment using a precision weighing scale.

v) Onset of water stress, which was determined via analysis of daily leaf elongation rate in comparison with a control group.

vi) Irrigation amount, manually supplied using a syringe and measured using a precision weighing scale.

Moisture measurement

Soil moisture plays an important role in plant physiological processes such as germination, transpiration, photosynthesis, and respiration. Soil moisture content can be expressed volumetrically (based on water volume) or gravimetrically (based on water mass), expressed as

$$WC_x = \frac{X_{water}}{X_{soil} + X_{water}}, \tag{4.1}$$

where

WC is the soil moisture content,
x is the moisture content evaluation approach- volumetric or gravimetric, and
X is volume (for volumetric) or mass (for gravimetric).

Due to the presence of air pockets within any growth substrate, necessary to facilitate physiological processes in plant roots, a gravimetric approach allows for more accurate assessment of moisture content, given the low density of air.

Manual determination of gravimetric soil moisture content had previously been achieved by daily measurements of pot mass using a precision weighing balance with a resolution of 0.01 g. The main limitation of manual measurements is the absence of real-time soil moisture values, necessary to enable monitoring and control of plant water stress in real time. A continuous measurement of soil moisture was developed, with two separate methodologies:

- based on continuous measurement of pot mass using electromechanical load cells, and
- based on continuous measurement of soil moisture using a capacitive moisture sensor.

Load cell-based soil moisture measurement

Electromechanical load cells transform mechanical force exerted due to application of mass into electrical signals. Three main types of load cells are commonly used, based on the nature of energy conversion:

i) Strain gauge-based load cells are designed based on the mechanical deformation experienced by an elastic material under tensile or compressive stress, based on Hooke's law. The resultant changes in dimension affect the electrical conductivity of the material, which is converted into an electrical signal (voltage or current) proportional to the applied force.

ii) Hydraulic load cells consist of a cylinder containing a liquid, whose pressure is influenced by external force applied via a connected piston. The pressure measurement can then be converted into an electric signal for further process control applications.

iii) Piezoelectric load cells comprise specialized crystals which emit a voltage when subjected to mechanical force. Amplification of the emitted signal allows determination of the applied force.

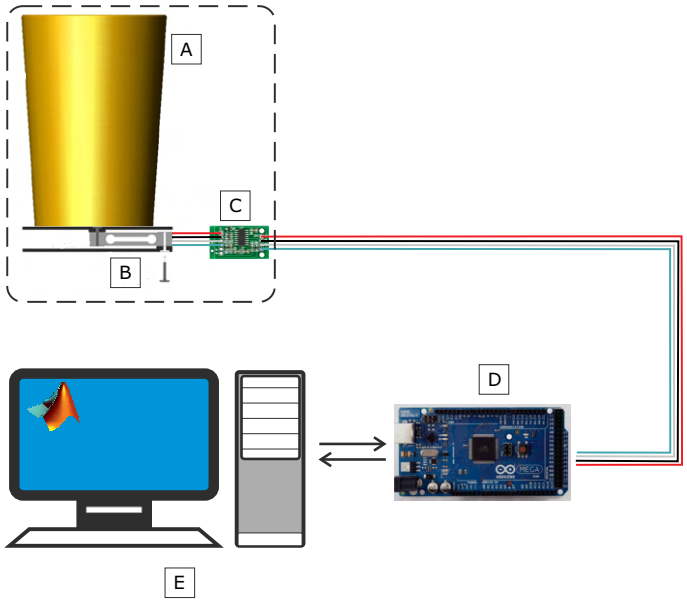

Figure 4.1: Load cell-based moisture measurement setup comprising
A: PET container with growth substrate; B: strain gauge-based load cell with 3D printed mounting; C: A/D converter HX711; D: Arduino Mega 2560 microcontroller; E: PC with MATLAB Software

Strain gauge-based load cells were applied for the automation of moisture content measurement due to high accuracy, low cost, and lower sensitivity to temperature. To determine the moisture content of the soil, initial dry mass of the pot and substrate was taken as a reference. Any additional mass was assumed to represent added water, with plant mass being neglected for the experiment duration.

The setup for achievement of load cell-based soil moisture measurement is illustrated in Figure 4.1.

Calibration of the strain gauges was performed, with measurements taken both incrementally and decrementally to assess the hysteresis behavior of the setup. The calibration curve is illustrated in Figure 4.2. An analysis of measurement accuracy indicated a mean absolute error of 0.67 g, RMSE of 0.82 g and a standard deviation of 0.53 g. The values obtained were considered acceptable for application within the greenhouse setup. Temperature compensation is achieved using a dynamic thermal

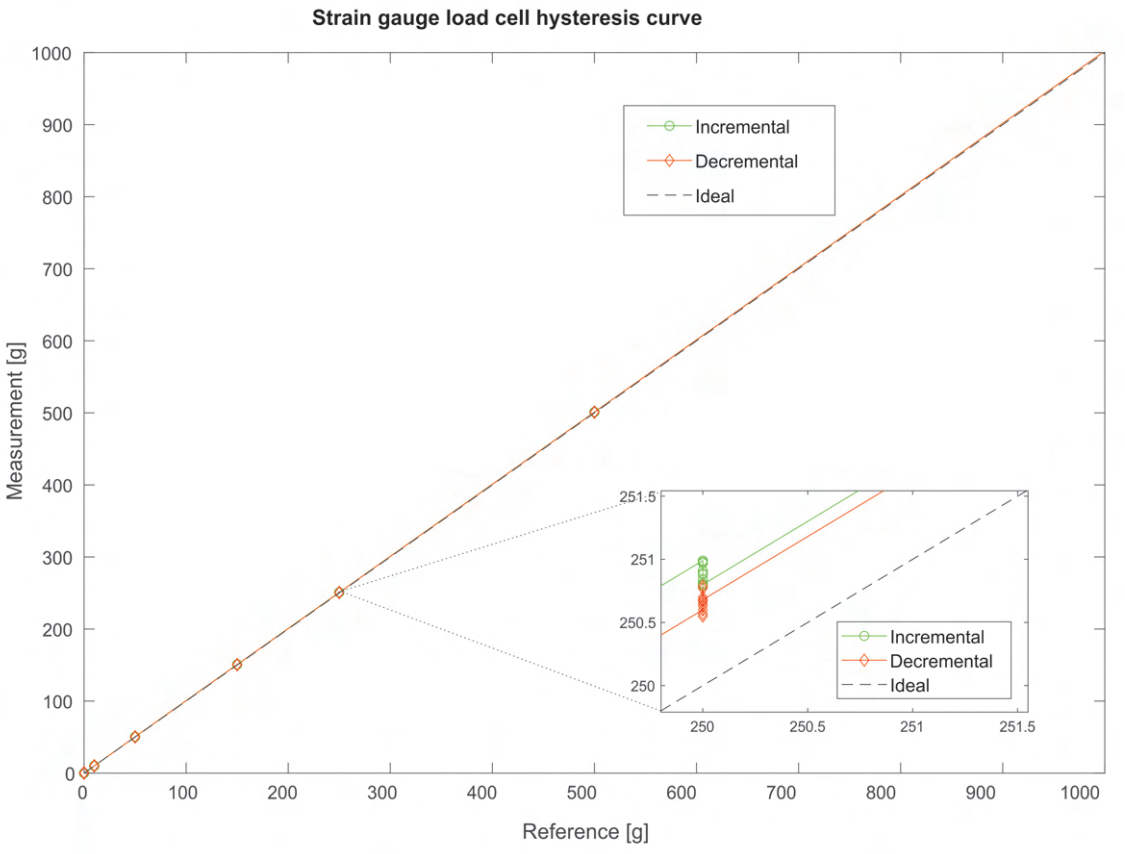

Figure 4.2: Hysteresis curve obtained during calibration of strain gauge-based load cell for real-time measurement of soil moisture content

coefficient α_k included in the strain gauge specifications. The relationship between changes in thermal coefficient and temperature changes is described by equation 4.2

$$\frac{\Delta k}{k} = \alpha_k \Delta T, \tag{4.2}$$

where

k is a scaling factor,
α_k is the thermal coefficient, and
ΔT is change in temperature.

Thermal induced deviations and measurement drift were analyzed over eight days using a known fixed mass subjected to periodic automatic measurements. Results presented in Figure 4.3 show variation in diurnal and nocturnal measurements for a sample of five load cells, with the magnitude of variation inconsistent across different sensors. This suggested that any corrections for thermal variations would need to be conducted independently for each load cell as part of the calibration procedure.

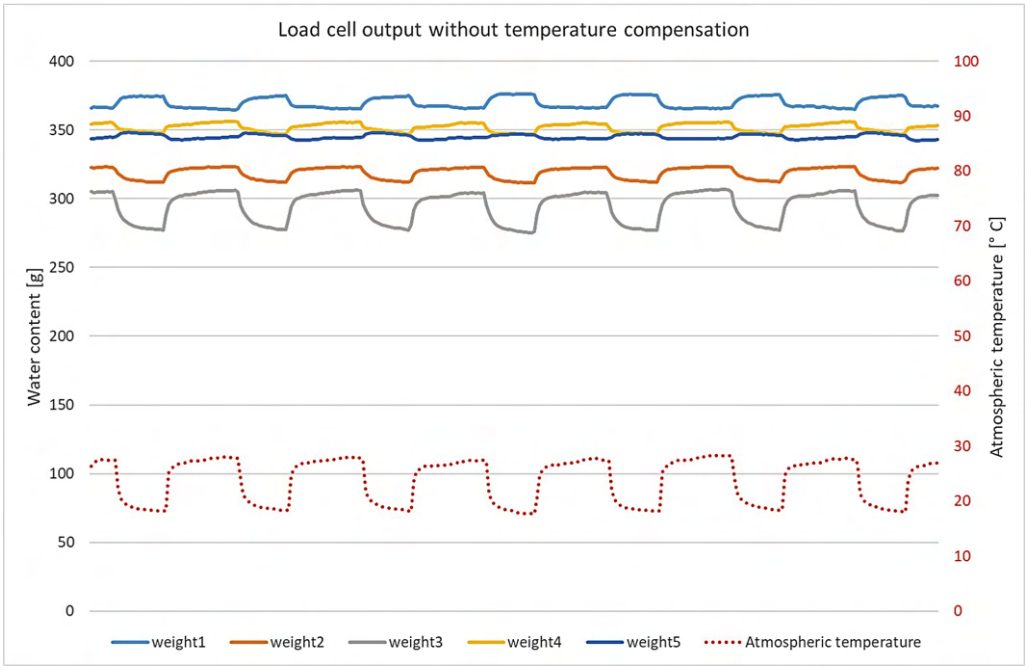

Figure 4.3: Load cell output without thermal compensation displaying variation in measured mass during diurnal and nocturnal cycles. Displayed results represent measurements taken at 30-minute intervals over an 8-day period.

Based on the thermal output characteristic (shown in Figure 4.4), an exponential correction formula was derived for real-time temperature compensation, with the adjusted thermal coefficient $\alpha_{k(adj)}$ for each sensor determined as

$$\alpha_{k(adj)} = A_1 \alpha_k^{A_2}, \tag{4.3}$$

where A_1 and A_2 are constants evaluated based on experimental data obtained during sensor calibration. The sensor output from the load cells after correction for

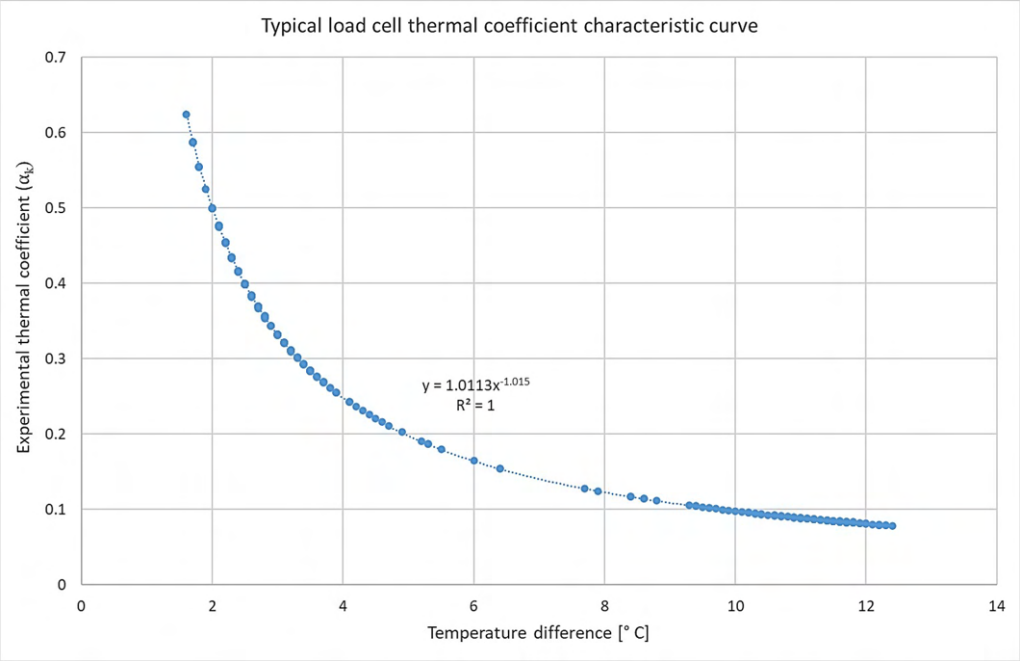

Figure 4.4: Typical thermal characteristic curve for load cell measurement output

thermal variation is represented in Figure 4.5, with output values relatively constant, with the exception of brief outlier values during the switch between day and night in the greenhouse.

Automated plant growth monitoring

Growth and development in plants results from the division, expansion, and differentiation of cells, which are related to different physiological processes. Cell expansion is primarily responsible for the production of above-ground biomass, which is expressed during the vegetative stage of plant growth as an increase in plant height, leaf length, and leaf area. Monitoring of growth characteristics expressed during the vegetative stage can be used for yield prediction in maize, with previous work reporting the application of plant height measurement for maize yield prediction ([YMJ+11]; [AMM+19]).

Plant height measurement defines the shortest distance between the ground level and the upper boundary of photosynthetic tissue (leaves, in the case of maize)

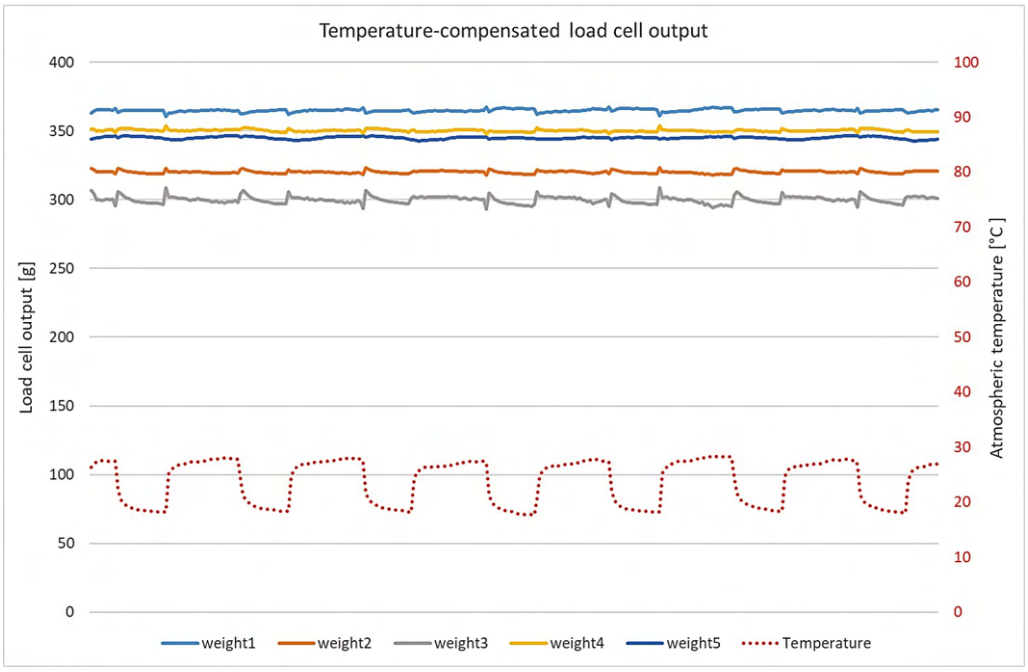

Figure 4.5: Temperature-compensated load cell output from sensor data presented in Figure 4.3

[PHDG+16]. For herbaceous plants, [PHDG+16] indicates that height-related developmental thresholds such as the cut-off between vegetative and reproductive stage may alternatively be defined based on leaf length, especially in species with leaves that bend as they elongate.

Image processing has been used to determine height of field-grown maize, with RGB images combined with depth assessment sensors to generate three-dimensional point clouds from data captured vertically above the maize plants. In [QZH22], the depth measurements are provided by an integrated infrared transmitter/camera within an RGBD camera, whereas [GZL+18] employs separately acquired LIDAR data for depth perception. An alternative approach is presented by [CWX+20], where sets of RGB images acquired at different oblique orientations are superimposed to generate depth-related data.

In this work, the indoor greenhouse setup (described in section 2.5) allows for acquisition of lateral images, allowing for direct determination of plant height via image processing techniques. A description of the steps applied in obtaining plant height and total leaf length estimates follows.

I) **Image capture**: an RGB camera mounted on a rotating platform equidistant from each of four groups of five plants each was programmed to take images

at intervals of 15 minutes per group. Infrared imaging was available, but due to the slow dynamics of leaf elongation, it was considered adequate to base data processing on the daytime images.

II) **Image segmentation**: Assessment of leaf height requires isolation of pixels representing the plants from the background. Color thresholding based on the location of green pixels was selected for purposes of segmentation, converting the RGB image into a binary file with individual pixels designated a value based on the presence or absence of green color. Determination of the specific color range designated "green" was achieved in a pre-processing stage, whereby individual pixels in a sample of plant images were manually tagged, and the resultant range of RGB values evaluated to specify the desired color range.

III) **Height determination**: A scaling factor is required to convert the pixel coordinates registered in the segmented image to plant height. The top diameter of the plant pot was used, with the total number of pixels in the x-direction extracted from captured images and compared to the actual measurements. It is assumed that no skewing of the camera during image capture occured. The plant height was then estimated based on the pixel with the highest registered y-coordinate.

IV) **Total leaf length estimation**: Regression analysis was carried out on historical measurement data to obtain a correlation between plant height (obtained via image processing performed on RGB images) and total leaf length (manually measured using a flexible rule). The obtained linear regression was incorporated into the image processing algorithm to estimate total leaf length in real time.

The linear regression model was evaluated to produce an R^2 value of 76% and an RMSE value of 9.17 cm during training with historical data. Application to test data yielded an R^2 value of 37% and an RMSE value of 27.45 cm, indicating that the selected model was not sufficiently accurate to estimate total leaf length.

It is to be noted that despite the environmental control within the indoor greenhouse, the plants nonetheless exhibited motion, both due to wind currents and the growth process itself. Additionally, the lighting angle and bending characteristics served to distort the registered color in some images, resulting in inaccurate and/or inconsistent height measurement (with some plants even showing significant reductions in height over subsequent daily measurements). These factors likely adversely affected the fully automated evaluation of leaf length based on image processing techniques, suggesting either application of alternative monitoring and measurement techniques, or use of a different variable to represent plant growth.

Thermal monitoring of plant water status

Plants exhibit a range of sophisticated responses to biotic and abiotic stresses, including water deficit [CLL$^+$09, Hsi73]. The concept of plant water stress can be distinguished as either external or internal [Tar96]. External water stress is defined by an imbalance between water supply and demand, taking into account only the soil/atmospheric water content at the plant boundary. Internal water stress is based on plant internal water status, which takes into account control mechanisms employed by the plant to sustain physiological processes even under water deficit conditions [Lar01].

In this work, the physiological response of interest with regard to water stress is the reduction in stomatal conductance, which results in partial or complete closure of stomatal apertures on the leaves. Due to the role of stomatal openings in thermoregulation of the plant through evapotranspiration, the physiological response to water stress can be observed as an increase in leaf surface temperature occasioned by the reduction in evapotransporative cooling. Extended increase in leaf surface temperature is visible observable as a wilting response. In the presence of reference plants maintained in fully watered condition, measurement of leaf surface temperature can serve as a reliable indicator of the onset and level of plant water stress due to the direct correlation between plant water status and leaf surface temperature.

The thermographic measurement principle is illustrated in the schematic diagram in figure 4.6, where 1 is the immediate surrounding of the measurement target, 2 is the target object, 3 is the atmosphere and 4 is the infrared (IR) camera. The target object emits its own energy with an emissivity ε and reflects radiation from its immediate surroundings with reflectivity $\rho = 1 - \varepsilon$. The energy received by the thermal camera experiences transmission losses due to transmittance of air and water vapor in the atmosphere. The final radiation energy received by the thermal camera is thus expressed as

$$W_{tot} = \varepsilon\tau W_{obj} + (1-\varepsilon)\tau W_{refl} + (1-\tau)W_{atm}, \tag{4.4}$$

where

W_tot is total energy received by the camera,
W_{obj} is the radiation energy of the target object,
W_{refl} is the radiation energy from the surroundings,
W_{atm} is the radiation energy in the atmosphere,
ε is the emissivity and
τ is transmittance of the atmosphere.

The results described in this work are obtained from an infrared camera FLIR a65sc

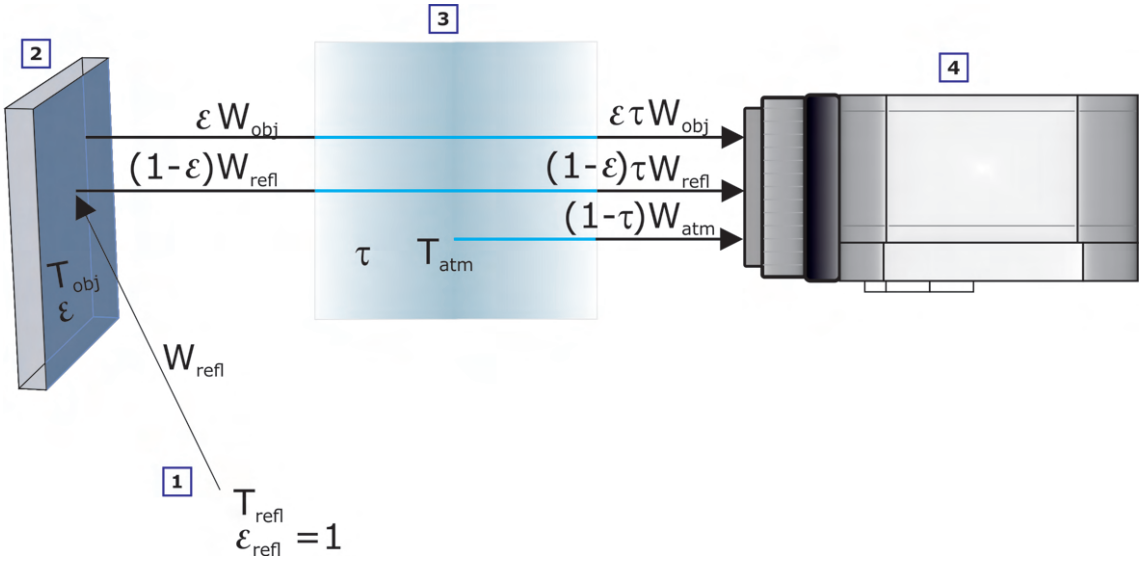

Figure 4.6: IR camera measurement principle with 1: Surrounding; 2: Object; 3: Atmosphere; 4: Camera

attached to an RGB camera. The setup rotates automatically through 90° steps, with the interval of image capture per plant group set to 15 minutes. Previous work reported in [Kög19] involved manual selection of individual pixels from previously recorded infrared images, which were then used to represent the entire leaf surface under consideration. In this work, isolation of plant-representative pixels allowed extraction of all relevant temperature data from each captured image, with temperature results comprising the mean value of all obtained values. The emissivity of the plant leaves is assumed to be constant at 0.97. Thermal data is converted into a 14-bit electrical signal based on the equation

$$p(x,y) = \left(\frac{R_1}{R_2} \cdot \frac{1}{e^{\frac{B}{T}} - F}\right) - O, \tag{4.5}$$

where

$p(x,y)$ refers to the radiation signal from a pixel located at the coordinate (x,y),
T is the temperature in Kelvin, and
R_1, R_2, F, O, and B are camera calibration constants, accessible from the camera settings.

The calibration constants and other relevant experimental parameters are presented in table 4.1. Additional variables required in the determination of leaf surface temperature are atmospheric temperature (taken to be equal to surrounding temperature) and relative humidity, which were measured in real time using a DHT22

temperature and humidity sensor, and integrated into the extraction algorithm.

Table 4.1: Parameter settings for themographic measurement of maize water stress

Parameter	**Description**	**Value [unit]**
$\frac{R_1}{R_2}$	camera reflectance coefficient	375918 [-]
B	camera calibration constant	1437.3 [-]
F	camera calibration constant	1 [-]
O	camera offset constant	483.266 [-]
ε_{leaf}	leaf emissivity	0.97 [-]
D	distance between target and camera	1 [m]

The image processing procedure followed a workflow described in the flowchart in Figure 4.7. Pre-processing is performed on the raw captured images adjust the contrast and intensity levels, resulting in a sharper image. The pre-processed IR image is then segmented with the help of a corresponding RGB image, with timestamp information used for matching. Color thresholding is applied to isolate green pixels, with other pixels set to black. To enable overlaying of the thresholded RGB image onto the IR image, a registration process involving translation, rotation and scaling was performed with the center of rotation coinciding with the image center of mass. This was done by generating an adjustment matrix obtained from a comparison of similarities and features of the pre-processed IR image and the RGB image. The adjustment matrix was then applied on the original IR image to generate a registered IR image. Temperature extraction was then performed based on equation 4.5, using the pixels on the registered IR image corresponding to the set of pixels isolated during the segmentation step. Figure 4.8 presents a sample heat map generated from processing the obtained IR images. An analysis of the sample image indicates observable variations in surface temperature even in individual plants. This underlines the importance of avoiding reliance on individually selected pixels to represent the temperature of an entire leaf surface.

4.2 Precision irrigation control background

Control techniques are broadly classified as open or closed loop, defining the existence of any kind of calculated or otherwise technically realized feedback (output to the input of the system considered). Open loop precision irrigation control relies on an accurate understanding (in the best case: a model) of plant water requirements,

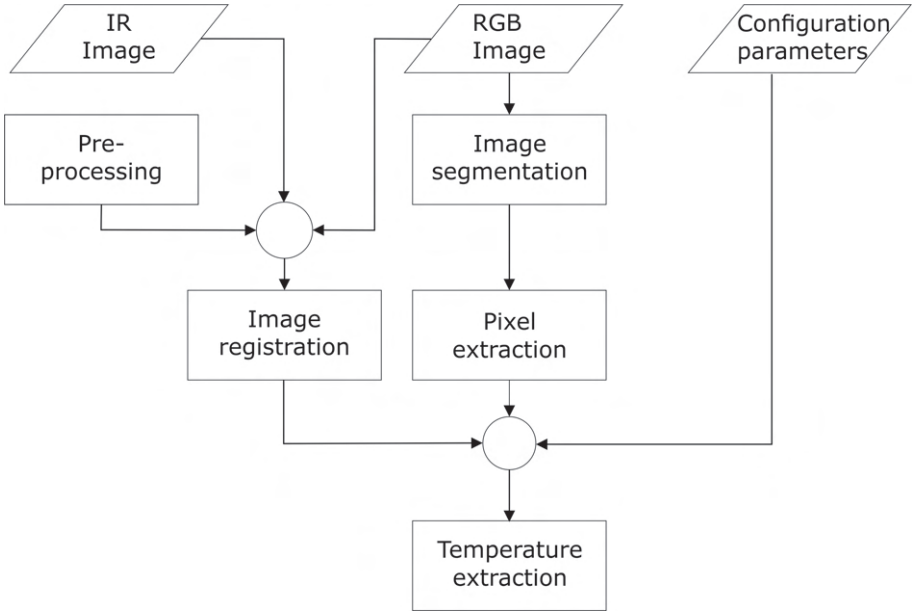

Figure 4.7: Flowchart representing image processing and temperature extraction workflow

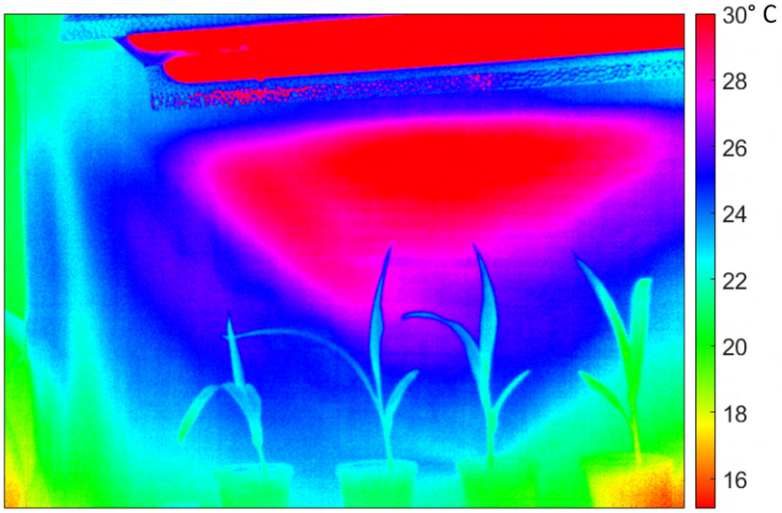

Figure 4.8: Sample heatmap representing pixel-specific temperature data generated from IR image

while closed loop methods include sensing mechanisms to dynamically adjust the control input to the irrigation system based on measured values.

The performance of precision irrigation control approaches depends on the definition

of plant water requirements. The characterization of plant water demand and the subsequent responses to the water application is described in Kögler [KS17] along a soil-plant-atmosphere continuum. Precision irrigation control approaches can thus be categorized into soil-based, plant-based, and atmosphere-based approaches. Further distinction is made between approaches targeted at enhancing precise delivery at field level, within irrigation management zones and at individual plant level.

Soil-based approaches

Growing plants obtain water required for their growth from the soil. The soil moisture content has therefore been applied as a measure of the water status of the plant, with a plant-specific lower limit describing the minimum moisture content required to maintain the plant above wilting point [BS11] and a soil-specific maximum water holding capacity, also referred to as the field capacity [VH31]. The main goal of traditional irrigation methods is to maintain soil moisture content at field capacity during the growth phases, with scheduling of irrigation events based on plant growth models such as FAO Aquacrop [SRH$^+$08] or multivariable models simulating soil moisture, plant growth, and evapotranspiration such as DSSAT [HPB$^+$19]. An overview of the current state-of-the art in soil-based precision irrigation control is presented in Table 4.2.

With regard to the current status of soil-based precision irrigation control approaches described in literature, it can be stated that the maintenance of soil moisture level between a user-defined lower boundary related to the wilting point and an upper boundary defined by the soil water capacity has been employed as the basis for control decisions. Challenges related to soil water dynamics arising from inherent hydraulic characteristics or changes in the spatial envelope defining root-available water have been solved.

Optimization of location and distribution of soil moisture sensors to allow accurate mapping of soil moisture distribution while minimizing the required number of sensors is a potential area for further work in the implementation of sensor-supported soil-based precision irrigation control. Variations in the upper soil moisture boundary during scheduling of irrigation quantity has not been considered in literature, signifying a gap in the application of soil-based precision irrigation methods to deficit irrigation strategies. Additionally, a significant gap exists in soil-based approaches applied at individual plant level.

Advancements in the field of wireless sensor networks, remote sensing and machine learning approaches are expected to drive future developments in soil-based precision irrigation control, allowing for more localized decision support systems and greater adaptability to individual plant water requirements.

Table 4.2: Summary of soil-based precision irrigation control approaches [OS22b]

Author	Year	Sensing/Measurement			Application scope			Modeling / Control approach
		Soil	Plant	Atm	Field	Zone	Plant	
Adeyemi et al.	2018	x		x	x			MPC with NN-based prediction
Andugula et al.	2017	x				x		Gaussian process regression
Bazzi et al.	2019	x				x		Fuzzy C-means algorithm
de Benedetto et al.	2018	x			x			Kriging with external drift
Benzekri & Refoufi	2006	x		x	x			Anticipatory on/off control
Capraro et al.	2008	x				x		on/off control with dynamic thresholds
Chen et al.	2020					x		Genetic algorithm
Egea et al.	2017	x			x			on/off control
Gu et al.	2021	x		x	x			NN-based on/off control
Hedley and Yule	2009	x				x		Daily prediction of soil water status
Jimenez et al.	2020	x			x			LSTM neural network
Liu & Xu	2018	x					x	On/off control
Lou et al.	2016	x	x		x			On/off control
Nahar et al.	2019	x		x	x			MPC with closed loop scheduling
Roy	2014	x			x			MPC with stochastic receding horizon
Song et al.	2016	x		x	x			Deep belief network (DBN)
Termite et al.	2019	x		x	x	x		Feedforward NN; ANFIS
Tseng et al.	2018		x		x		x	Deep convolutional neural network
Wei et al.	2013	x			x			On/off control
Xiao et al.	2010	x			x			on/off control
Zhao et al.	2007	x			x			On/off, Time control and fuzzy hybrid control

Atmosphere-based approaches

Atmosphere-based precision irrigation control approaches involve balancing the water supplied to the plant with the water released to the atmosphere through evapotranspiration. Achievement of the high accuracy required in precision irrigation is either accomplished by refining evapotranspiration models for use in open loop control or by incorporation of sensor feedback in closed loop control. Common models of evapotranspiration incorporated into precision irrigation include FAO's Penman-Monteith model [All98], the Hargreaves-Samani model [HS85] and the Surface Energy Balance model (SEBAL) [BMFH98].

An alternative atmospheric-based approach relies on prediction of precipitation rather than evapotranspiration [Roy14, TKP+16]. Irrigation scheduling is adjusted based on predicted timing and quantities of precipitation.

Hybrid approaches combining ET estimation with soil moisture sensing [LMA+16, NZB+19, BHB+20] or plant-based methods [TKP+16, GLM+19] have also been used to achieve greater accuracy in precision irrigation control. These allow compensation of weather-related disturbances to the evapotranspiration model by integrating the dynamic behavior of soil moisture or of the plant. However the related reliability depends on the accuracy of crop coefficients used in determination of actual evapotranspiration. An overview of the current state of research on atmosphere-based precision irrigation control approaches is presented in Table 4.3.

A major challenge in atmospheric-based precision irrigation approaches arises from the difficulty in differentiating between evaporation (from the soil surface) and transpiration (from the plants), requiring dynamic adjustment of irrigation control algorithms as plant cover increases during the growth season. A recent approach described by Chen et al. [CHM20] involves the partitioning of evapotranspiration values into its two components through machine learning techniques. This could provide a key to achieving greater accuracy in precision irrigation control, allowing the focusing of water delivery to meet actual plant demand rather than maintaining constant soil moisture levels, including in areas where no plant growth is present.

A move towards simplification of evapotranspiration and weather forecasting models to reduce sensing requirements and incorporation of machine learning and remote measurement has been observed.

Atmosphere-based approaches however face the challenge of not taking into consideration the plant response, and therefore have generally been integrated into control approaches where feedback is obtained from plant-based or soil-based measurements. Application at plant level is also not widespread. Advances in spatial and temporal precision in modeling and measurement of atmospheric parameters are expected to extend the application of atmosphere-based approaches to plant level.

Table 4.3: Summary of atmosphere-based precision irrigation control approaches

Author	Year	Sensing/Measurement			Application scope			Modeling / Control approach
		Soil	Plant	Atm	Field	Zone	Plant	
Barker et al.	2018			x		x	x	VRI with remote sensing-based water balance model
Bhatti et al.	2019			x	x			Satellite and airbone imagery-based VRI
Dominguez-Nino et al.	2020	x		x		x		Model predictive control (IRRIX software)
Farooque et al.	2021			x				Deep learning model-based ET prediction
Fourati et al.	2014	x		x	x	x		FAO56 ET model-based on/off control
Gobbo et al.	2019	x		x		x		VRI with dynamic zone delineation
Gordin et al.	2019	x		x	x	x		Hargreaves-Samani ET model-based on/off control
Incrocci et al.	2014	x		x		x	x	Soil moisture-based vs ET-based automated drip irrigation
Linker et al.	2018			x	x			MPC with real-time multi-objective optimization
Lorite et al.	2015			x	x			Weather forecast-derived ET-based deficit irrigation
Lozoya et al.	2016	x		x	x	x		Model predictive control with soil moisture measurement
Ma et al.	2017	x		x	x			Weather forecast-derived ET-based deficit irrigation
Pelosi et al.	2019		x	x	x			Calibrated Hargreaves-Samani for ET modeling
Robinson	2017			x	x	x		Plant species-specific Penman-Monteith model-based control
Roy	2014	x		x	x	x		MPC with stochastic receding horizon
Sidhu et al.	2020			x	x			Regression-based on/off scheduling
Tsakmakis et al.	2016	x		x	x	x		Interoperable model coupling for irrigation scheduling (IMCIS)

Plant-based approaches

To alleviate the gaps inherent in soil-based and atmospheric-based precision control approaches, plant-based precision irrigation control has been widely seen as the best approach in accurately determining and meeting plant water requirements [Jon04].

The timing and quantity of irrigation is based on the plant physiological response to lack of water, which results in changes in leaf surface temperature, water potential, or turgor [AP07]. Other emerging methods of assessing plant water status that could provide useful feedback for precision irrigation control include measurement of leaf thickness [SSL11], trunk diameter [CMO+11, MDC+17], leaf reflectance [KEF+16] and various applications of image analysis [HM09,COLM18,MAGMRC+19,XQH+20].

A summary of emerging approaches in plant-based precision irrigation control is presented in Table 4.4.

While plant-based approaches provide the closest match to plant water requirements, there still exist open questions regarding the determination of appropriate irrigation quantity, the distinguishing of physiological responses to water stress from other stresses, and the dynamic adaptation of irrigation control to account for physiological coping mechanisms employed by plants in response to water stress.

4.3 Precision deficit irrigation-based control and optimization of maize growth

The incorporation of spatial variability in the management of irrigation is a key concept in distinguishing between traditional irrigation and precision irrigation [SESC05,SB09]. In Smith et al. [SBM+10], a distinction is made between traditional definitions of precision irrigation, which focus on maximizing efficiency through precise determination of volume, location and timing of irrigation, with uniform application over the entire system, and an updated definition that incorporates spatial and temporal variation in irrigation treatment. The focus is shifted from field level to management zones within the field [Fer17,GDGZTF14], or to individual plant level [KKMD+18, KHH+18]. Camp et al. describe precision irrigation as "site-specific water management, specifically the application of water to a given site in a volume and at a time needed for optimum crop production, profitability, or other management objectives at that specific site" [CSE06]. In this section, the supporting technologies are considered with regard to their flexibility in allowing variable precision irrigation of individual plants or zones, rather than achieving efficiency through generation of uniform irrigation schedules.

Traditional definitions of precision irrigation consider the "precise amount" of water to be applied to be the full amount of water required to meet the plant demand,

Table 4.4: Summary of plant-based precision irrigation control approaches

Author	Year	Sensing/Measurement			Application scope			Modeling / Control approach
		Soil	Plant	Atm	Field	Zone	Plant	
Acevedo-Opazo et al.	2010		x	x			x	Stem water potential-based regulated deficit irrigation
Andrade et al.	2018	x	x	x		x		ANN-based model predictive control
Bellvert et al.	2015		x			x		Regulated deficit irrigation with dynamic management zones
Blanco-Cipollone et al.	2017		x	x			x	Deficit irrigation with on/off control and static thresholds
Gonzalez-Dugo et al.	2013		x		x	x	x	Canopy air temperature differential-based CWSI thresholding
Gutierrez et al.	2018		x	x	x			Reduced error pruning tree-based VRI
Kizer et al.	2018		x	x	x			CWSI- and stem water potential-based VRI
Livellara et al.	2011		x	x			x	Variable rate drip irrigation
Martinez et al.	2016		x	x	x		x	IR image-based deficit irigation
Matese et al.	2018	x	x		x			Stem water potential-based on/off control
Meron et al.	2010	x	x			x		Inverse distance-weighted interpolation of CWSI data
Miras-Avalos et al.	2016	x	x	x	x			Stem water potential-based regulated deficit irrigation
O'Shaughnessy et al.	2016	x	x		x	x		CWSI and time threshold-based on/off control
Osroosh et al.	2015	x	x	x	x	x	x	Adaptive on/off control with dynamic threshold
Pocas et al.	2020		x		x			Bayesian and tree-based regression algorithms
Rojo et al.	2016	x	x			x		Unsupervised fuzzy classification-based VRI
Ruiz-Sanchez et al.	2018	x	x			x	x	Takagi-Sugeno-Kang fuzzy inference system
Tung et al.	2018		x			x	x	Modified partial least squares regression-based LWP modeling

which has commonly been determined based on the relationship between crop evapotranspiration and environmental factors [MMC+15, LMA+16]. Current irrigation practices that explore the cultivation of irrigated crops under regulated water deficit provide a new frontier for precision irrigation, where the required amount to be delivered is determined with a goal of avoiding irreversible water stress damage, without necessarily fully matching evapotranspiration-based plant demands. This provides further avenues for improvement of water use efficiency. Deficit irrigation-based applications of precision irrigation approaches have been employed in control of both pre- and post-harvest yield quality [LMPSR+19, PPRSM+07, VMP+21].

Maize growth model description

The growth rate of maize plants during the vegetative phase has been found to have a correlation with the quantity of soil available water as reported by [Çak04] with respect to reductions in plant height and leaf area development in plants subjected to short term water stress. Irrecoverable damage is however observed when the duration and severity of water stress is prolonged, as reported in [SJH19]. When appropriate deficit irrigation scheduling is applied, the growth rate and subsequent yield of plants subjected to mild water stress during the vegetative phase are observed to match fully irrigated maize plants, with the additional benefit of buffering the plant against yield losses due to water stress in the flowering and maturation stages as reported in [CTD+19].

This work is based on an initial state-machine model of maize growth described in [SKO19]. Three primary stress levels are defined:

i) Plants whose water content is maintained above the upper stress level boundary (mild stress boundary) by daily replenishment to the maximum holding capacity of the growth substrate are described as experiencing no stress. This watering scheme is also referred to in this work as full irrigation.

ii) Plants whose water content is maintained between the upper and lower level boundaries, and whose stress duration does not exceed the chronological damage boundary are described as experiencing mild stress

iii) Plants whose water content falls below the lower level boundary, or which remain between the upper and lower level boundary for a time exceeding the chronological damage boundary are described as experiencing high stress.

The stress level at step n (SL_n) can thus be represented using the level boundaries based on gravimetric water content (in this work, though the boundaries could also be experimentally obtained for volumetric water content), LB_{MS} representing the transition point from an unstressed condition to mild stress, observable as a

reversible reduction in growth rate, and LB_{HS} representing the transition point from mild stress to high stresss, observable as a irreversible reduction in growth rate, also defined as damage. The additional temporal boundary CB_{HS} represents the maximum duration a plant can be subjected to water content levels characterised as mild stress without showing irreversible growth retardation.

Hence

$$SL_n = \begin{cases} 0, & \text{if } WC > LB_{MS} \\ 1, & \text{if } LB_{MS} \geq WC > LB_{HS} \& \ CB_{HS} = 0 \\ 2, & \text{otherwise.} \end{cases} \tag{4.6}$$

It has been shown in previous research that plants subjected to abiotic stresses retain a memory of the stress event for a certain duration, resulting in a catch-up phenomenon when the stress is withdrawn [LB17, KS20]. Withdrawal of the stress for an extended duration results in loss of memory. A chronological flag, CB_{Mem} is used to represent the memory retention period, becoming activated when the plant experiences stress, and deactivated when the duration of recovery after experiencing stress crosses the experimentally determined memory retention threshold. The memory of the plant can thus be represented as a binary state, with

$$M_n = \begin{cases} 1, & \text{if } (WC \leq LB_{MS} \| M_{n-1} = 1) \& \ CB_{Mem} = 1, \\ 0, & \text{otherwise.} \end{cases} \tag{4.7}$$

When a plant is exposed to high stress, it experiences damage, which is observed as an irreversible retardation of growth rate even when the stress is later relieved by reirrigating the plant. The damage level can thus also be expressed as a binary state with

$$D_n = \begin{cases} 1, & \text{if } WC \leq LB_{HS} \| \ D_{n-1} = 1 \| \ CB_{HS} = 1, \\ 0, & \text{otherwise.} \end{cases} \tag{4.8}$$

The concept of deficit irrigation-based growth control involves maintaining the test plants within the two states where presence of memory and absence of damage intersect, cycling the plants between periods of mild stress and subsequent recovery through reirrigation. Reducing the complexity of the initial model, in this work a truncated growth model is presented as illustrated in Figure 4.9, where dashed arrows represent no stress and continuous arrows represent mild stress. The transitions are described using a three-bit code, with the initial bit representing the presence of memory M_n, the second bit representing the current stress level SL_n (with 0 as no stress and 1 as mild stress) and the third bit representing the next state SL_{n+1}.

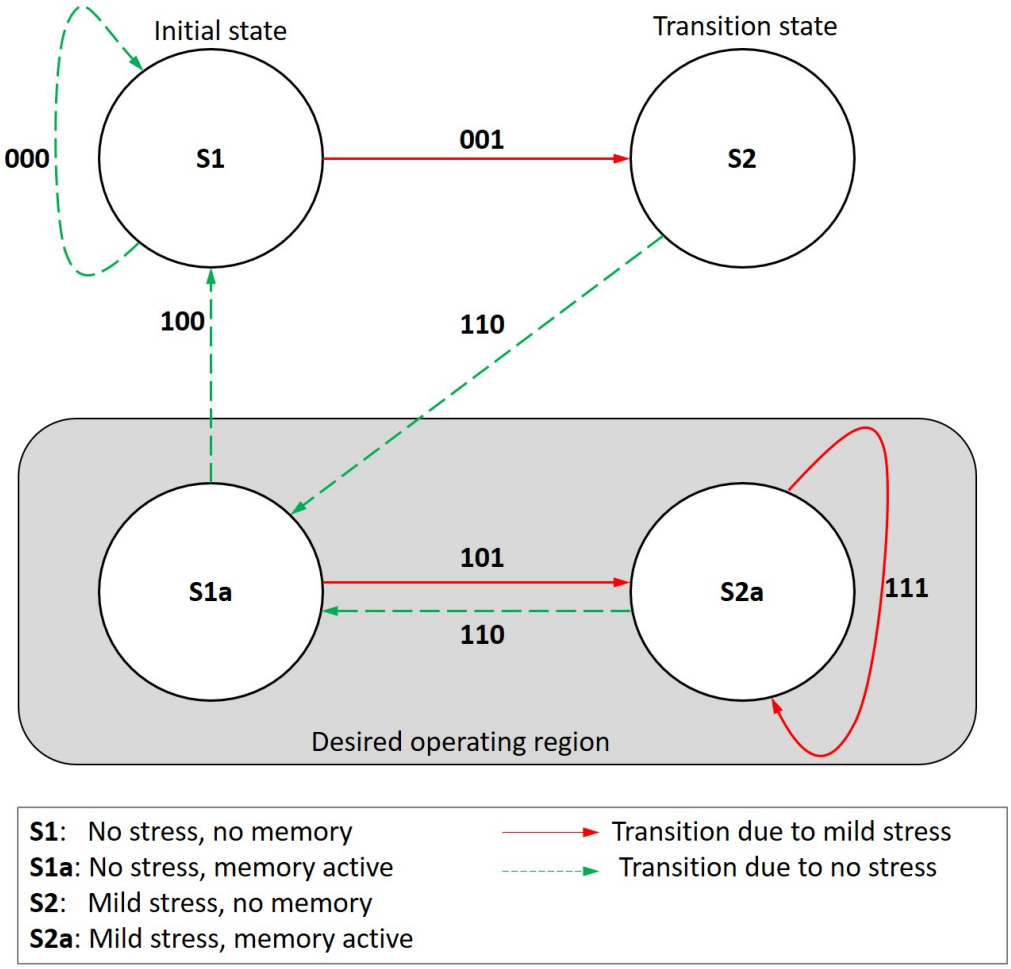

Figure 4.9: Modified state machine model of maize growth with S_i denoting states of the model and arrows representing transitions [OS22c]

Optimization of state level thresholds

A description of the NSGA-II optimization algorithm has been presented in subsection 3.1. In previous work [Kög19,JKS19], the optimization algorithm was applied to experimental data with a fixed number of iterations, which is a function of the population size and maximum number of generations. In this case the default values were set to 50 and 200 respectively, resulting in an optimization cycle encompassing 1000 iterations.

A key observation made using the fixed number of iterations was that the threshold values obtained were non-reproducible, resulting in overlaps between both level and chronological thresholds. A statistical analysis of 10 consecutive runs yielded the values presented in Table 4.5.

Table 4.5: Analysis of state thresholds obtained from NSGA-II optimization algorithm with default number of iterations (all values represent water content in g)

	FI Threshold	**MS Threshold**	**HS Threshold**
Minimum	53.6323	12.5725	10.2949
Maximum	149.2605	87.8742	78.9513
Median	107.8239	66.6766	46.4354
Std. Deviation	29.5333	19.5941	22.7483

An algorithm was created to examine alternative population sizes and maximum generations to identify if convergence was achievable in the optimization process. With the population size fixed at 50, the maximum number of generations was varied between 20 and 10,000 in increments of 20 steps. The absolute error and RMSE values were found to converge within the first 500 generations. The process was repeated with the maximum generations varied from 100 to 500 in increments of 2. Convergence was found to occur at 200 generations. An evaluation of the threshold values produced however, showed significant variations and overlaps between all three stress levels. This is observable in Figure 4.10.

A further examination of the performance of the optimization algorithm with varying population sizes was carried out, with the maximum number of generations set at 500. The population size was varied from 12 to 50. It was observed that population sizes up to 30 produced similar, low RMSE values, with erratic behavior at higher values.

An investigation varying population size between 2 and 38 in increments of 2, and varying maximum number of generations between 200 and 5000 in intervals of 50 was carried out. A 3D plot representing the convergence behavior is presented in Figure 4.11.

Rotation of the 3D plot suggested a minimum RMSE value which repeatedly occured at different combinations of population size and maximum number of genera-tions. Multiple iterations produced similar results, with the modal value of RMSE appearing as either the best performance, or having a negligible difference from the best performing error value (in the order of 1×10^{-5}). The algorithm was modified to identify and count the instances of each unique RMSE value, with the process terminating as soon as any error value had been repeated 50 times.

A comparison of the stress thresholds produced using the parameters at convergence however indicated great variations, therefore thresholds based on NSGA-II optimization were not applied in any further experiments, and stress boundaries were set based on expert knowledge obtained by observing variations in leaf elongation rate in comparison with a fully irrigated control group.

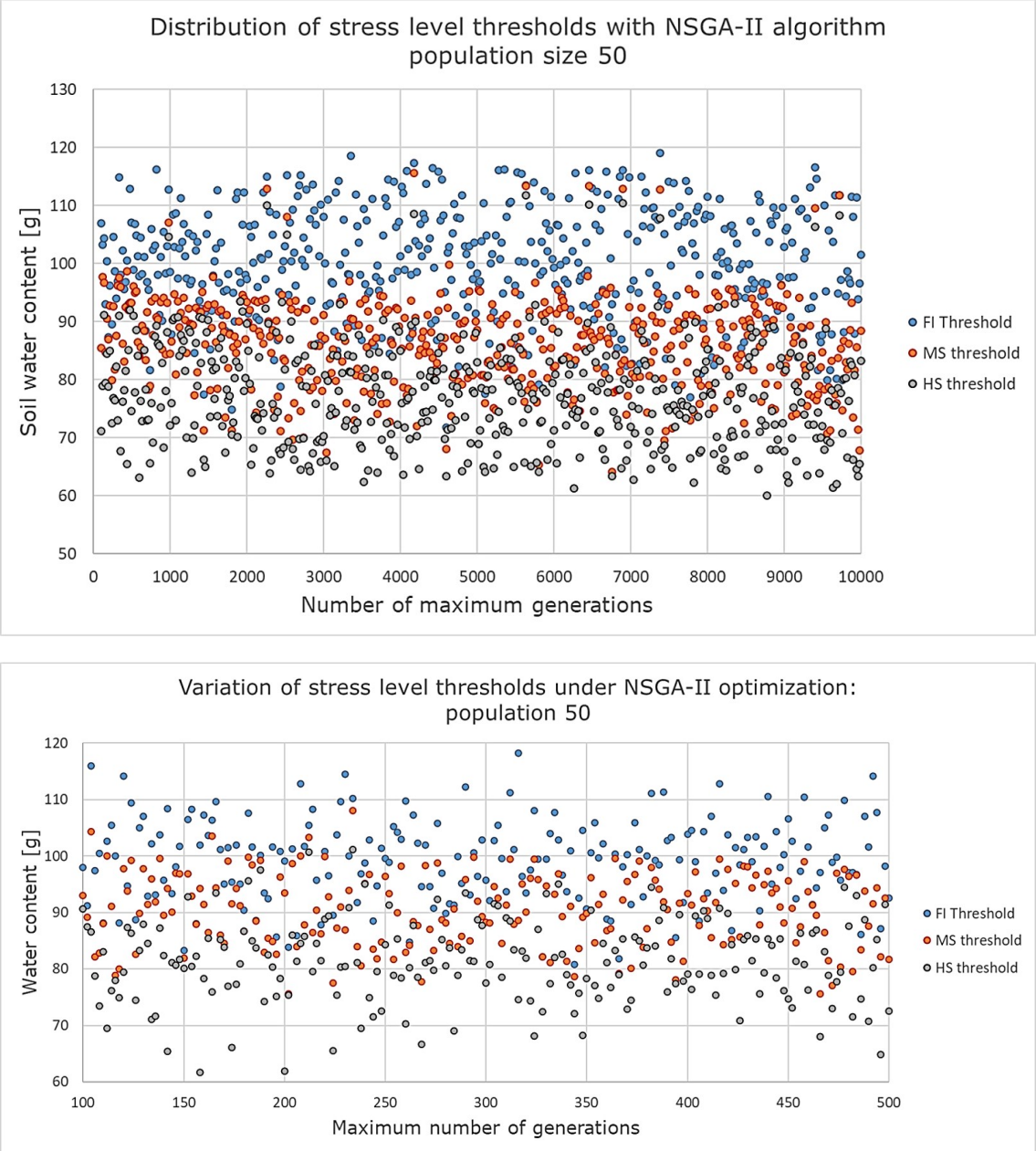

Figure 4.10: Variation of stress level thresholds with different settings of maximum number of generations. Population size in this case remains constant at 50.

A machine learning-based approach involving clustering of leaf elongation rates for determination of stress level boundaries was examined. Selected experimental growth data was segmented according to the total number of visibly appeared leaves, and clustering performed on the dataset, with the number of required groupings set

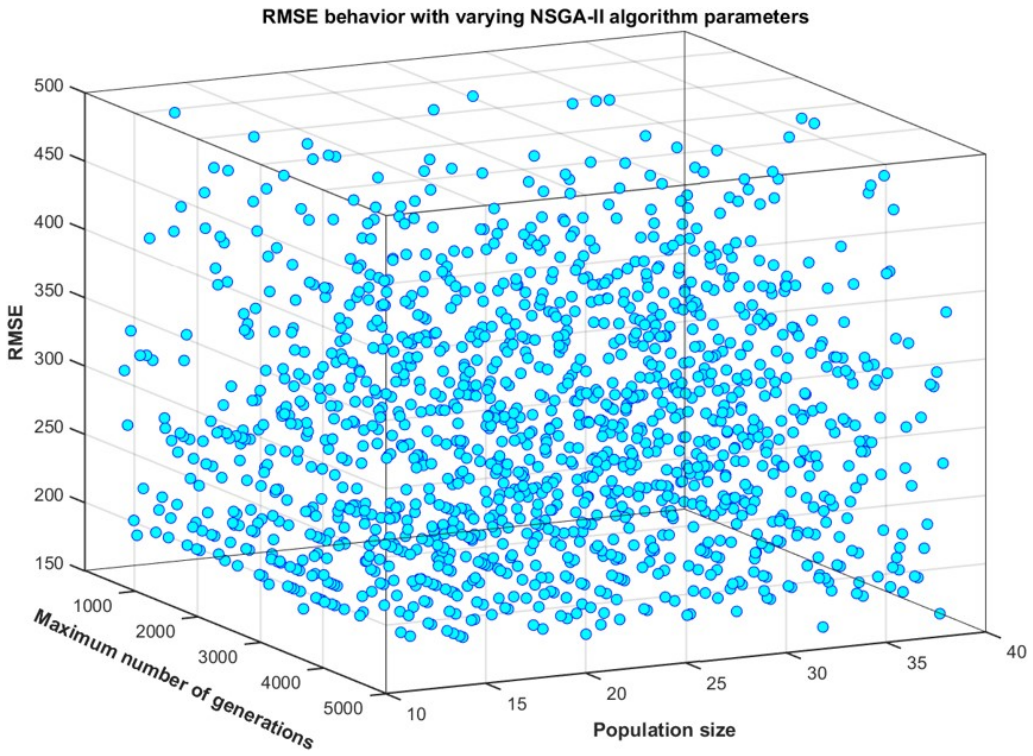

Figure 4.11: Variation of prediction accuracy under varying NSGA-II parameter settings

to two for data corresponding to plants with three leaves, and three clusters for plants with four and five leaves. Results are presented in Figure 4.12.

From the obtained clusters, a clear downwards trend in the stress level boundaries with time is observed, suggesting a need for dynamic stress level boundaries rather than static water content values. It is hypothesized that the contribution of root expansion to extending the range of available water within the growing pot is responsible for the changes in stress boundaries, suggesting a need to decouple the definition of plant water stress status from irrigation deficit levels, which are generally expressed in relation to total soil water holding capacity rather than plant physiological response.

Evaluation of clustering performance was done by classification of test data based on the selected clusters. The achieved prediction accuracy is presented in Table 4.6.

Available experimental data shows relatively crisp boundaries between no stress and high stress data, with fuzzier boundaries for the mild stress region, indicating a need for improved approaches for identifying plants exhibiting mild stress responses.

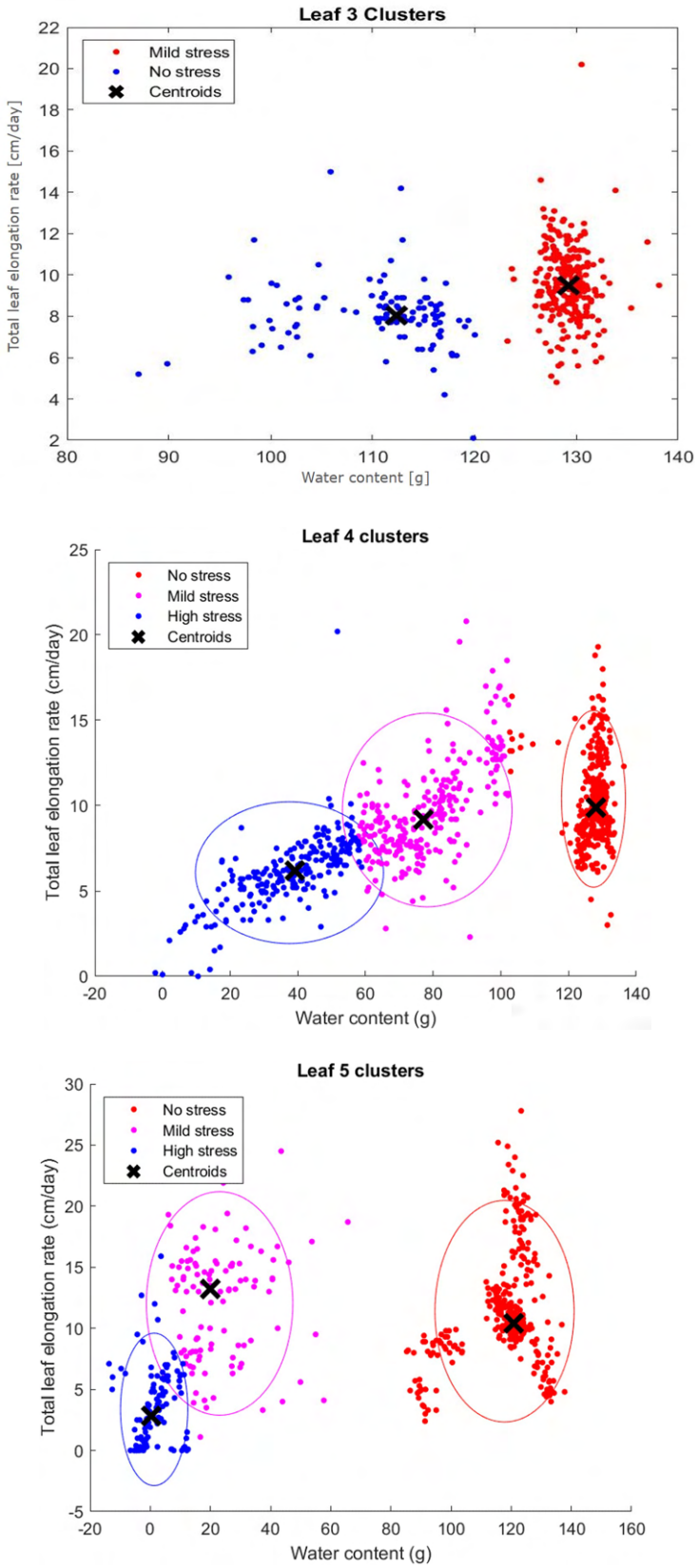

Figure 4.12: Evaluation of stress level thresholds using clustering approach

Table 4.6: Classification accuracy for stress level threshold determination approaches

Prediction accuracy [%]	No stress		Mild stress		High Stress	
	NSGA-II	Clustered	NSGA-II	Clustered	NSGA-II	Clustered
Three leaves	57.6	85.1	37.2	44.8	–	–
Four leaves	81.4	83.2	25.2	53.2	82.6	79.6
Five leaves	74.7	89.9	33.3	20	75.7	60

Trellis diagram approach

Trellis diagrams are used in telecommunications to represent coded sequences of bits that are encoded stepwise, with transitions between different states recorded in memory, and the output as a function of the current state and the input. Decoding of trellis code involves identification of the intermediate states taken to arrive at a given final output, given the initial conditions. Common decoding approaches include the Viterbi algorithm, a maximum likelihood approach described in [Vit67], which produces the shortest path through a trellis diagram by examining all possible paths, and the sequential decoding algorithms, which use a sequential search for the shortest path through a trellis, with new paths only being computed as extensions of previously selected paths, and all other possible sequences systematically discarded along the way, as described by [For74].

The initial progression of plant growth through the states is clearly represented in the trellis diagram shown in Figure 4.13. The initial state of the plants involves no stress and no memory, represented as S1. Subsequent transitions eventually evolve into a repetitive cycle, represented by the section after step k3. Linear

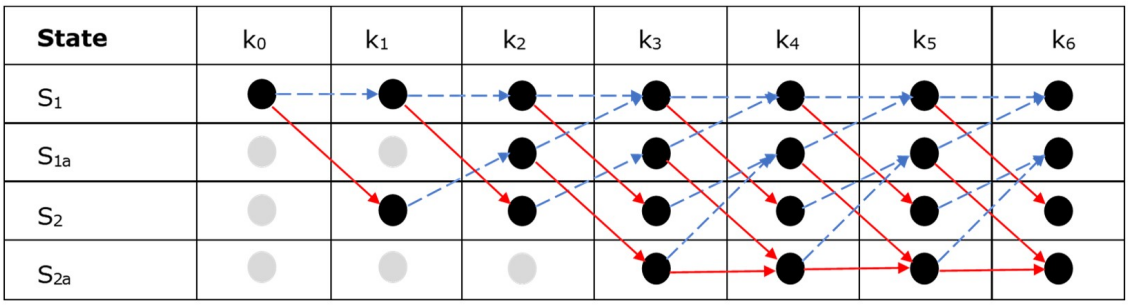

Figure 4.13: Trellis diagram representation of state transitions

regression is applied on historical experimental data representing each state to obtain distinct state equations to characterize the daily growth rate, expressed as total leaf elongation rate, and the evapotranspiration rate, which is represented by a function of minimum and maximum daily temperatures, minimum and maximum

daily relative humidity, current total leaf length and stress state. A model predictive controller, described in the next section, is developed to achieve closed loop growth control.

Model-based predictive control

Model predictive control, as described by [CST61], utilizes a model of the controlled system to generate a control variable based on predicted future error. A set of predictions is made over a specified number of time steps, known as the prediction horizon. A set of control variables is calculated based on the predicted error over a specified number of steps, known as the control horizon. The controller applies the calculated control variable for the next time step, after which system measurements are used to update the error value. A new set of predictions and control variables, and a possibly updated system model are then generated using the updated error, a concept referred to as moving horizon. The basic procedure followed during model predictive control is summarized in Figure 4.14.

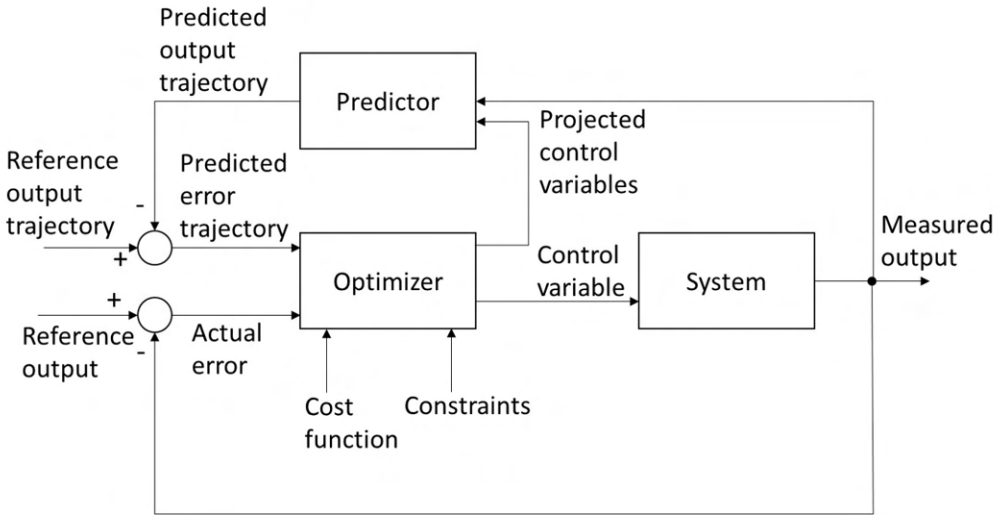

Figure 4.14: Block diagram representing model predictive control

Control algorithm design

The control goal in this work is to achieve specific total leaf length within a fixed time period, with a secondary goal of minimizing water consumption. The state-specific elongation rate and evapotranspiration equations allow prediction of growth and water consumption given a specific watering sequence and the representative water

content for fully irrigated and mild stress conditions. To achieve growth control, it is necessary to generate the closest matching irrigation sequence that would produce the required growth within the specified time. For this purpose, a hybrid algorithm combining elements of model predictive control and trellis diagram decoding was developed. A block diagram representing the steps followed in designing the controller algorithm is shown in figure 4.15. In the development of a plant growth controller,

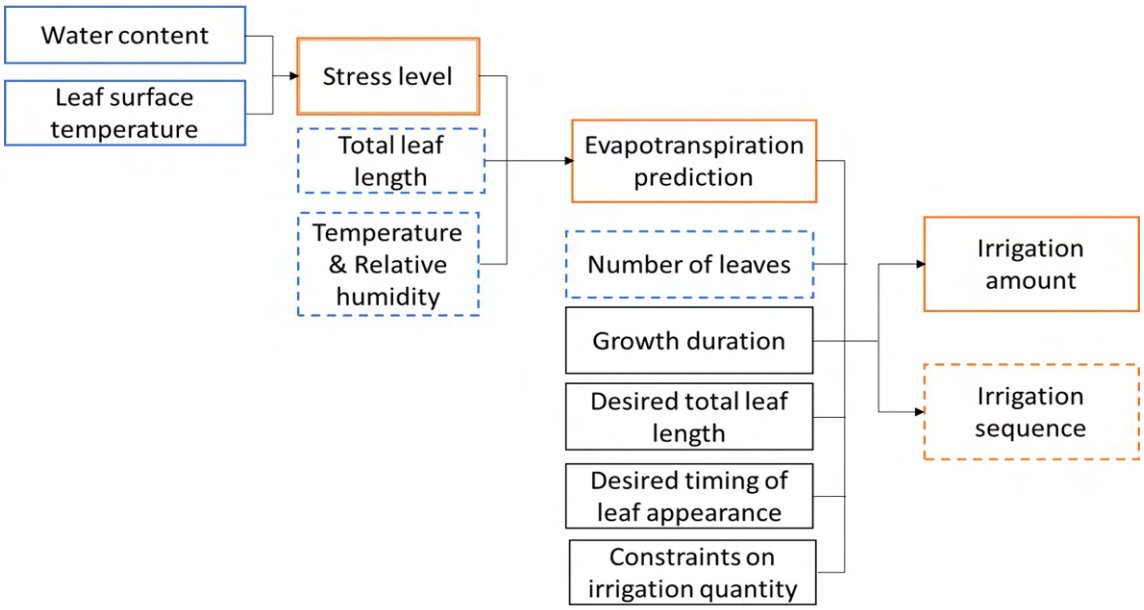

Figure 4.15: Overview of plant growth control strategy based on precision deficit irrigation

the system outputs are a sum of intermediate outputs generated from related growth and evapotranspiration equations associated with each successive state the individual goes through. Additionally, the goal of common decoding algorithms is to find the fastest path out of the trellis code, whereas the goal in this work is to find the closest matching result within a fixed duration. As a result, traditional maximum likelihood or sequential decoding approaches cannot be directly applied.

The main characteristics of each approach were considered in creating a decoding algorithm for determining the optimal path through the trellis for achieving targeted plant growth. A maximum likelihood approach provides the advantage of greater achievable accuracy, since all possible outcomes are generated before a path is selected. Multiple optimization goals can be integrated in the control decision-making, making it a more flexible approach. A sequential approach has the advantage of lower memory and processing requirements because unpursued paths are discarded at each step, allowing for longer possible prediction and control horizons.

A simplified search algorithm following the maximum likelihood approach was developed for generation of optimal irrigation sequences for achievement of the desired total leaf length. The choice was based on the relatively slow dynamics of maize growth during the vegetative stage, and constraints on the optimal length of the prediction horizon, brought about by the need to adjust the growth and evapotranspiration equations upon the appearance of new leaves. For these reasons, the advantages offered by a sequential approach are irrelevant to the application.

A description of the resultant model predictive algorithm integrating decoding of the generated trellis diagram follows. The process is visually summarized in Figure 4.16.

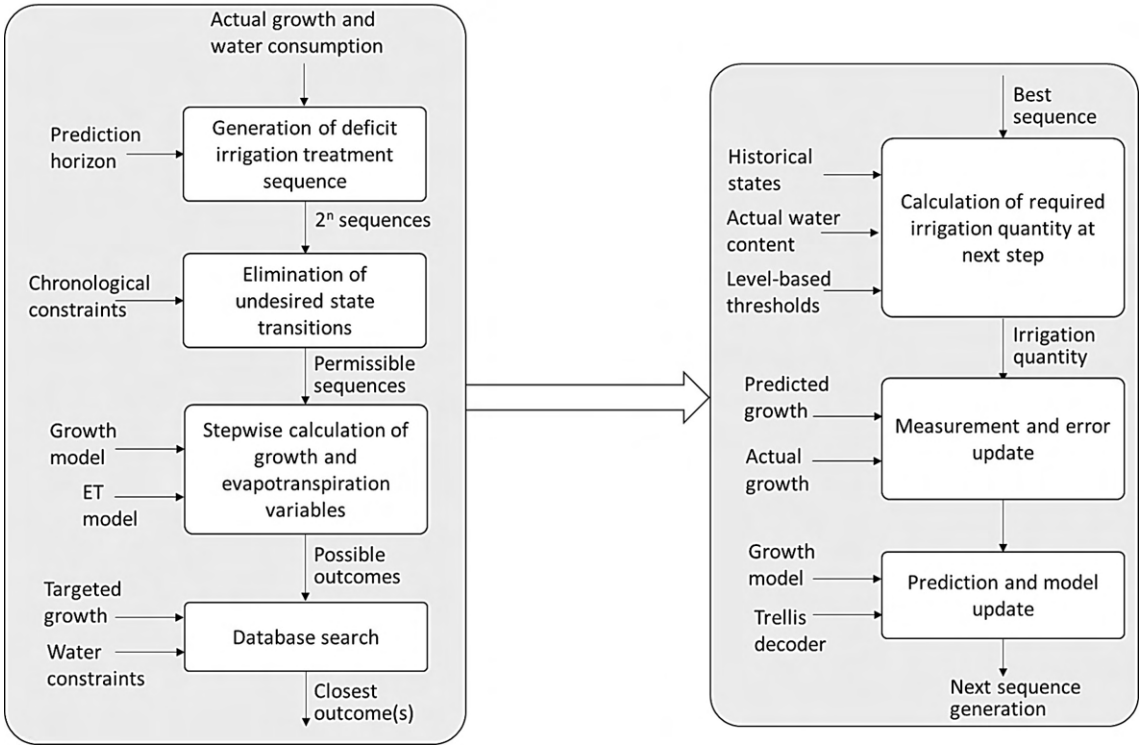

Figure 4.16: Overview of plant growth control algorithm

(1) All possible irrigation sequences over a prediction horizon of duration n are generated as binary codes, with 0 representing no stress and 1 representing mild stress. The output of this step is 2^n possible combinations.

(2) Chronological constraints related to damage under prolonged mild stress and loss of memory due to an extended recovery period are applied to the search space to eliminate undesired transitions. In this work, both parameters have

been set to three days based on past experimental data. The elimination process is achieved by searching the binary codes generated in the first step for consecutively occurring 0s (representing loss of memory) and consecutively occurring 1s (representing transition to damaged state).

(3) The total leaf length and cumulative water consumption for all acceptable irrigation sequences is calculated based on the state-specific leaf elongation rate and evapotranspiration equations. The calculation must be done in a stepwise manner because the functions describing elongation rate and evapotranspiration are both dependent on current total leaf length.

(4) The database is searched for the value closest to the desired total leaf length at the end of the specified time period, and the corresponding sequence selected as the output.

(5) The first bit of the generated sequence is used to calculate the required amount of irrigation to achieve the prescribed state.

(6) The next set of measurements is taken.

(7) Step (1) to (5) are repeated using the new measurements to generate a new set of predictions and control output.

(8) From the third iteration, the sum of the three most recently generated control output bits is restricted to values of 1 or 2 (to prevent loss of memory or damage due to prolonged mild stress).

An advantage of generating all possible output values is the possibility of determining the acceptable range for growth targets, with the user prompted to enter a growth target between a pre-calculated minimum and maximum. In addition, the algorithm can readily be expanded to include optimization of water consumption by comparing a specified range of closest results, and selecting based on minimum water consumption. Conversely, a search can be made with minimization of water consumption as the main goal, and the maximum achievable growth used as a secondary goal to search the resultant subset of closest matches.

Experimental setup

Experimental work was carried out in an indoor greenhouse housed in the Chair of Dynamics and Control at the University of Duisburg-Essen, Germany. Maize plants (*Zea mays*, KWS Ronaldinio variety) were grown in 500 ml capacity PET tumblers filled with Seramis^{TM} clay granulate and positioned under artificial grow lamps which were automatically switched on and off to maintain a day length of 14 hours. Irrigation was applied once daily to levels determined by the required irrigation

sequence. Fertigation was supplied using Seramis Vitalnährung für Grünpflanzen^{TM}, which provided adequate nutrition for the vegetative phase.

Four sets of five plants each were positioned in a square configuration with an infrared camera at the center. A single maize seed was sown in each pot, and the plants were maintained under full irrigation until the third leaf tip was visible on all plants, which occured eleven days after planting. One set was designated as the control group, and received full irrigation for the entire duration of the experiment. A second group was used for validation of the stress boundaries, with the plants cycled through no stress, mild stress and high stress before being reirrigated. The remaining two groups were irrigated based on sequences generated by the developed control algorithm. The water content of the plants was monitored continously through a load cell-based measurement system on which each plant was mounted. Additional measurements taken included daily maximum and minimum temperature and relative humidity values, total leaf length and number of appeared leaves.

The stress boundaries were initially set based on expert knowledge, with plants in mild stress maintained at a water content approximately between 40 % and 70% of the holding capacity of the growth substrate. The upper stress boundary was confirmed during the course of the experiment by infrared imagery of leaf surface temperatures, which confirmed an observable deviation between the control group and the designated stress boundary validation group when the average water content in the stressed group reached a value approximately 55 % of the average water content in the control group.

Three sets of experiments were carried out as described:

Experiment 1: 60 plants were planted in the indoor greenhouse, with 20 individuals selected as test subjects for growth control. The control goal was achievement of a specified final total leaf length after the specified period, without optimization of either plant growth or water consumption. Implementation of the irrigation schedule commenced when all plants had at least three visibly appeared leaves. An initial common goal of 95 cm total leaf length after 5 days was set, with each plant receiving an individualized irrigation prescription to best match the target. Due to appearance of the fourth leaf on the second day of treatment with the associated rapid increase in total leaf length at the beginning of the active elongation phase, a section of test plants were determined to have attained levels of growth that would place their lowest possible growth target above the preset target. Based on the obtained measurements, a revision of growth targets was made, with ten plants receiving a new growth target of 105 cm, and ten plants retaining the original growth target of 95 cm. The irrigation schedules for the evaluated plants are shown in Figure 4.17. Full irrigation was performed by increasing the water content to total holding capacity of the substrate, with the exception of days when the next step involved mild stress. Irrigation was then applied to a level based on the projected evapotranspiration, with an aim of just crossing the boundary from

no stress into mild stress. On days requiring mild stress irrigation amount was dependent on projected evapotranspiration based on achieved total leaf length with a lower boundary set to prevent transition into high stress. Upon the appearance of

Group B watering schedule													
		Initial TLL		Target	Duration		D1	D2	D3	D4	D5	D6	Projected
ALPHA	9	29,5		95	6		0	1	1	0	0	0	94,723
ALPHA	10	35,2		95	6		0	0	0	1	0	1	95,383
ALPHA	11	39,7		105	6		1	1	1	0	0	0	104,854
ALPHA	13	29,9		95	6		0	1	0	0	1	0	95,032
ALPHA	15	34,1		95	6		0	1	1	1	0	0	94,997
BETA	1	44,7		105	6		1	0	1	1	0	1	105,023
BETA	3	38,2		105	6		0	1	0	0	0	1	105,271
BETA	5	27,2		95	6		1	1	0	0	0	0	94,431
BETA	6	30,3		95	6		0	0	0	1	0	0	95,139
BETA	7	43,3		105	6		0	0	0	1	0	1	104,875
GAMMA	9	40,9		105	6		0	0	1	0	0	1	105,439
GAMMA	10	33,1		95	6		0	0	0	0	1	0	95,147
GAMMA	11	35,1		105	6		1	1	0	0	0	0	104,558
GAMMA	13	40,9		105	6		0	0	1	0	0	1	105,439
GAMMA	15	38,1		105	6		0	1	0	0	0	1	105,147
DELTA	1	28,3		95	6		1	0	0	0	0	1	95,464
DELTA	3	42,8		105	6		0	1	0	0	1	1	105,190
DELTA	5	24,4		95	6		1	0	0	0	0	0	95,982
DELTA	6	24,4		95	6		1	0	0	0	0	0	95,982
DELTA	7	37,5		105	6		0	1	1	0	0	0	104,676

Figure 4.17: Irrigation schedule for uniform final total leaf length, with 0 representing no stress/full irrigation, and 1 representing mild stress.

leaf 5 on the sixth day of the irrigation sequence, the results were evaluated using the expected attained growth for the individual plants by day 6, rather than the day 7 targets.

Experiment 2: The set target for control was achievement of uniform cumulative water consumption, with a target set to 350 ml over a period of seven days. Individual plants with different total leaf lengths and initial values of cumulative water consumption were subjected to irrigation sequences targeted at meeting the target within the specified time. A total of 20 plants were involved in the experiment. Water content levels for the different stress states were influenced both by the required stress state for a specific day, and the next expected stress state based on the generated sequence. This required continous prediction of evapotranspiration levels at each step, with irrigation quantity set to prevent transition into an undesired stress state. A plant expected to remain in a state of no stress for two consecutive days thus received more water than one required to transition into mild stress the next day, with the latter receiving just enough water to cross the mild stress threshold based on daily evaporation rates.

Experiment 3: Optimal values of plant growth and water consumption were selected based on two different weighting ratios, with constraints obtained from the database of prediction values generated by the controller algorithm. Ranking of growth and water consumption values as ratios of the best case results (highest growth or lowest water consumption) was performed, and weighting was allocated with two separate optimization scenarios.

In the examined optimization scenario, equal weighting was attached to maximizing growth and minimizing water consumption, thus the final ranking of irrigation schedules was obtained by addition of the individual ranking obtained for each of the two variables to be optimized. The irrigation sequences corresponding to the highest ranked performance were then selected for implementation. Due to different initial measurements and different final targets for each individual, irrigation sequences were unique and could be considered to be random.

Results and Discussion

Results obtained relating to the control goal of attaining identical total leaf length at the end of the selected growth period from plants with varying initial measurement through imposition of appropriate irrigation sequences are presented in figure 4.18. Total leaf length without addition of leaf 5 is also presented for comparison. The

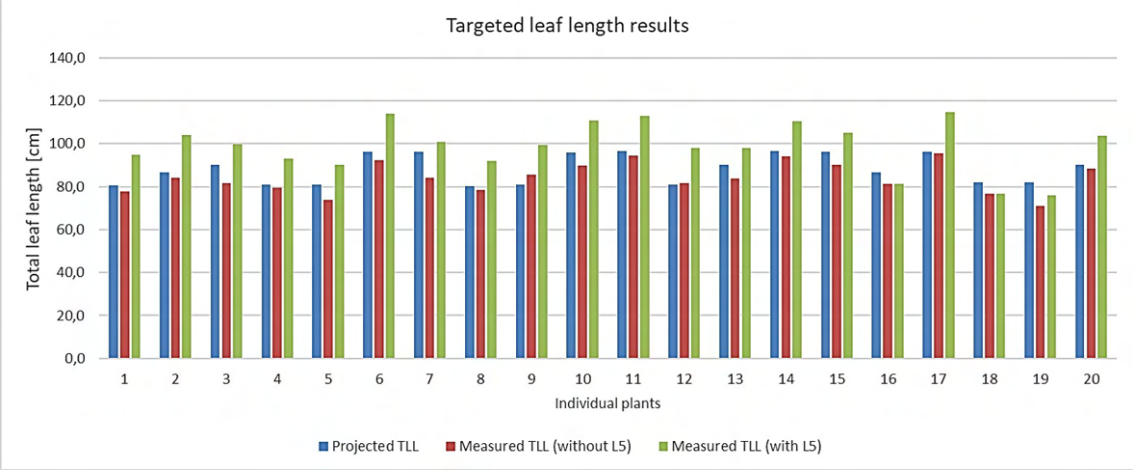

Figure 4.18: Targeted growth control results

measured total leaf length at the end of the growth period closely matched the projected total leaf length predicted for day 6 under the irrigation sequences applied to the individual plants. The mean percentage error was obtained as -4.6 % of total leaf length, with a standard deviation of 4.394 cm.

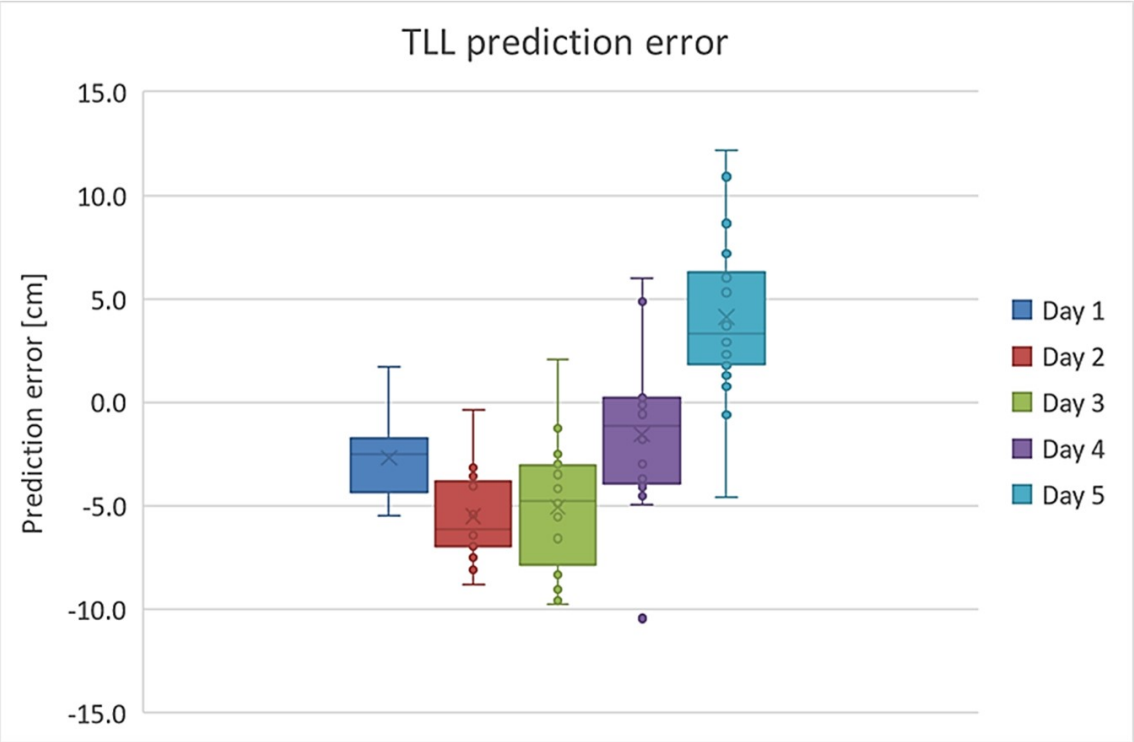

Figure 4.19: Trajectory of control error over time for uniform final total leaf length

An overview of the behavior of the error value over the duration of the experiment is captured in Figure 4.19. It can be observed that the range of error values increased over time, with a tendency to overestimation of total leaf length with time. The overall control error remained within 10 % of the total leaf length for all individuals throughout the experiment, with the exception of two outliers.

Achievement of a fixed target with regards to water consumption was also achieved for the test groups in Experiment 2. The results are presented in Figure 4.20. In this experiment, the results tracked closely the targeted cumulative water consumption, with error values within ±10 % for all individuals in the test group, with the exception of one outlier. Deviations in water consumption tended in the negative, that is, most of the observations were slightly lower than predicted cumulative water consumption, which is preferable in an implementation scenario where water availability is a major constraint, and the cost of overwatering is greater than the associated penalty for underwatering.

A control goal attaching equal weights to the dual goals of minimizing total water consumption and maximizing total leaf length was set for the test groups. The projected total leaf lengths were calculated based on the optimal irrigation sequences obtained from the algorithm. Measurements were taken on day 3 and day 7 of

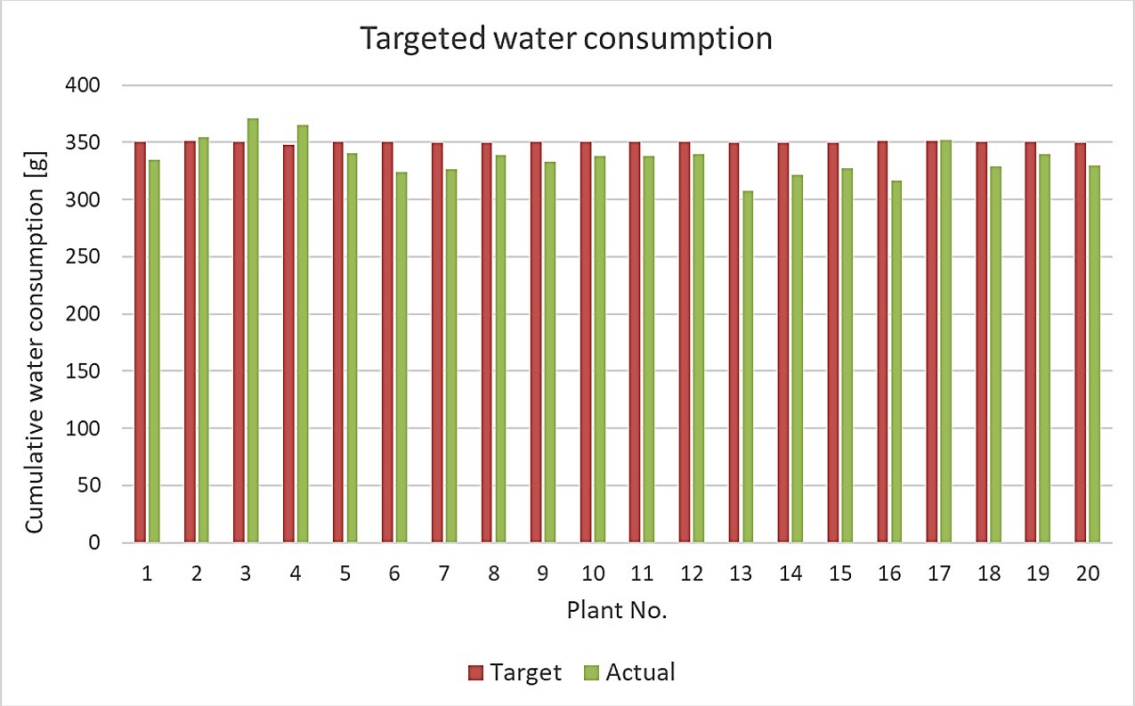

Figure 4.20: Controller performance for targeted cumulative water consumption

the experiments, with the irrigation sequence updated on day 4 based on obtained measurements. In Figure 4.21 resultant total leaf lengths obtained on application of the growth control algorithm after three and seven days of irrigation respectively are shown. The measured total leaf length tracks the projections closely, with a mean absolute percentage error of 4.24 % on day 3, and 8.39 % on day 7. The prediction error distribution (as a percentage of measured total leaf length) is graphically illustrated in Figure 4.22.

The upward drift in error is attributed to the development of the plant, with the fifth leaf making an appearance on day 6 for most of the test group. To avoid distortion of the output by the unaccounted-for new leaf, the length of leaf 5 was not included in the analysis.

During the experiment, a dynamic shift of the level boundaries demarcating the region of mild stress was observed. This is possibly due to the cultivation of the maize plants in pots. As the plants develop, the threshold values for transition into stressed state trends lower, suggesting that the developing root systems of the plants are able to extract moisture from the substrate even at relatively low gravimetric water content levels.

The effect of this shift in the state transition boundaries is not addressed in this work, and will be explored in future, in addition to possible shifting in the chronological

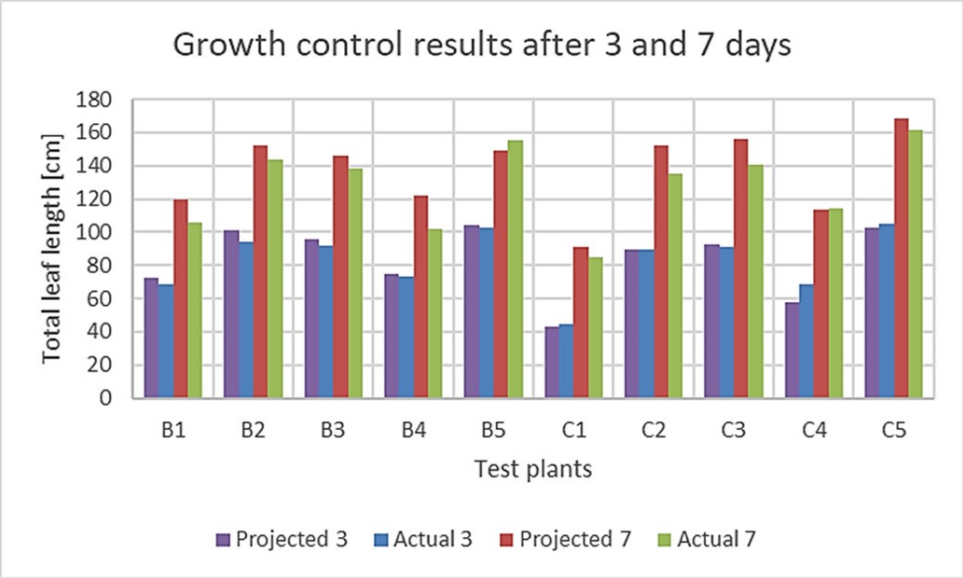

Figure 4.21: Targeted growth control results

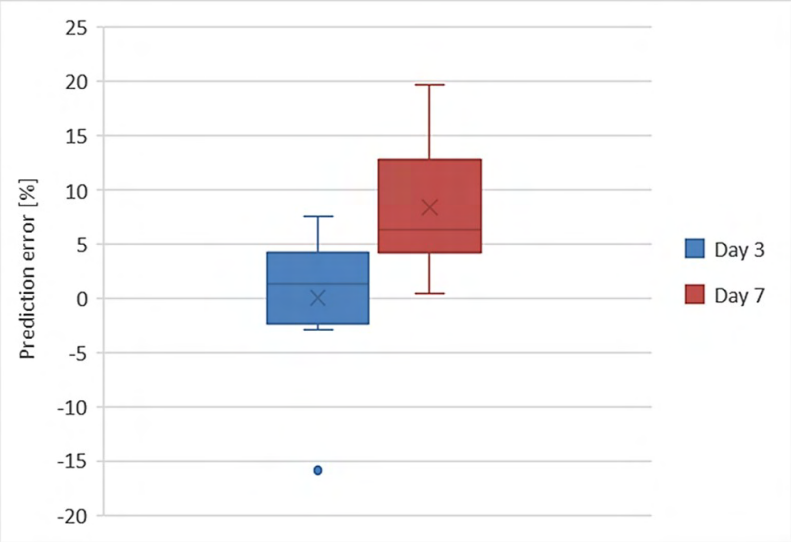

Figure 4.22: Percentage error in total leaf length on days 3 and 7

memory and damage thresholds.

4.4 Summary

Implementation of a state machine model for representation of growth of a maize plant during the vegetative phase has been experimentally validated, with generation of state-specific models of leaf elongation and evapotranspiration, which are then employed in a model predictive control setup to achieve optimal plant growth while minimizing water consumption.

The definition of the necessary thresholds required to describe the state machine model presented has been attempted using an NSGA-II optimization algorithm, with variation of parameters controlling the number of iterations performed. Despite achievement of convergent error metrics for different combinations of population size and maximum number of generations, the specific threshold values required to define state boundaries exhibit large ranges with considerable overlap for all stress levels. An additional challenge faced is non-reproducibility of threshold values, with repeated runs of the optimization process producing vastly different outcomes. As a result, for purposes of developing a control algorithm, both the chronological and level-based stress boundaries have been set based on expert knowledge. For future work, the employment of dynamic stress thresholds over the course of plant growth is recommended, as observation of clustering results indicates that onset and severity of stress varies over the duration of plant growth, probably due to root growth dynamics which were not explored within this work.

Development of the control algorithm employed a hybrid approach combining a decoding procedure intended to select an optimal path through a trellis diagram, combined with a model predictive control algorithm with a variable prediction horizon. Goals related to achieving specific growth and water consumption without optimization, as well as achieving optimal growth and water consumption with equal weighting assigned to the competing targets were experimentally achieved, with control error for all experiments falling within a range of ± 10 % for all values, inclusive of a couple of outliers whose initial measurements resulted in less reliable prediction of expected trajectory.

5 Summary, conclusion, and outlook

This work describes the modeling, control and optimization of maize growth based on precision deficit irrigation. The growth and development of maize plants is modeled using state machine representation, allowing the definition of incremental leaf extension, appearance of new leaves, generation of biomass and daily evapotranspiration depending on identified water stress levels. A model predictive controller is developed capable of achieving specified growth or water consumption within a fixed duration. Optimization is achievable by varying weighting of the two main control variables of interest- the total leaf length and the total water consumption. This enables meeting the twin goals of maximizing plant growth and minimizing total irrigation water consumption.

5.1 Summary and conclusion

In the first part of the thesis (section 2), a detailed analysis of existing literature in the modeling of various aspects related to plant growth and physiology are considered. The focus is on parameters that serve as variables in the control of plant growth based on irrigation. The section considers the applicability of existing approaches to the envisioned test environment, which is an indoor greenhouse, and emphasis is given to literature focusing on growth and development of maize. Key conclusions from this chapter are as follows:

Modeling of plant growth:
Growth of maize during the vegetative phase can be described based on the elongation rate, surface area, and rate of appearance of leaves. Existing literature assumes static thermal functions for maize growth modeling, with exposure to water stress integrated primarily as a factor causing retardation in growth. Studies related to the catch-up effect exhibited by plants in the immediate period of recovery from applied stress and the priming phenomenon that increases resilience to future stress events suggest a need for modeling approaches that encompass variations in growth under water deficit conditions. A modeling approach based on state machine description and applied to leaf elongation is considered. Extension of state-based modeling incorporating effects of water deficit to description of leaf appearance and biomass modeling is considered necessary to fully describe the water status-related growth of maize plants during the vegetative stage.

Evapotranspiration modeling:
The main driver of water loss in growing plants is evapotranspiration, making it a key variable of interest in determining the timing and quantity of irrigation water supply. As with morphological models of plant growth and development, existing evapotranspiration modeling assumes a dependence on environmental factors, and

neglects the effect of current and previous water stress events on plant physiological response, in this case, rate of transpiration. Advances have been made in simplifying the required variables for effective modeling of evapotranspiration, with the most popularly applied approaches based on thermal factors and exposed surface area of the plant. Integration of variations resulting from physiological response to ongoing or previous exposure to water stress events is a key requirement for precision deficit irrigation control, allowing for more accurate assessment of water requirements in plants periodically subjected to water deficit.

The second part of this thesis (section 3) describes approaches developed for morphological and physiological modeling of plant growth and development, with a focus to leaf elongation, leaf appearance, biomass estimation and evapotranspiration.

Leaf elongation model:
Working from an existing state machine model with seven distinct states related to level and duration of exposure to water stress, with state thresholds initially determined using an NSGA-II optimization algorithm, validation of model accuracy was carried out using experimental growth data. Significant errors were found to occur in the projection of plant growth, particularly in application to plants under full irrigation conditions. Implementation of a trust-region-reflexive least squares optimization algorithm produced greater prediction accuracy, however the projections related to full irrigation conditions still exhibited rising inaccuracy with time, implying a need to either adjust the growth-related equations or develop a new model to describe leaf elongation.

An evaluation of model performance using the NSGA-II optimization model with similar equations for all growth states produced greater prediction accuracy, but led to level thresholds that contained significant overlaps between the mild stress and high stress conditions, which made this approach unsuitable for use in this work, as one of the goals of precision deficit irrigation in this case is to avoid subjecting the plants to high stress to avoid damage. Reversing the two equations initially used to represent large changes in observed values and minor changes resulted in clearly distinguishable regions of high stress and mild stress, with some overlapping observable in the regions of mild stress and no stress. The prediction accuracy is significantly greater than the other examined cases (involving all three forms of the growth equation as initially described, and only using one form of the growth equation), making the overall rating of this approach inconclusive.

A data-driven linear regression model based on historical data was developed, resulting in a reduced set of equations representing six of the seven described states. The undescribed state was as a result of insufficient experimental growth data. The results from prediction using linear regression equations to describe each of the six considered states produced RMSE values of 17.09 cm, with prediction accuracy relatively robust even for a ten-step prediction horizon.

Biomass estimation:
Using the presented state machine description, cumulative above ground biomass is predicted by a direct application of the optimized state machine model for leaf length prediction. This approach is not pursued further due to significantly large error values attributed to inadequate training data for intermediate biomass values.

An allometric function is developed as a linear regression model based on leaf area, with stepwise prediction of biomass accumulation. A prediction accuracy of between 80 % and 95 % is achieved, and a comparison with the Aquacrop growth model indicates close agreement of both intermediate and final biomass accumulation predictions.

Leaf appearance model:
A modeling approach based on linear degradation models employed in continuous health monitoring of mechanical systems is applied to prediction of leaf appearance, with elongation trajectories of existing leaves used to predict new leaf appearance. Based on analysis of existing experimental plant growth data, leaf elongation rate thresholds are identified representing the transition of existing leaves from an active elongation phase to a mature phase during which no further extension is experienced. These thresholds demarcate the appearance of new leaves, with a three-leaf interval identified as the optimal separation between the leaf under observation and the new leaf whose appearance is to be predicted.

Prediction results for the fourth and fifth leaves in maize plants under different irrigation treatments are presented, showing a close match to projected timing of leaf appearance.

Data driven evapotranspiration model:
The third part of this thesis (section 4) focuses on the development of a growth control approach based on precision deficit irrigation. A model predictive control scheme based on the state machine model description of plant growth and evapotranspiration is combined with a trellis decoding approach to achieve targeted growth control through generation of specific irrigation sequences. Optimization options allow for variation of weighting of the twin goals of maximizing plant growth (defined by the total leaf length) and minimizing water consumption.

Growth control results:
Implementation of a model predictive controller integrating a trellis decoding algorithm based on a brute force approach on control of plant growth and cumulative water consumption was experimentally validated on a group of test plants. Fixed growth and water consumption targets imposed on plants with different initial measurements and levels of cumulative water consumption were achieved for the plants within the test groups. Optimization of both water consumption and plant growth was tested with equal weights for both targets, with results evaluated on the basis of final achieved total leaf lengths. The performance of the control algorithm

was found to be satisfactory for the selected duration. It was however noted that the control error exhibited an upwards drift with time, implying the need to dynamically adjust stress thresholds as the plants grow.

5.2 Outlook

Application of a state machine-based representation for maize growth during the vegetative stage has been experimentally validated. However, the definition of stress thresholds has remained a challenge, leading to a hypothesis that dynamic stress thresholds for pot-grown plants may lead to greater modeling accuracy, particularly as the plants grow beyond the 6-leaf stage. This is attributable to the extension of plant roots with time, resulting in greater accessibility to water even at significantly lower soil water content. This results in a seemingly delayed response to water deficit, with reduced levels of stress not fully attributable to the priming effect developed after an initial exposure to water stress. Exploration of the development of the root system would be particularly useful in further refining the growth models with respect to stress boundaries. An alternative would be to rely purely on sensing of physiological response to identify and quantify water stress, which however requires high precision, high resolution sensors, thereby implying increased costs.

Initial testing of irrigation-based growth control shows it to be feasible, with optimization of both growth-related and water-related goals achievable. Exploration of the effect of different optimization scenarios, involving adjusting the weighting of growth and water consumption as targets needs to be experimentally verified to ascertain the practical limits of achievable control goals.

The extent of experimental validation of different growth-related parameters has been limited by the dimensions of the experimental space, with pot size limiting root expansion and distance to internal lighting limiting the maximum achievable plant height. Further experiments involving larger pots and more vertical room for plant growth could be useful in evaluating the performance of the growth controller over the entire vegetative stage, particulary because greater reliability in estimation of final maize yield is achieved by considering later stages of vegetative growth. Other plants exhibiting similar physiological responses to water stress but with lower space requirements would also provide an ideal option to test the performance of the growth controller, provided initial preparatory experiments are carried out to obtain training data for model parametrization.

Bibliography

[AGd+17] Arborea, S. ; Giannoccaro, G. ; de Gennaro, B. ; Iacobellis, V. ; Piccinni, A.: Cost–Benefit Analysis of Wastewater Reuse in Puglia, Southern Italy. In: *Water* 9 (2017), feb, Nr. 3, pp. 175. http://dx.doi.org/10.3390/w9030175. – DOI 10.3390/w9030175

[AGM20] Arena, C. ; Genco, M. ; Mazzola, M. R.: Environmental Benefits and Economical Sustainability of Urban Wastewater Reuse for Irrigation—A Cost-Benefit Analysis of an Existing Reuse Project in Puglia, Italy. In: *Water* 12 (2020), oct, Nr. 10, pp. 2926. http://dx.doi.org/10.3390/w12102926. – DOI 10.3390/w12102926

[AHB06] Andrieu, B. ; Hillier, J. ; Birch, C.: Onset of Sheath Extension and Duration of Lamina Extension are Major Determinants of the Response of Maize Lamina Length to Plant Density. In: *Annals of Botany* 98 (2006), aug, Nr. 5, pp. 1005–1016. http://dx.doi.org/10.1093/aob/mcl177. – DOI 10.1093/aob/mcl177

[All98] Allen, R. G.: *Crop evapotranspiration : guidelines for computing crop water requirements- FAO Irrigation and drainage paper 56*. Rome : Food and Agriculture Organization of the United Nations, 1998. – ISBN 9251042195

[AMB+21] Adak, A. ; Murray, S. C. ; Božinović, S. ; Lindsey, R. ; Nakasagga, S. ; Chatterjee, S. ; Anderson, S. L. ; Wilde, S.: Temporal Vegetation Indices and Plant Height from Remotely Sensed Imagery Can Predict Grain Yield and Flowering Time Breeding Value in Maize via Machine Learning Regression. In: *Remote Sensing* 13 (2021), may, Nr. 11, pp. 2141. http://dx.doi.org/10.3390/rs13112141. – DOI 10.3390/rs13112141

[AMC+20] Anderson, S. L. ; Murray, S. C. ; Chen, Y. ; Malambo, L. ; Chang, A. ; Popescu, S. ; Cope, D. ; Jung, J.: Unoccupied aerial system enabled functional modeling of maize height reveals dynamic expression of loci. In: *Plant Direct* 4 (2020), may, Nr. 5. http://dx.doi.org/10.1002/pld3.223. – DOI 10.1002/pld3.223

[AMER+21] Amazirh, A. ; Merlin, O. ; Er-Raki, S. ; Bouras, E. ; Chehbouni, A.: Implementing a new texture-based soil evaporation reduction coefficient in the FAO dual crop coefficient method. In: *Agricultural Water Management* 250 (2021), may, pp.

106827. http://dx.doi.org/10.1016/j.agwat.2021.106827. – DOI 10.1016/j.agwat.2021.106827

[AMM+19] Anderson, S. L. ; Murray, S. C. ; Malambo, L. ; Ratcliff, C. ; Popescu, S. ; Cope, D. ; Chang, A. ; Jung, J. ; Thomasson, J. A.: Prediction of Maize Grain Yield before Maturity Using Improved Temporal Height Estimates of Unmanned Aerial Systems. In: *The Plant Phenome Journal* 2 (2019), jan, Nr. 1, pp. 1–15. http://dx.doi.org/10.2135/tppj2019.02.0004. – DOI 10.2135/tppj2019.02.0004

[AP07] Ayars, J. E. ; Phene, C. J.: 7. Automation. Version: 2007. http://dx.doi.org/10.1016/s0167-4137(07)80010-2. In: *Developments in Agricultural Engineering* Bd. Microirrigation for Crop Production: Design, Operation and Management. Elsevier, 2007, pp. 259–284. – DOI 10.1016/s0167–4137(07)80010–2

[BAF02] Birch, C. J. ; Andrieu, B. ; Fournier, C.: Dynamics of internode and stem elongation in three cultivars of maize. In: *Agronomie* 22 (2002), jul, Nr. 5, pp. 511–524. http://dx.doi.org/10.1051/agro:2002030. – DOI 10.1051/agro:2002030

[BAM+16] Battude, M. ; Al Bitar, A. ; Morin, D. ; Cros, J. ; Huc, M. ; Sicre, C. M. ; Le Dantec, V. ; Demarez, V.: Estimating maize biomass and yield over large areas using high spatial and temporal resolution Sentinel-2 like remote sensing data. In: *Remote Sensing of Environment* 184 (2016), oct, pp. 668–681. http://dx.doi.org/10.1016/j.rse.2016.07.030. – DOI 10.1016/j.rse.2016.07.030

[BBD+14] Bassu, S. ; Brisson, N. ; Durand, J. ; Boote, K. ; Lizaso, J. ; Jones, J. W. ; Rosenzweig, C. ; Ruane, A. C. ; Adam, M. ; Baron, C. ; Basso, B. ; Biernath, C. ; Boogaard, H. ; Conijn, S. ; Corbeels, M. ; Deryng, D. ; De Sanctis, G. ; Gayler, S. ; Grassini, P. ; Hatfield, J. ; Hoek, S. ; Izaurralde, C. ; Jongschaap, R. ; Kemanian, A. R. ; Kersebaum, K. C. ; Kim, S. ; Kumar, N. S. ; Makowski, D. ; Müller, C. ; Nendel, C. ; Priesack, E. ; Pravia, M. V. ; Sau, F. ; Shcherbak, I. ; Tao, F. ; Teixeira, E. ; Timlin, D. ; Waha, K.: How do various maize crop models vary in their responses to climate change factors? In: *Global Change Biology* 20 (2014), apr, Nr. 7, pp. 2301–2320. http://dx.doi.org/10.1111/gcb.12520. – DOI 10.1111/gcb.12520

[BC62] Blaney, H. F. ; Criddle, W. D.: *Determining Consumptive Use and Irrigation Water Requirements*. US Department of Agriculture, 1962 (1275). http://dx.doi.org/10.22004/AG.ECON.171000. http://dx.doi.org/10.22004/AG.ECON.171000

[BHB+20] Bhatti, S. ; Heeren, D. M. ; Barker, J. B. ; Neale, C. M. U. ; Woldt, W. E. ; Maguire, M. S. ; Rudnick, D. R.: Site-specific irrigation management in a sub-humid climate using a spatial evapotranspiration model with satellite and airborne imagery. In: *Agricultural Water Management* 230 (2020), mar, pp. 105950. http://dx.doi.org/10.1016/j.agwat.2019.105950. – DOI 10.1016/j.agwat.2019.105950

[BHH+14] Brown, H. E. ; Huth, N. I. ; Holzworth, D. P. ; Teixeira, E. I. ; Zyskowski, R. F. ; Hargreaves, J. N. G. ; Moot, D. J.: Plant Modelling Framework: Software for building and running crop models on the APSIM platform. In: *Environmental Modelling and Software* 62 (2014), dec, pp. 385–398. http://dx.doi.org/10.1016/j.envsoft.2014.09.005. – DOI 10.1016/j.envsoft.2014.09.005

[BKA+10] Ben-Gal, A. ; Kool, D. ; Agam, N. ; van Halsema, G. E. ; Yermiyahu, U. ; Yafe, A. ; Presnov, E. ; Erel, R. ; Majdop, A. ; Zipori, I. ; Segal, E. ; Rüger, S. ; Zimmermann, U. ; Cohen, Y. ; Alchanatis, V. ; Dag, A.: Whole-tree water balance and indicators for short-term drought stress in non-bearing 'Barnea' olives. In: *Agricultural Water Management* 98 (2010), dec, Nr. 1, pp. 124–133. http://dx.doi.org/10.1016/j.agwat.2010.08.008. – DOI 10.1016/j.agwat.2010.08.008

[BLB+04] Bennouna, B. ; Lahrouni, A. ; Bethenod, O. ; Fournier, C. ; Andrieu, B. ; Khabba, S.: Development of Maize Internode under Drought Stress. In: *Journal of Agronomy* 3 (2004), mar, Nr. 2, pp. 94–102. http://dx.doi.org/10.3923/ja.2004.94.102. – DOI 10.3923/ja.2004.94.102

[BMFH98] Bastiaanssen, W. G. M. ; Menenti, M. ; Feddes, R. A. ; Holtslag, A. A. M.: A remote sensing surface energy balance algorithm for land (SEBAL). 1. Formulation. In: *Journal of Hydrology* 212-213 (1998), dec, pp. 198–212. http://dx.doi.org/10.1016/s0022-1694(98)00253-4. – DOI 10.1016/s0022–1694(98)00253–4

[BMR+98] Brisson, N. ; Mary, B. ; Ripoche, D. ; Jeuffroy, M. ; Ruget, F. ; Nicoullaud, B. B. ; Gate, P. ; Devienne-Barret, F. ;

Antonioletti, R. ; Dürr, C. ; Richard, G. ; Beaudoin, N. ; Recous, S. ; Tayot, X. ; Plenet, D. ; Cellier, P. ; Machet, J. ; Meynard, J. M. ; Delécolle., R.: STICS: a generic model for the simulation of crops and their water and nitrogen balances. I. Theory and parameterization applied to wheat and corn. In: *Agronomie, EDP Sciences* 18 (1998), Nr. 5–6, pp. 311–346

[BS11] Briggs, L. J. ; Shantz, H. L.: A Wax Seal Method for Determining the Lower Limit of Available Soil Moisture. In: *Botanical Gazette* 51 (1911), Nr. 3, 210–219. http://www.jstor.org/stable/2466810. – ISSN 00068071

[BS17] Beganovic, N. ; Söffker, D.: Remaining lifetime modeling using State-of-Health estimation. In: *Mechanical Systems and Signal Processing* 92 (2017), aug, pp. 107–123. http://dx.doi.org/10.1016/j.ymssp.2017.01.031. – DOI 10.1016/j.ymssp.2017.01.031

[BVK+98] Birch, C. J. ; Vos, J. ; Kiniry, J. ; Bos, H. J. ; Elings, A.: Phyllochron responds to acclimation to temperature and irradiance in maize. In: *Field Crops Research* 59 (1998), dec, Nr. 3, pp. 187–200. http://dx.doi.org/10.1016/s0378-4290(98)00120-8. – DOI 10.1016/s0378–4290(98)00120–8

[BWB06] Brisson, N. ; Wery, J. ; Boote, K.: Fundamental concepts of crop models illustrated by a comparative approach. In: *Working with Dynamic Crop Models*. , Oxford : Elsevier LTD, 2006, pp. 257–280

[Çak04] Çakir, R.: Effect of water stress at different development stages on vegetative and reproductive growth of corn. In: *Field Crops Research* 89 (2004), sep, Nr. 1, pp. 1–16. http://dx.doi.org/10.1016/j.fcr.2004.01.005. – DOI 10.1016/j.fcr.2004.01.005

[CC12] Chianucci, F. ; Cutini, A.: Digital hemispherical photography for estimating forest canopy properties: current controversies and opportunities. In: *iForest - Biogeosciences and Forestry* 5 (2012), dec, Nr. 1, pp. 290–295. http://dx.doi.org/10.3832/ifor0775-005. – DOI 10.3832/ifor0775–005

[CCHK16] Cobaner, M. ; Citakoğlu, H. ; Haktanir, T. ; Kisi, O.: Modifying Hargreaves–Samani equation with meteorological variables for estimation of reference evapotranspiration in Turkey. In: *Hydrology Research* 48 (2016), may, Nr. 2, pp. 480–497. http://dx.doi.org/10.2166/nh.2016.217. – DOI 10.2166/nh.2016.217

[CEB+17] Colaizzi, P. D. ; Evett, S. R. ; Brauer, D. K. ; Howell, T. A. ; Tolk, J. A. ; Copeland, K. S.: Allometric Method to Estimate Leaf Area Index for Row Crops. In: *Agronomy Journal* 109 (2017), may, Nr. 3, pp. 883–894. http://dx.doi.org/10.2134/agronj2016.11.0665. – DOI 10.2134/agronj2016.11.0665

[CHM20] Chen, H. ; Huang, J. J. ; McBean, E.: Partitioning of daily evapotranspiration using a modified shuttleworth-wallace model, random Forest and support vector regression, for a cabbage farmland. In: *Agricultural Water Management* 228 (2020), feb, pp. 105923. http://dx.doi.org/10.1016/j.agwat.2019.105923. – DOI 10.1016/j.agwat.2019.105923

[CLL+09] Chaerle, L. ; Lenk, S. ; Leinonen, I. ; Jones, H. G. ; Van der Straeten, D. ; Buschmann, C.: Multi-sensor plant imaging: Towards the development of a stress-catalogue. In: *Biotechnology Journal* 4 (2009), aug, Nr. 8, pp. 1152–1167. http://dx.doi.org/10.1002/biot.200800242. – DOI 10.1002/biot.200800242

[CMO+11] Conejero, W. ; Mellisho, C. D. ; Ortuño, M. F. ; Moriana, A. ; Moreno, F. ; Torrecillas, A.: Using trunk diameter sensors for regulated deficit irrigation scheduling in early maturing peach trees. In: *Environmental and Experimental Botany* 71 (2011), Juli, Nr. 3, pp. 409–415. http://dx.doi.org/10.1016/j.envexpbot.2011.02.014. – DOI 10.1016/j.envexpbot.2011.02.014

[COLM18] Chen, A. ; Orlov-Levin, V. ; Meron, M.: Applying High-Resolution Visible-Channel Aerial Scan of Crop Canopy to Precision Irrigation Management. In: *Proceedings of the 2nd International Electronic Conference on Remote Sensing* 2 (2018), mar, Nr. 7, pp. 335. http://dx.doi.org/10.3390/ecrs-2-05148. – DOI 10.3390/ecrs–2–05148

[CR27] Cummings, N. W. ; Richardson, B.: Evaporation from Lakes. In: *Physical Review* 30 (1927), oct, Nr. 4, pp. 527–534. http://dx.doi.org/10.1103/physrev.30.527. – DOI 10.1103/physrev.30.527

[CSE06] *Kapitel* Precision Water Management: Current realities, possibilities and trends. In: Camp, C. R. ; Sadler, J. E. ; Evans, R. G.: *In: Srinivasan A. editor. Handbook of Precision Agriculture.* Binghamton, New York : Haworth Press, 2006, pp. 153–183

[CST61] Chestnut, H. ; Sollecito, W. E. ; Troutman, P. H.: Predictive-control system application. In: *Transactions of the*

American Institute of Electrical Engineers, Part II: Applications and Industry 80 (1961), jul, Nr. 3, pp. 128–139

[CTD+19] Comas, L. H. ; Trout, T. J. ; DeJonge, K. C. ; Zhang, H. ; Gleason, S. M.: Water productivity under strategic growth stage-based deficit irrigation in maize. In: *Agricultural Water Management* 212 (2019), feb, pp. 433–440. http://dx.doi.org/10.1016/j.agwat.2018.07.015. – DOI 10.1016/j.agwat.2018.07.015

[CTM+19] Calou, V. B. C. ; Teixeira, A. . ; Moreira, L. C. J. ; Neto, O. C. . ; da Silva, J. A.: Estimation of maize biomass using unmanned aerial vehicles. In: *Engenharia Agrícola* 39 (2019), dec, Nr. 6, pp. 744–752

[CWX+20] Che, Y. ; Wang, Q. ; Xie, Z. ; Zhou, L. ; Li, S. ; Hui, F. ; Wang, X. ; Li, B. ; Ma, Y.: Estimation of maize plant height and leaf area index dynamics using an unmanned aerial vehicle with oblique and nadir photography. In: *Annals of Botany* 126 (2020), may, Nr. 4, pp. 765–773. http://dx.doi.org/10.1093/aob/mcaa097. – DOI 10.1093/aob/mcaa097

[dAC+22] dos Santos, C. L. ; Abendroth, L. J. ; Coulter, J. A. ; Nafziger, E. D. ; Suyker, A. ; Yu, J. ; Schnable, P. S. ; Archontoulis, S. V.: Maize Leaf Appearance Rates: A Synthesis From the United States Corn Belt. In: *Frontiers in Plant Science* 13 (2022), apr. http://dx.doi.org/10.3389/fpls.2022.872738. – DOI 10.3389/fpls.2022.872738

[Dal98] Dalton, J.: Experimental essays, on the constitution of mixed gases; on the force of steam or vapour from water and other liquids in different temperatures, both in a Torricellian vacuum and in air; on evaporation; and on the expansion of gases by heat. In: *Memoirs of the Literary and Philosophical Society of Manchester* 5 (1798), 535–602. https://www.biodiversitylibrary.org/part/308525

[dBF+19] de Wit, A. ; Boogaard, H. ; Fumagalli, D. ; Janssen, S. ; Knapen, R. ; van Kraalingen, D. ; Supit, I. ; van der Wijngaart, R. ; van Diepen, K.: 25 years of the WOFOST cropping systems model. In: *Agricultural Systems* 168 (2019), jan, pp. 154–167. http://dx.doi.org/10.1016/j.agsy.2018.06.018. – DOI 10.1016/j.agsy.2018.06.018

[DGBA17] Davoodi, E. ; Ghasemieh, H. ; Batelaan, O. ; Abdollahi, K.: Spatial-Temporal Simulation of LAI on Basis of Rainfall and

Growing Degree Days. In: *Remote Sensing* 9 (2017), nov, Nr. 12, pp. 1207. http://dx.doi.org/10.3390/rs9121207. – DOI 10.3390/rs9121207

[DP03] Drouet, J.-L. ; Pagès, L.: GRAAL: a model of GRowth, Architecture and carbon ALlocation during the vegetative phase of the whole maize plant. In: *Ecological Modelling* 165 (2003), jul, Nr. 2-3, pp. 147–173. http://dx.doi.org/10.1016/s0304-3800(03)00072-3. – DOI 10.1016/s0304–3800(03)00072–3

[dSV+18] da Silveira, A. C. ; Schorr, L. P. B. ; Vuaden, E. ; Aguiar, J. T. ; Cuchi, T. ; Moraes, G. C.: Modelagem da Altura e do Incremento em Área Transversal de Louro Pardo. In: *Nativa* 6 (2018), mar, Nr. 2, pp. 191. http://dx.doi.org/10.31413/nativa.v6i2.4790. – DOI 10.31413/nativa.v6i2.4790

[EDB+15] Egle, R. B. ; Domingo, A. J. ; Bueno, C. ; Laurena, A. C. ; Aguilar, E. A. ; Cruz, P. S. ; Clerget, B.: Variability and Synchronism of Leaf Appearance and Leaf Elongation Rates of Eleven Contrasting Rice Genotypes. In: *Agricultural Sciences* 06 (2015), Nr. 10, pp. 1207–1219. http://dx.doi.org/10.4236/as.2015.610116. – DOI 10.4236/as.2015.610116

[Ett51] Etter, A. G.: How Kentucky Bluegrass Grows. In: *Annals of the Missouri Botanical Garden* 38 (1951), sep, Nr. 3, pp. 293. http://dx.doi.org/10.2307/2394639. – DOI 10.2307/2394639

[FA00] Fournier, C. ; Andrieu, B.: Dynamics of the Elongation of Internodes in Maize (Zea mays L.): Analysis of Phases of Elongation and their Relationships to Phytomer Development. In: *Annals of Botany* 86 (2000), sep, Nr. 3, pp. 551–563. http://dx.doi.org/10.1006/anbo.2000.1217. – DOI 10.1006/anbo.2000.1217

[FAO98] FAO: Crop Evapotranspiration- Guidelines for computing crop water requirements / Food and Agriculture Organization of the United Nations. Rome, 1998 (FAO Irrigation and drainage paper 56). – techreport

[FAO18] FAO: The future of food and agriculture- alternative pathways to 2050. Rome, 2018. – techreport

[FAO20] FAO: *The State of Food and Agriculture 2020*. Rome : Rome. FAO, 2020. http://dx.doi.org/10.4060/cb1447en. http://dx.doi.org/10.4060/cb1447en

[FDL+05] Fournier, C. ; Durand, J. L. ; Ljutovac, S. ; Schäufele, R. ; Gastal, F. ; Andrieu, B.: A functional–structural model of elongation of the grass leaf and its relationships with the phyllochron. In: *New Phytologist* 166 (2005), mar, Nr. 3, pp. 881–894. http://dx.doi.org/10.1111/j.1469-8137.2005.01371.x. – DOI 10.1111/j.1469–8137.2005.01371.x

[Fer17] Fernández, J.: Plant-Based Methods for Irrigation Scheduling of Woody Crops. In: *Horticulturae* 3 (2017), jun, Nr. 2, pp. 35. http://dx.doi.org/10.3390/horticulturae3020035. – DOI 10.3390/horticulturae3020035

[FIU+22] FAO ; IFAD ; UNICEF ; WFP ; WHO: *The State of Food Security and Nutrition in the World 2022. Repurposing food and agricultural policies to make healthy diets more affordable.* Repurposing food and agricultural policies to make healthy diets more affordable. Rome : Rome, FAO, 2022. http://dx.doi.org/10.4060/cc0639en. http://dx.doi.org/10.4060/cc0639en

[For74] Forney, G. D.: Convolutional codes III. Sequential decoding. In: *Information and Control* 25 (1974), jul, Nr. 3, pp. 267–297. http://dx.doi.org/10.1016/s0019-9958(74)90876-6. – DOI 10.1016/s0019–9958(74)90876–6

[FZS+07] Fourcaud, T. ; Zhang, X. ; Stokes, A. ; Lambers, H. ; Korner, C.: Plant Growth Modelling and Applications: The Increasing Importance of Plant Architecture in Growth Models. In: *Annals of Botany* 101 (2007), aug, Nr. 8, pp. 1053–1063. http://dx.doi.org/10.1093/aob/mcn050. – DOI 10.1093/aob/mcn050

[GBB95] Giauffret, C. ; Bonhomme, R. ; Bonhomme, M.: Genotypic differences for temperature response of leaf appearance rate and leaf elongation in field-grown maize. In: *Agronomie, EDP Sciences* 15 (1995), Nr. 2, pp. 123–137

[GDGZTF14] Gonzalez-Dugo, V. ; Goldhamer, D. ; Zarco-Tejada, P. J. ; Fereres, E.: Improving the precision of irrigation in a pistachio farm using an unmanned airborne thermal system. In: *Irrigation Science* 33 (2014), sep, Nr. 1, pp. 43–52. http://dx.doi.org/10.1007/s00271-014-0447-z. – DOI 10.1007/s00271–014–0447–z

[GEA+18] Gafurov, Z. ; Eltazarov, S. ; Akramov, B. ; Yuldashev, T. ; Djumaboev, K. ; Anarbekov, O.: Modifying Hargreaves-Samani Equation for Estimating Reference Evapotranspiration in Dryland Regions of Amudarya River Basin. In: *Agricultural*

Sciences 09 (2018), Nr. 10, pp. 1354–1368. http://dx.doi.org/10.4236/as.2018.910094. – DOI 10.4236/as.2018.910094

[GHHM00] Grenfell, B. P. ; Hunt, A. S. ; Hogarth, D. G. ; Milne, J. G.: *Fayûm towns and their papyri*. Egypt exploration fund: Graeco-Roman branch https://archive.org/details/faymtownsandthe00milngoog/page/n8/mode/2up

[GLM+19] Gobbo, S. ; Lo Presti, S. ; Martello, M. ; Panunzi, L. ; Berti, A. ; Morari, F.: Integrating SEBAL with in-Field Crop Water Status Measurement for Precision Irrigation Applications—A Case Study. In: *Remote Sensing* 11 (2019), sep, Nr. 17, pp. 2069. http://dx.doi.org/10.3390/rs11172069. – DOI 10.3390/rs11172069

[GQS+20] Gong, X. ; Qiu, R. ; Sun, J. ; Ge, J. ; Li, Y. ; Wang, S.: Evapotranspiration and crop coefficient of tomato grown in a solar greenhouse under full and deficit irrigation. In: *Agricultural Water Management* 235 (2020), may, pp. 106154. http://dx.doi.org/10.1016/j.agwat.2020.106154. – DOI 10.1016/j.agwat.2020.106154

[GRS06] Giordano, M. A. (Hrsg.) ; Rijsberman, F. R. (Hrsg.) ; Saleth, R. M. (Hrsg.): *More Crop per Drop*. London, UK. : IWA Publishing, 2006. – ISBN 9781843391128

[GZL+18] Gao, Z. ; Zhu, Y. ; Liu, C. ; Qian, H. ; Cao, W. ; Ni, J.: Design and Test of a Soil Profile Moisture Sensor Based on Sensitive Soil Layers. In: *Sensors* 18 (2018), may, Nr. 5, pp. 1648. http://dx.doi.org/10.3390/s18051648. – DOI 10.3390/s18051648

[HB07] Hofius, D. ; Börnke, F. A. J.: Photosynthesis, carbohydrate metabolism and source–sink relations. Version: 2007. http://dx.doi.org/10.1016/b978-044451018-1/50055-5. In: *Potato Biology and Biotechnology*. Elsevier, 2007, pp. 257–285. – DOI 10.1016/b978–044451018–1/50055–5

[HBC19] Hao, Y. ; Baik, J. ; Choi, M.: Developing a soil water index-based Priestley–Taylor algorithm for estimating evapotranspiration over East Asia and Australia. In: *Agricultural and Forest Meteorology* 279 (2019), dec, pp. 107760. http://dx.doi.org/10.1016/j.agrformet.2019.107760. – DOI 10.1016/j.agrformet.2019.107760

[HI71] Hanway, J. J. ; Iowa State University. Cooperative Extension Service: *How a Corn Plant Develops*. Iowa State

University of Science and Technology, Co-operative Extension Services (Special report (Iowa State University. Agricultural and Home Economics Experiment Station)). https://books.google.de/books?id=CGxLHAAACAAJ

[HM09] Hendrawan, Y. ; Murase, H.: Precision Irrigation for Sunagoke Moss Production using Intelligent Image Analysis. In: *Environment Control in Biology* 47 (2009), Nr. 1, pp. 21–36. http://dx.doi.org/10.2525/ecb.47.21. – DOI 10.2525/ecb.47.21

[HORB+19] Hagenvoort, J. ; Ortega-Reig, M. ; Botella, S. ; García, C. ; de Luis, A. ; Palau-Salvador, G.: Reusing Treated Waste-Water from a Circular Economy Perspective—The Case of the Real Acequia de Moncada in Valencia (Spain). In: *Water* 11 (2019), sep, Nr. 9, pp. 1830. http://dx.doi.org/10.3390/w11091830. – DOI 10.3390/w11091830

[HPB+19] Hoogenboom, G. ; Porter, C. H. ; Boote, K. J. ; Shelia, V. ; Wilkens, P. W. ; Singh, U. ; White, J. W. ; Asseng, S. ; Lizaso, J. I. ; Moreno, L. P. ; Pavan, W. ; Ogoshi, R. ; Hunt, L. A. ; Tsuji, G. Y. ; Jones, J. W.: The DSSAT crop modeling ecosystem. Version: dec 2019. http://dx.doi.org/10.19103/as.2019.0061.10. In: *Advances in crop modelling for a sustainable agriculture*. Burleigh Dodds Science Publishing, dec 2019, pp. 173–216. – DOI 10.19103/as.2019.0061.10

[HS82] Hargreaves, G. H. ; Samani, Z. A.: Estimating Potential Evapotranspiration. In: *Journal of the Irrigation and Drainage Division* 108 (1982), sep, Nr. 3, pp. 225–230. http://dx.doi.org/10.1061/jrcea4.0001390. – DOI 10.1061/jrcea4.0001390

[HS85] Hargreaves, G. H. ; Samani, Z. A.: Reference Crop Evapotranspiration from Temperature. In: *Applied Engineering in Agriculture* 1 (1985), Nr. 2, pp. 96–99. http://dx.doi.org/10.13031/2013.26773. – DOI 10.13031/2013.26773

[Hsi73] Hsiao, T. C.: Plant response to water stress. In: *Annual review of plant physiology* 24 (1973), Nr. 1, pp. 519–570

[HWRZ88] Hesketh, J. D. ; Warrinton, J. ; Reid, J. F. ; Zur, B.: The dynamics of corn canopy development: Phytomer ontogeny. In: *Biotronics* 17 (1988), pp. 69–77

[HYD+19] Han, L. ; Yang, G. ; Dai, H. ; Xu, B. ; Yang, H. ; Feng, H. ; Li, Z. ; Yang, X.: Modeling maize above-ground biomass based

on machine learning approaches using UAV remote-sensing data. In: *Plant Methods* 15 (2019), feb, Nr. 1. http://dx.doi.org/10.1186/s13007-019-0394-z. – DOI 10.1186/s13007–019–0394–z

[HZZ+22] Han, X. ; Zhou, Q. ; Zhang, B. ; Che, Z. ; Wei, Z. ; Qiu, R. ; Chen, H. ; Li, Y. ; Du, T.: Real-time methods for short and medium-term evapotranspiration forecasting using dynamic crop coefficient and historical threshold. In: *Journal of Hydrology* 606 (2022), mar, pp. 127414. http://dx.doi.org/10.1016/j.jhydrol.2021.127414. – DOI 10.1016/j.jhydrol.2021.127414

[JCR99] Jame, Y. W. ; Cutforth, H. W. ; Ritchie, J. T.: Temperature response function for leaf appearance rate in wheat and corn. In: *Canadian Journal of Plant Science* 79 (1999), pp. 1–10

[JDPS19] Jha, K. ; Doshi, A. ; Patel, P. ; Shah, M.: A comprehensive review on automation in agriculture using artificial intelligence. In: *Artificial Intelligence in Agriculture* 2 (2019), jun, pp. 1–12. http://dx.doi.org/10.1016/j.aiia.2019.05.004. – DOI 10.1016/j.aiia.2019.05.004

[JFN+04] Jonckheere, I. ; Fleck, S. ; Nackaerts, K. ; Muys, B. ; Coppin, P. ; Weiss, M. ; Baret, F.: Review of methods for in situ leaf area index determination. In: *Agricultural and Forest Meteorology* 121 (2004), jan, Nr. 1-2, pp. 19–35. http://dx.doi.org/10.1016/j.agrformet.2003.08.027. – DOI 10.1016/j.agrformet.2003.08.027

[JGH+15] Jägermeyr, J. ; Gerten, D. ; Heinke, J. ; Schaphoff, S. ; Kummu, M. ; Lucht, W.: Water savings potentials of irrigation systems: global simulation of processes and linkages. In: *Hydrology and Earth System Sciences* 19 (2015), jul, Nr. 7, pp. 3073–3091. http://dx.doi.org/10.5194/hess-19-3073-2015. – DOI 10.5194/hess–19–3073–2015

[JK86] Jones, C. A. (Hrsg.) ; Kiniry, J. R. (Hrsg.): *CERES-Maize: A simulation model of maize growth and development*. College Station : Texas A & M Univ. Press, 1986

[JKS19] Jihin, R. ; Kögler, F. ; Söffker, D.: Data Driven State Machine Model for Industry 4.0 Lifetime Modeling and Identification of Irrigation Control Parameters. In: *2019 Global IoT Summit (GIoTS)*, 2019, pp. 1–6

[JKT+14] Jiang, X. ; Kang, S. ; Tong, L. ; Li, F. ; Li, D. ; Ding, R. ; Qiu, R.: Crop coefficient and evapotranspiration of grain

maize modified by planting density in an arid region of northwest China. In: *Agricultural Water Management* 142 (2014), aug, pp. 135–143. http://dx.doi.org/10.1016/j.agwat.2014.05.006. – DOI 10.1016/j.agwat.2014.05.006

[JLG+20] Jiang, T. ; Liu, J. ; Gao, Y. ; Sun, Z. ; Chen, S. ; Yao, N. ; Ma, H. ; Feng, H. ; Yu, Q. ; He, J.: Simulation of plant height of winter wheat under soil Water stress using modified growth functions. In: *Agricultural Water Management* 232 (2020), apr, pp. 106066. http://dx.doi.org/10.1016/j.agwat.2020.106066. – DOI 10.1016/j.agwat.2020.106066

[JMC05] Jonckheere, I. ; Muys, B. ; Coppin, P.: Allometry and evaluation of in situ optical LAI determination in Scots pine: a case study in Belgium. In: *Tree Physiology* 25 (2005), jun, Nr. 6, pp. 723–732. http://dx.doi.org/10.1093/treephys/25.6.723. – DOI 10.1093/treephys/25.6.723

[Jon04] Jones, H. G.: Irrigation scheduling: advantages and pitfalls of plant-based methods. In: *Journal of Experimental Botany* 55 (2004), sep, Nr. 407, pp. 2427–2436. http://dx.doi.org/10.1093/jxb/erh213. – DOI 10.1093/jxb/erh213

[Jon07] Jones, H. G.: Monitoring plant and soil water status: Established and novel methods revisited and their relevance to studies of drought tolerance. In: *J. Exp. Bot.* 58 (2007), pp. 119–130. http://dx.doi.org/10.1093/jxb/erl118. – DOI 10.1093/jxb/erl118

[JSS+20] Jin, S. ; Su, Y. ; Song, S. ; Xu, K. ; Hu, T. ; Yang, Q. ; Wu, F. ; Xu, G. ; Ma, Q. ; Guan, H. ; Pang, S. ; Li, Y. ; Guo, Q.: Non-destructive estimation of field maize biomass using terrestrial lidar: an evaluation from plot level to individual leaf level. In: *Plant Methods* 16 (2020), may, Nr. 1. http://dx.doi.org/10.1186/s13007-020-00613-5. – DOI 10.1186/s13007–020–00613–5

[KCH+03] Keating, B. A. ; Carberry, P. S. ; Hammer, G. L. ; Probert, M. E. ; Robertson, M. J. ; Holzworth, D. ; Huth, N. I. ; Hargreaves, J. N. G. ; Meinke, H. ; Hochman, Z. ; McLean, G. ; Verburg, K. ; Snow, V. ; Dimes, J. P. ; Silburn, M. ; Wang, E. ; Brown, S. ; Bristow, K. L. ; Asseng, S. ; Chapman, S. ; McCown, R. L. ; Freebairn, D. M. ; Smith, C. J.: An overview of APSIM, a model designed for farming systems simulation. In: *European Journal of Agronomy* 18 (2003), jan, Nr. 3-4, pp. 267–288. http://dx.doi.org/10.1016/s1161-0301(02)00108-9. – DOI 10.1016/s1161–0301(02)00108–9

[KEF+16] Katsoulas, N. ; Elvanidi, A. ; Ferentinos, K. P. ; Kacira, M. ; Bartzanas, T. ; Kittas, C.: Crop reflectance monitoring as a tool for water stress detection in greenhouses: A review. In: *Biosystems Engineering* 151 (2016), nov, pp. 374–398. http://dx.doi.org/10.1016/j.biosystemseng.2016.10.003. – DOI 10.1016/j.biosystemseng.2016.10.003

[KHH+18] Klein, L. J. ; Hamann, H. F. ; Hinds, N. ; Guha, S. ; Sanchez, L. ; Sams, B. ; Dokoozlian, N.: Closed Loop Controlled Precision Irrigation Sensor Network. In: *IEEE Internet of Things Journal* 5 (2018), dec, Nr. 6, pp. 4580–4588. http://dx.doi.org/10.1109/jiot.2018.2865527. – DOI 10.1109/jiot.2018.2865527

[KIWO20] Kukal, M. S. ; Irmak, S. ; Walia, H. ; Odhiambo, L.: Spatio-temporal calibration of Hargreaves-Samani model to estimate reference evapotranspiration across U.S. High Plains. In: *Agronomy Journal* 112 (2020), jul, Nr. 5, pp. 4232–4248. http://dx.doi.org/10.1002/agj2.20325. – DOI 10.1002/agj2.20325

[KKMD+18] Kizer, E. ; Ko-Madden, C. ; Drechsler, K. ; Meyers, J. ; Jiang, C. ; Santos, R. . ; Upadhyaya, S. K.: Precision irrigation in Almonds based on plant water status. In: *Amazonian Journal of Plant Research* 2 (2018), Nr. 1, pp. 113–116. http://dx.doi.org/10.26545/ajpr.2018.b00015x. – DOI 10.26545/ajpr.2018.b00015x

[Kög19] Kögler, F.: *Deficit irrigation model-based control of plant growth*, University of Duisburg-Essen, Diss., März 2019

[KPKS12] Kloss, S. ; Pushpalatha, R. ; Kamoyo, K. J. ; Schütze, N.: Evaluation of Crop Models for Simulating and Optimizing Deficit Irrigation Systems in Arid and Semi-arid Countries Under Climate Variability. In: *Water Resour. Manag.* 26 (2012), pp. 997–1014. http://dx.doi.org/10.1007/s11269-011-9906-y. – DOI 10.1007/s11269–011–9906–y

[KRJH91] *Kapitel* 5. In: Kiniry, J. R. ; Rosenthal, W. D. ; Jackson, B. S. ; Hoogenboom, G.: *Predicting leaf development of crop plants*. CRC Press, 1991 (In T. Hodges (ed.), Predicting Crop Phenology), pp. 29–42

[KS17] Kögler, F. ; Söffker, D.: Water (stress) models and deficit irrigation: System-theoretical description and causality mapping. In: *Ecological Modelling* 361 (2017), oct, pp. 135–156. http://dx.doi.org/10.1016/j.ecolmodel.2017.07.037. – DOI 10.1016/j.ecolmodel.2017.07.037

[KS18] Kögler, F. ; Söffker, D.: Steuerung des Pflanzenwachstums durch Bewässerung. In: H. Stützel, L. Francke-Weltmann (Hrsg.): *61.e Jahrestagung der Gesellschaft für Pflanzenbauwissenschaften*. Göttingen : Verlag Liddy Halm, September 2018, pp. 116–119

[KS20] Kögler, F. ; Söffker, D.: State-based open-loop control of plant growth by means of water stress training. In: *Agricultural Water Management* 230 (2020), mar, pp. 105963. http://dx.doi.org/10.1016/j.agwat.2019.105963. – DOI 10.1016/j.agwat.2019.105963

[KWGD92] Kiniry, J. R. ; Williams, J. R. ; Gassman, P. W. ; Debaeke, P.: A General, Process-Oriented Model for Two Competing Plant Species. In: *Transactions of the ASAE* 35 (1992), Nr. 3, pp. 801–810. http://dx.doi.org/10.13031/2013.28665. – DOI 10.13031/2013.28665

[KYT+12] Kim, S. ; Yang, Y. ; Timlin, D. J. ; Fleisher, D. H. ; Dathe, A. ; Reddy, V. R. ; Staver, K.: Modeling Temperature Responses of Leaf Growth, Development, and Biomass in Maize with MAIZSIM. In: *Agronomy Journal* 104 (2012), nov, Nr. 6, pp. 1523–1537. http://dx.doi.org/10.2134/agronj2011.0321. – DOI 10.2134/agronj2011.0321

[Lar01] Larcher, W.: *Ökophysiologie der Pflanzen : Leben, Leistung und Streßbewältigung der Pflanzen in ihrer Umwelt*. 6., neubearb. Aufl. Stuttgart : Ulmer, 2001 (UTB für Wissenschaft 8074 : Botanik, Agrar- und Forstwissenschaften, Ökologie, Geographie). – ISBN 3825280748

[LB17] Lämke, J. ; Bäurle, I.: Epigenetic and chromatin-based mechanisms in environmental stress adaptation and stress memory in plants. In: *Genome Biology* 18 (2017), jun, Nr. 1. http://dx.doi.org/10.1186/s13059-017-1263-6. – DOI 10.1186/s13059–017–1263–6

[LBJ+11] Lizaso, J. I. ; Boote, K. J. ; Jones, J. W. ; Porter, C. H. ; Echarte, L. ; Westgate, M. E. ; Sonohat, G.: CSM-IXIM: A New Maize Simulation Model for DSSAT Version 4.5. In: *Agronomy Journal* 103 (2011), may, Nr. 3, pp. 766–779. http://dx.doi.org/10.2134/agronj2010.0423. – DOI 10.2134/agronj2010.0423

[LdO+22] Lima, E. . ; de Souza, Z. M. ; Oliveira, S. R. . ; Montanari, R. ; Farhate, C. V. V.: Random forest model to predict the height of Eucalyptus. In: *Engenharia Agrícola* 42 (2022), Nr. spe. http://dx.doi.org/10.1590/1809-4430-Eng.Agric.v42nepe20210153/2022. – DOI 10.1590/1809–4430–Eng.Agric.v42nepe20210153/2022

[LGH+19] Liu, H. ; Gleason, S. M. ; Hao, G. ; Hua, L. ; He, P. ; Goldstein, G. ; Ye, Q.: Hydraulic traits are coordinated with maximum plant height at the global scale. In: *Science Advances* 5 (2019), feb, Nr. 2. http://dx.doi.org/10.1126/sciadv.aav1332. – DOI 10.1126/sciadv.aav1332

[LIS+16] Linker, R. ; Ioslovicha, I. ; Sylaiosb, G. ; Plauborgc, F. ; Battilanid, A.: Optimal model-based deficit irrigation scheduling using AquaCrop: A simulation study with cotton, potato and tomato. In: *Agric. Water Manag.* 163 (2016), pp. 236–243. http://dx.doi.org/10.1016/j.agwat.2015.09.011. – DOI 10.1016/j.agwat.2015.09.011

[LLT+19] Laxa, M. ; Liebthal, M. ; Telman, W. ; Chibani, K. ; Dietz, K.: The Role of the Plant Antioxidant System in Drought Tolerance. In: *Antioxidants* (2019), 04

[LMA+16] Lozoya, C. ; Mendoza, C. ; Aguilar, A. ; Román, A. ; Castelló, R.: Sensor-Based Model Driven Control Strategy for Precision Irrigation. In: *Journal of Sensors* (2016), pp. 1–12. http://dx.doi.org/10.1155/2016/9784071. – DOI 10.1155/2016/9784071. – ISSN 1687–725X

[LMPSR+19] Lipan, L. ; Martín-Palomo, M. J. ; Sánchez-Rodríguez, L. ; Cano-Lamadrid, M. ; Sendra, E. ; Hernández, F. ; Burló, F. ; Vázquez-Araújo, L. ; Andreu, L. ; Carbonell-Barrachina, Á. A.: Almond fruit quality can be improved by means of deficit irrigation strategies. In: *Agricultural Water Management* 217 (2019), may, pp. 236–242. http://dx.doi.org/10.1016/j.agwat.2019.02.041. – DOI 10.1016/j.agwat.2019.02.041

[LNW+15] Li, W. ; Niu, Z. ; Wang, C. ; Huang, W. ; Chen, H. ; Gao, S. ; Li, D. ; Muhammad, S.: Combined Use of Airborne LiDAR and Satellite GF-1 Data to Estimate Leaf Area Index, Height, and Aboveground Biomass of Maize During Peak Growing Season. In: *IEEE Journal of Selected Topics in Applied Earth*

Observations and Remote Sensing 8 (2015), sep, Nr. 9, pp. 4489–4501. http://dx.doi.org/10.1109/jstars.2015.2496358. – DOI 10.1109/jstars.2015.2496358

[LSG+22] Lu, H. ; Shi, W. ; Guo, Y. ; Guan, W. ; Lei, C. ; Yu, G.: Materials Engineering for Atmospheric Water Harvesting: Progress and Perspectives. In: *Advanced Materials* (2022), feb, pp. 2110079. http://dx.doi.org/10.1002/adma.202110079. – DOI 10.1002/adma.202110079

[LY21] Lestari, T. E. ; Yuansa, R. D. T. Y.: Response Surface Regression with LTS and MM-Estimator to Overcome Outliers on Red Roselle Flowers. In: *Jurnal Varian* 4 (2021), apr, Nr. 2, pp. 91–98. http://dx.doi.org/10.30812/varian.v4i2.882. – DOI 10.30812/varian.v4i2.882

[LYL+22] Linder, E. R. ; Young, S. ; Li, X. ; Inoa, S. H. ; Suchoff, D. H.: The Effect of Transplant Date and Plant Spacing on Biomass Production for Floral Hemp (Cannabis sativa L.). In: *Agronomy* 12 (2022), aug, Nr. 8, pp. 1856. http://dx.doi.org/10.3390/agronomy12081856. – DOI 10.3390/agronomy12081856

[LZW+16] Liu, K. ; Zhou, Q. ; Wu, W. ; Xia, T. ; Tang, H.: Estimating the crop leaf area index using hyperspectral remote sensing. In: *Journal of Integrative Agriculture* 15 (2016), feb, Nr. 2, pp. 475–491. http://dx.doi.org/10.1016/s2095-3119(15)61073-5. – DOI 10.1016/s2095–3119(15)61073–5

[LZZ+21] LaPotin, A. ; Zhong, Y. ; Zhang, L. ; Zhao, L. ; Leroy, A. ; Kim, H. ; Rao, S. R. ; Wang, E. N.: Dual-Stage Atmospheric Water Harvesting Device for Scalable Solar-Driven Water Production. In: *Joule* 5 (2021), jan, Nr. 1, pp. 166–182. http://dx.doi.org/10.1016/j.joule.2020.09.008. – DOI 10.1016/j.joule.2020.09.008

[MAGMRC+19] Mateo-Aroca, A. ; García-Mateos, G. ; Ruiz-Canales, A. ; Molina-García-Pardo, J. M. ; Molina-Martínez, J. M.: Remote Image Capture System to Improve Aerial Supervision for Precision Irrigation in Agriculture. In: *Water* 11 (2019), feb, Nr. 2, pp. 255. http://dx.doi.org/10.3390/w11020255. – DOI 10.3390/w11020255

[MC89] Muchow, R. C. ; Carberry, P. S.: Environmental control of phenology and leaf growth in a tropically adapted maize. In: *Field Crops Research* 20 (1989), apr, Nr. 3, pp. 221–236. http://dx.

doi.org/10.1016/0378-4290(89)90081-6. – DOI 10.1016/0378–4290(89)90081–6

[MCZZ16] Mao, L. ; Chen, S. ; Zhang, J. ; Zhou, G.: Altitudinal patterns of maximum plant height on the Tibetan Plateau. In: *Journal of Plant Ecology* (2016), dec, pp. rtw128. http://dx.doi.org/10.1093/jpe/rtw128. – DOI 10.1093/jpe/rtw128

[MDC+17] Meng, Z. ; Duan, A. ; Chen, D. ; Dassanayake, K. B. ; Wang, X. ; Liu, Z. ; Liu, H. ; Gao, S.: Suitable indicators using stem diameter variation-derived indices to monitor the water status of greenhouse tomato plants. In: *PLOS ONE* 12 (2017), feb, Nr. 2, pp. e0171423. http://dx.doi.org/10.1371/journal.pone.0171423. – DOI 10.1371/journal.pone.0171423

[MF16] Mihai, H. ; Florin, S.: Biomass prediction model in maize based on satellite images. In: *AIP Conference Proceedings* 1738, 350009 (2016). http://dx.doi.org/10.1063/1.4952132. – DOI 10.1063/1.4952132

[MMC+15] Morillo, J. G. ; Martín, M. ; Camacho, E. ; Díaz, J. A. R. ; Montesinos, P.: Toward precision irrigation for intensive strawberry cultivation. In: *Agricultural Water Management* 151 (2015), mar, pp. 43–51. http://dx.doi.org/10.1016/j.agwat.2014.09.021. – DOI 10.1016/j.agwat.2014.09.021

[MN20] Mousavi, S. M. N. ; Nagy, J.: Evaluation of plant characteristics related to grain yield of FAO410 and FAO340 hybrids using regression models. In: *Cereal Research Communications* 49 (2020), sep, Nr. 1, pp. 161–169. http://dx.doi.org/10.1007/s42976-020-00076-3. – DOI 10.1007/s42976–020–00076–3

[Mon11] Montgomery, E. G.: Correlation studies in corn. In: *Agricultural Experiment Station of Nebraska, Lincoln, Annual Report* 24 (1911), pp. 108–159

[Mon65] Monteith, J. L.: Evaporation and Environment. In: *Symposia of the Society for Experimental Biology* 19 (1965), pp. 205–234

[MPH+20] Morel, J. ; Parsons, D. ; Halling, M. A. ; Kumar, U. ; Peake, A. ; Bergkvist, G. ; Brown, H. ; Hetta, M.: Challenges for Simulating Growth and Phenology of Silage Maize in a Nordic Climate with APSIM. In: *Agronomy* 10 (2020), may, Nr. 5, pp. 645. http://dx.doi.org/10.3390/agronomy10050645. – DOI 10.3390/agronomy10050645

[MPM+18] Malambo, L. ; Popescu, S. C. ; Murray, S. C. ; Putman, E. ; Pugh, N. A. ; Horne, D. W. ; Richardson, G. ; Sheridan, R. ; Rooney, W. L. ; Avant, R. ; Vidrine, M. ; McCutchen, B. ; Baltensperger, D. ; Bishop, M.: Multitemporal field-based plant height estimation using 3D point clouds generated from small unmanned aerial systems high-resolution imagery. In: *International Journal of Applied Earth Observation and Geoinformation* 64 (2018), feb, pp. 31–42. http://dx.doi.org/10.1016/j.jag.2017.08.014. – DOI 10.1016/j.jag.2017.08.014

[MQS+17] Ma, L. ; Qi, Z. ; Shen, Y. ; He, L. ; Xu, S. ; Kisekka, I. ; Sima, M. ; Malone, R. W. ; Yu, Q. ; Fang, Q.: Optimizing Et-Based Irrigation Scheduling for Wheat and Maize with Water Constraints. In: *Transactions of the ASABE* 60 (2017), Nr. 6, pp. 2053–2065. http://dx.doi.org/10.13031/trans.12363. – DOI 10.13031/trans.12363

[MRT01] Muller, B. ; Reymond, M. ; Tardieu, F.: The elongation rate at the base of a maize leaf shows an invariant pattern during both the steady-state elongation and the establishment of the elongation zone. In: *Journal of Experimental Botany* 52 (2001), jun, Nr. 359, pp. 1259–1268. http://dx.doi.org/10.1093/jexbot/52.359.1259. – DOI 10.1093/jexbot/52.359.1259

[MTS+10] Mokhtarpour, H. ; Teh, C. B. S. ; Saleh, G. ; Selamat, A. B. ; Asadi, M. E. ; Kamkar, B.: Non-destructive estimation of maize leaf area, fresh weight, and dry weight using leaf length and leaf width. In: *Communications in Biometry and Crop Sciences* 5 (2010), Mai, Nr. 1, pp. 19–26

[MWW+09] Moles, A. T. ; Warton, D. I. ; Warman, L. ; Swenson, N. G. ; Laffan, S. W. ; Zanne, A. E. ; Pitman, A. ; Hemmings, F. A. ; Leishman, M. R.: Global patterns in plant height. In: *Journal of Ecology* 97 (2009), sep, Nr. 5, pp. 923–932. http://dx.doi.org/10.1111/j.1365-2745.2009.01526.x. – DOI 10.1111/j.1365–2745.2009.01526.x

[NH19] Nemeskéri, E. ; Helyes, L.: Physiological Responses of Selected Vegetable Crop Species to Water Stress. In: *Agronomy* 9 (2019), aug, Nr. 8, pp. 447. http://dx.doi.org/10.3390/agronomy9080447. – DOI 10.3390/agronomy9080447

[NMW+19] Nagano, S. ; Moriyuki, S. ; Wakamori, K. ; Mineno, H. ; Fukuda, H.: Leaf-Movement-Based Growth Prediction Model Using Optical Flow Analysis and Machine Learning in

Plant Factory. In: *Frontiers in Plant Science* 10 (2019), mar. http://dx.doi.org/10.3389/fpls.2019.00227. – DOI 10.3389/fpls.2019.00227

[NR92] NeSmith, D. S. ; Ritchie, J. T.: Short- and Long-Term Responses of Corn to a Pre-Anthesis Soil Water Deficit. In: *Agronomy Journal* 84 (1992), jan, Nr. 1, pp. 107–113. http://dx.doi.org/10.2134/agronj1992.00021962008400010021x. – DOI 10.2134/agronj1992.00021962008400010021x

[NZB+19] Nocco, M. A. ; Zipper, S. C. ; Booth, E. G. ; Cummings, C. R. ; Loheide, S. P. ; Kucharik, C. J.: Combining Evapotranspiration and Soil Apparent Electrical Conductivity Mapping to Identify Potential Precision Irrigation Benefits. In: *Remote Sensing* 11 (2019), oct, Nr. 21, pp. 2460. http://dx.doi.org/10.3390/rs11212460. – DOI 10.3390/rs11212460

[OEE+21] Ogunrinde, A. T. ; Emmanuel, I. ; Enaboifo, M. A. ; Ajayi, T. A. ; Pham, Q. B.: Spatio-temporal calibration of Hargreaves–Samani model in the Northern Region of Nigeria. In: *Theoretical and Applied Climatology* 147 (2021), dec, Nr. 3-4, pp. 1213–1228. http://dx.doi.org/10.1007/s00704-021-03897-2. – DOI 10.1007/s00704–021–03897–2

[OHKS19] Owino, L. ; Hilkens, M. ; Kögler, F. ; Söffker, D.: Automated Measurement and Control of Germination Paper Water Content. In: *Sensors* 19 (2019), may, Nr. 10, pp. 2232. http://dx.doi.org/10.3390/s19102232. – DOI 10.3390/s19102232

[OPRW21] Ofori, S. ; Pušká̌čová, A. ; Růžičková, I. ; Wanner, J.: Treated wastewater reuse for irrigation: Pros and cons. In: *Science of The Total Environment* 760 (2021), pp. 144026. http://dx.doi.org/10.1016/j.scitotenv.2020.144026. – DOI 10.1016/j.scitotenv.2020.144026

[OS19a] Owino, L. ; Söffker, D.: Deficit irrigation-based control of leaf appearance in early vegetative stages of Maize growth. In: *Mitteilungen der Gesellschaft für Pflanzenbauwissenschaften Band 31*. Berlin : Verlag Liddy Halm, Göttingen, September 2019 (62), pp. 63–64

[OS19b] Owino, L. ; Söffker, D.: Development and Test of Prediction Model for Maize Leaf Appearance during Vegetative Phase. In: *IFAC-PapersOnLine* 52 (2019), Nr. 30, pp. 126–131

[OS22a] Owino, L. ; Söffker, D.: Deficit irrigation-based growth control of maize plants using hybrid model predictive / trellis decoding algorithm. In: *IFAC-PapersOnLine* 55 (2022), Nr. 32, pp. 183–187. http://dx.doi.org/10.1016/j.ifacol.2022.11.136. – DOI 10.1016/j.ifacol.2022.11.136

[OS22b] Owino, L. ; Söffker, D.: How much is enough in watering plants? State-of-the-art in irrigation control: Advances, challenges, and opportunities with respect to precision irrigation. In: *Frontiers in Control Engineering* 3 (2022), sep. http://dx.doi.org/10.3389/fcteg.2022.982463. – DOI 10.3389/fcteg.2022.982463

[OS22c] Owino, L. ; Söffker, D.: Modeling and prediction of corn growth during vegetative phase. In: *AgEng2021 Proceedings*, 2022, pp. 433

[OS23] Owino, L. ; Söffker, D.: *Dynamic water stress threshold determination for precision irrigation control using clustering and regression algorithms.* Juli 2023. – Accepted (To be presented at IFAC World Congress, Yokohama (2023))

[OSCA20] Oubelkacem, A. ; Scardigno, A. ; Choukr-Allah, R.: Treated Wastewater Reuse on Citrus in Morocco: Assessing the Economic Feasibility of Irrigation and Nutrient Management Strategies. In: *Integrated Environmental Assessment and Management* 16 (2020), sep, Nr. 6, pp. 898–909. http://dx.doi.org/10.1002/ieam.4314. – DOI 10.1002/ieam.4314

[PBD22] Paramanik, S. ; Behera, M. D. ; Dash, J.: Symbolic regression-based allometric model development of a mangrove forest LAI using structural variables and digital hemispherical photography. In: *Applied Geography* 139 (2022), feb, pp. 102649. http://dx.doi.org/10.1016/j.apgeog.2022.102649. – DOI 10.1016/j.apgeog.2022.102649

[Pen48] Penman, H. L.: Natural evaporation from open water, bare soil and grass. In: *Proceedings of the Royal Society of London. Series A. Mathematical and Physical Sciences* 193 (1948), apr, Nr. 1032, pp. 120–145. http://dx.doi.org/10.1098/rspa.1948.0037. – DOI 10.1098/rspa.1948.0037

[PHDG+16] Pérez-Harguindeguy, N. ; Díaz, S. ; Garnier, E. ; Lavorel, S. ; Poorter, H. ; Jaureguiberry, P. ; Bret-Harte, M. S. ; Cornwell, W. K. ; Craine, J. M. ; Gurvich, D. E. ; Urcelay, C. ; Veneklaas, E. J. ; Reich, P. B. ; Poorter, L. ; Wright, I. J. ; Ray, P. ; Enrico, L. ; Pausas, J. G. ; de Vos, A. C. ;

Buchmann, N. ; Funes, G. ; Quétier, F. ; Hodgson, J. G. ; Thompson, K. ; Morgan, H. D. ; ter Steege, H. ; Sack, L. ; Blonder, B. ; Poschlod, P. ; Vaieretti, M. V. ; Conti, G. ; Staver, A. C. ; Aquino, S. ; Cornelissen, J. H. C.: Corrigendum to: New handbook for standardised measurement of plant functional traits worldwide. In: *Australian Journal of Botany* 64 (2016), Nr. 8, pp. 715. http://dx.doi.org/10.1071/BT12225. – DOI 10.1071/BT12225

[PO05] Padilla, J. M. ; Otegui, M. E.: Co-ordination between Leaf Initiation and Leaf Appearance in Field-grown Maize (Zea mays): Genotypic Differences in Response of Rates to Temperature. In: *Annals of Botany* 96 (2005), Nr. 6, pp. 997–1007. http://dx.doi.org/10.1093/aob/mci251. – DOI 10.1093/aob/mci251

[PPM+20] Pereira, L. S. ; Paredes, P. ; Melton, F. ; Johnson, L. ; Wang, T. ; López-Urrea, R. ; Cancela, J. J. ; Allen, R. G.: Prediction of crop coefficients from fraction of ground cover and height. Background and validation using ground and remote sensing data. In: *Agricultural Water Management* 241 (2020), pp. 106197. http://dx.doi.org/10.1016/j.agwat.2020.106197. – DOI 10.1016/j.agwat.2020.106197

[PPRSM+07] Pérez-Pastor, A. ; Ruiz-Sánchez, M. C. ; Martínez, J. A. ; Nortes, P. A. ; Artés, F. ; Domingo, R.: Effect of deficit irrigation on apricot fruit quality at harvest and during storage. In: *Journal of the Science of Food and Agriculture* 87 (2007), Nr. 13, pp. 2409–2415. http://dx.doi.org/10.1002/jsfa.2905. – DOI 10.1002/jsfa.2905

[PSM+17] Phogat, V. ; Skewes, M. A. ; McCarthy, M. G. ; Cox, J. W. ; Šimůnek, J. ; Petrie, P. R.: Evaluation of crop coefficients, water productivity, and water balance components for wine grapes irrigated at different deficit levels by a sub-surface drip. In: *Agricultural Water Management* 180 (2017), pp. 22–34. http://dx.doi.org/10.1016/j.agwat.2016.10.016. – DOI 10.1016/j.agwat.2016.10.016

[PT72] Priestley, C. H. B. ; Taylor, R. J.: On the Assessment of Surface Heat Flux and Evaporation Using Large-Scale Parameters. In: *Monthly Weather Review* 100 (1972), Nr. 2, pp. 81–92

[QZH22] Qiu, R. ; Zhang, M. ; He, Y.: Field estimation of maize plant height at jointing stage using an RGB-D camera. In: *The Crop*

Journal 10 (2022), oct, Nr. 5, pp. 1274–1283. http://dx.doi.org/10.1016/j.cj.2022.07.010. – DOI 10.1016/j.cj.2022.07.010

[RHT18] Rezazadeh, A. ; Harkess, R. ; Telmadarrehei, T.: The Effect of Light Intensity and Temperature on Flowering and Morphology of Potted Red Firespike. In: *Horticulturae* 4 (2018), oct, Nr. 4, pp. 36. http://dx.doi.org/10.3390/horticulturae4040036. – DOI 10.3390/horticulturae4040036

[Roy14] Roy, S.: Feedback control of soil moisture in precision-agriculture systems: Incorporating stochastic weather forecasts. In: *2014 American Control Conference*, 2014. – ISSN 2378–5861, pp. 2694–2698

[RPR+12] Rosa, R. D. ; Paredes, P. ; Rodrigues, G. C. ; Fernando, R. M. ; Alves, I. ; Pereira, L. S. ; Allen, R. G.: Implementing the dual crop coefficient approach in interactive software: 2. Model testing. In: *Agricultural Water Management* 103 (2012), jan, pp. 62–77. http://dx.doi.org/10.1016/j.agwat.2011.10.018. – DOI 10.1016/j.agwat.2011.10.018

[SB09] Smith, R. J. ; Baillie, J. N.: Defining precision irrigation: A new approach to irrigation management. In: *Irrigation Australia 2009: Irrigation Australia Irrigation and Drainage Conference: Irrigation Today - Meeting the Challenge*, Swan Hill, Australia, Oktober 2009

[SBM+10] Smith, R. J. ; Baillie, J. ; McCarthy, A. ; Raine, S. ; Baillie, C.: Review of precision irrigation technologies and their application, 2010

[SCST07] Schleppi, P. ; Conedera, M. ; Sedivy, I. ; Thimonier, A.: Correcting non-linearity and slope effects in the estimation of the leaf area index of forests from hemispherical photographs. In: *Agricultural and Forest Meteorology* 144 (2007), jun, Nr. 3-4, pp. 236–242. http://dx.doi.org/10.1016/j.agrformet.2007.02.004. – DOI 10.1016/j.agrformet.2007.02.004

[SESC05] Sadler, E. J. ; Evans, R. G. ; Stone, K. C. ; Camp, C. R.: Opportunities for conservation with precision irrigation. In: *Journal of Soil and Water Conservation* 60 (2005), Nr. 6, 371–378. https://www.jswconline.org/content/60/6/371. – ISSN 0022–4561

[SGW+11] Sakamoto, T. ; Gitelson, A. A. ; Wardlow, B. D. ; Arkebauer, T. J. ; Verma, S. B. ; Suyker, A. E. ;

Shibayama, M.: Application of day and night digital photographs for estimating maize biophysical characteristics. In: *Precision Agriculture* 13 (2011), sep, Nr. 3, pp. 285–301. http://dx.doi.org/10.1007/s11119-011-9246-1. – DOI 10.1007/s11119–011–9246–1

[SHZ+21] Shao, G. ; Han, W. ; Zhang, H. ; Liu, S. ; Wang, Y. ; Zhang, L. ; Cui, X.: Mapping maize crop coefficient Kc using random forest algorithm based on leaf area index and UAV-based multispectral vegetation indices. In: *Agricultural Water Management* 252 (2021), jun, pp. 106906. http://dx.doi.org/10.1016/j.agwat.2021.106906. – DOI 10.1016/j.agwat.2021.106906

[SJH19] Song, L. ; Jin, J. ; He, J.: Effects of Severe Water Stress on Maize Growth Processes in the Field. In: *Sustainability* 11 (2019), sep, Nr. 18, pp. 5086. http://dx.doi.org/10.3390/su11185086. – DOI 10.3390/su11185086

[SKA+20] Sim, H. S. ; Kim, D. S. ; Ahn, M. G. ; Ahn, S. R. ; Kim, S. K.: Prediction of Strawberry Growth and Fruit Yield based on Environmental and Growth Data in a Greenhouse for Soil Cultivation with Applied Autonomous Facilities. In: *Horticultural Science and Technology* 38 (6) (2020), pp. 840–849. http://dx.doi.org/10.7235/HORT.20200076. – DOI 10.7235/HORT.20200076

[SKO19] Söffker, D. ; Kögler, F. ; Owino, L.: Crop Growth Modeling-a New Data-driven Approach. In: *IFAC-PapersOnLine* 52 (2019), Nr. 30, pp. 132–136. http://dx.doi.org/10.1016/j.ifacol.2019.12.510. – DOI 10.1016/j.ifacol.2019.12.510

[Sla69] Slatyer, R. O.: Physiological significance of internal water relations to crop yield. In: *Agronomy and Horticulture–Faculty Publications* 186 (1969), pp. 53–88

[SLH93] Smith, B. N. ; Lytle, C. M. ; Hansen, L. D.: Predicting Plant Growth Rates from Dark Respiration Rates: an Experimental Approach. In: Roundy, B. A. (Hrsg.) ; McArthur, E. D. (Hrsg.) ; Haley, J. S. (Hrsg.) ; Mann, D. K. (Hrsg.): *Proceedings: wildland shrub and arid land restoration symposium.* Las Vegas, NV, Oktober 1993

[SPA17] Sudana, I. M. ; Purnawirawan, O. ; Arief, U. M.: Prediction system of hydroponic plant growth and development

using algorithm Fuzzy Mamdani method. (2017), pp. 020052–(1–12). http://dx.doi.org/10.1063/1.4976916. – DOI 10.1063/1.4976916

[SRH+08] Steduto, P. ; Raes, D. ; Hsiao, T. C. ; Fereres, E. ; Heng, L. ; Izzi, G. ; Hoogeveen, J.: AquaCrop: a new model for crop prediction under water deficit conditions. In: López-Francos, A. (Hrsg.): *Drought management: scientific and technological innovations CIHEAM, (Options Méditerranéennes : Série A. Séminaires Méditerranéens* Bd. 80. Zaragoza : Academic Press, 2008, pp. 285–292

[SSL11] Seelig, H. ; Stoner, R. J. ; Linden, J. C.: Irrigation control of cowpea plants using the measurement of leaf thickness under greenhouse conditions. In: *Irrigation Science* 30 (2011), mar, Nr. 4, pp. 247–257. http://dx.doi.org/10.1007/s00271-011-0268-2. – DOI 10.1007/s00271–011–0268–2

[SSPG18] Shadrin, D. ; Somov, A. ; Podladchikova, T. ; Gerzer, R.: Pervasive agriculture: Measuring and predicting plant growth using statistics and 2D/3D imaging. In: *2018 IEEE International Instrumentation and Measurement Technology Conference (I2MTC)*, IEEE, may 2018

[Str03] Streck, N. A.: Incorporating a Chronology Response into the Prediction of Leaf Appearance Rate in Winter Wheat. In: *Annals of Botany* 92 (2003), jun, Nr. 2, pp. 181–190. http://dx.doi.org/10.1093/aob/mcg121. – DOI 10.1093/aob/mcg121

[SUST19] Sakurai, S. ; Uchiyama, H. ; Shimada, A. ; Taniguchi, R.: Plant Growth Prediction using Convolutional LSTM. (2019). http://dx.doi.org/10.5220/0007404901050113. – DOI 10.5220/0007404901050113

[TAMG00] Turner, D. P. ; Acker, S. A. ; Means, J. E. ; Garman, S. L.: Assessing alternative allometric algorithms for estimating leaf area of Douglas-fir trees and stands. In: *Forest Ecology and Management* 126 (2000), feb, Nr. 1, pp. 61–76. http://dx.doi.org/10.1016/s0378-1127(99)00083-3. – DOI 10.1016/s0378–1127(99)00083–3

[Tar96] Tardieu, F.: Drought perception by plants: Do cells of droughted plants experience water stress? In: *Plant Growth Regulation* 20 (1996), nov, Nr. 2, pp. 93–104. http://dx.doi.org/10.1007/bf00024005. – DOI 10.1007/bf00024005

[TBZ+14] Tang, H. ; Brolly, M. ; Zhao, F. ; Strahler, A. H. ; Schaaf, C. L. ; Ganguly, S. ; Zhang, G. ; Dubayah, R.: Deriving and validating Leaf Area Index (LAI) at multiple spatial scales through lidar remote sensing: A case study in Sierra National Forest, CA. In: *Remote Sensing of Environment* 143 (2014), mar, pp. 131–141. http://dx.doi.org/10.1016/j.rse.2013.12.007. – DOI 10.1016/j.rse.2013.12.007

[TCPR00] Traore, S. B. ; Carlson, R. E. ; Pilcher, C. D. ; Rice, M. E.: Bt and Non-Bt Maize Growth and Development as Affected by Temperature and Drought Stress. In: *Agronomy Journal* 92 (2000), sep, Nr. 5, pp. 1027–1035. http://dx.doi.org/10.2134/agronj2000.9251027x. – DOI 10.2134/agronj2000.9251027x

[Tho48] Thornthwaite, C. W.: An Approach toward a Rational Classification of Climate. In: *Geographical Review* 38 (1948), jan, Nr. 1, pp. 55. http://dx.doi.org/10.2307/210739. – DOI 10.2307/210739

[TKP+16] Tsakmakis, I. ; Kokkos, N. ; Pisinaras, V. ; Papaevangelou, V. ; Hatzigiannakis, E. ; Arampatzis, G. ; Gikas, G. D. ; Linker, R. ; Zoras, S. ; Evagelopoulos, V. ; Tsihrintzis, V. A. ; Battilani, A. ; Sylaios, G.: Operational Precise Irrigation for Cotton Cultivation through the Coupling of Meteorological and Crop Growth Models. In: *Water Resources Management* 31 (2016), nov, Nr. 1, pp. 563–580. http://dx.doi.org/10.1007/s11269-016-1548-7. – DOI 10.1007/s11269–016–1548–7

[TWZW18] Tu, Y. ; Wang, R. ; Zhang, Y. ; Wang, J.: Progress and Expectation of Atmospheric Water Harvesting. In: *Joule* 2 (2018), aug, Nr. 8, pp. 1452–1475. http://dx.doi.org/10.1016/j.joule.2018.07.015. – DOI 10.1016/j.joule.2018.07.015

[UN 15] UN General Assembly: Transforming our world : the 2030 Agenda for Sustainable Development. (2015), Oktober, Nr. A/RES/70/1. https://www.refworld.org/docid/57b6e3e44.html

[VAP+17] Varela, S. ; Assefa, Y. ; Prasad, P. V. V. ; Peralta, N. R. ; Griffin, T. W. ; Sharda, A. ; Ferguson, A. ; Ciampitti, I. A.: Spatio-temporal evaluation of plant height in corn via unmanned aerial systems. In: *Journal of Applied Remote Sensing* 11 (2017), aug, Nr. 03, pp. 1. http://dx.doi.org/10.1117/1.jrs.11.036013. – DOI 10.1117/1.jrs.11.036013

[vGv97a] van Laar, H. H. (Hrsg.) ; Goudriaan, J. (Hrsg.) ; van Keulen, H. (Hrsg.): *Simulation of crop growth for potential and water-limited production situations, as applied to spring wheat.* Wageningen/Haren, 1997

[vGv97b] van Laar, H. H. ; Goudriaan, J. ; van Keulen, H.: *SUCROS97: Simulation of crop growth for potential and water-limited production situations. As applied to spring wheat.* AB-DLO, TPE (Quantitative Approaches in Systems Analysis : 14). https://edepot.wur.nl/4426

[VH31] Veihmeyer, F. J. ; Hendrickson, A. H.: The moisture equivalent as a measure of the field capacity of soils. In: *Soil Science* 32 (1931), September, Nr. 3, pp. 181–194

[Vit67] Viterbi, A.: Error bounds for convolutional codes and an asymptotically optimum decoding algorithm. In: *IEEE Transactions on Information Theory* 13 (1967), apr, Nr. 2, pp. 260–269. http://dx.doi.org/10.1109/tit.1967.1054010. – DOI 10.1109/tit.1967.1054010

[VK22] Vasantha, S. V. ; Kiranmai, B.: Machine Learning-Based Breeding Values Prediction System (ML-BVPS). (2022), pp. 259–266. http://dx.doi.org/10.1007/978-981-16-6289-8_22. – DOI 10.1007/978–981–16–6289–8_22

[VMP+21] Venturi, M. ; Manfrini, L. ; Perulli, G. D. ; Boini, A. ; Bresilla, K. ; Grappadelli, L. C. ; Morandi, B.: Deficit Irrigation as a Tool to Optimize Fruit Quality in Abbé Fetél Pear. In: *Agronomy* 11 (2021), jun, Nr. 6, pp. 1141. http://dx.doi.org/10.3390/agronomy11061141. – DOI 10.3390/agronomy11061141

[vWvR89] van Diepen, C. A. ; Wolf, J. ; van Keulen, H. ; Rappoldt, C.: WOFOST: a simulation model of crop production. In: *Soil Use and Management* 5 (1989), März, Nr. 1, pp. 16–24

[WA02] Williams, L. E. ; Araujo, F. J.: Correlations among Predawn Leaf, Midday Leaf, and Midday Stem Water Potential and their Correlations with other Measures of Soil and Plant Water Status in Vitis vinifera. In: *J. Am. Soc. Hortic. Sci.* 127 (2002), pp. 448–454

[WBB95] Weiss, A. ; Budak, N. ; Baenziger, P. S.: Using transpiration to characterize plant height in winter wheat in different environments:

A simulation study. In: *Canadian Journal of Plant Science* 75 (1995), jul, Nr. 3, pp. 583–587. http://dx.doi.org/10.4141/cjps95-101. – DOI 10.4141/cjps95–101

[WBS+04] Weiss, M. ; Baret, F. ; Smith, G. J. ; Jonckheere, I. ; Coppin, P.: Review of methods for in situ leaf area index (LAI) determination. In: *Agricultural and Forest Meteorology* 121 (2004), jan, Nr. 1-2, pp. 37–53. http://dx.doi.org/10.1016/j.agrformet.2003.08.001. – DOI 10.1016/j.agrformet.2003.08.001

[WE98] Wang, E. ; Engel, T.: Simulation of phenological development of wheat crops. In: *Agricultural Systems* 58 (1998), sep, Nr. 1, pp. 1–24. http://dx.doi.org/10.1016/s0308-521x(98)00028-6. – DOI 10.1016/s0308–521x(98)00028–6

[Wes19] Westermann, W. L.: The development of the irrigation system of Egypt. In: *Classical Philology* 14 (1919), April, Nr. 2, pp. 158–164

[WGA+17] Watanabe, K. ; Guo, W. ; Arai, K. ; Takanashi, H. ; Kajiya-Kanegae, H. ; Kobayashi, M. ; Yano, K. ; Tokunaga, T. ; Fujiwara, T. ; Tsutsumi, N. ; Iwata, H.: High-Throughput Phenotyping of Sorghum Plant Height Using an Unmanned Aerial Vehicle and Its Application to Genomic Prediction Modeling. In: *Frontiers in Plant Science* 8 (2017), mar. http://dx.doi.org/10.3389/fpls.2017.00421. – DOI 10.3389/fpls.2017.00421

[WNX+16] Wang, C. ; Nie, S. ; Xi, X. ; Luo, S. ; Sun, X.: Estimating the Biomass of Maize with Hyperspectral and LiDAR Data. In: *Remote Sensing* 9 (2016), dec, Nr. 1, pp. 11. http://dx.doi.org/10.3390/rs9010011. – DOI 10.3390/rs9010011

[WSA+20] Wong, J. ; Sha, H. ; Al Hasan, M. ; Mohler, G. ; Becker, S. ; Wiltse, C.: Automated Corn Ear Height Prediction Using Video-Based Deep Learning. (2020), dec. http://dx.doi.org/10.1109/bigdata50022.2020.9378115. – DOI 10.1109/bigdata50022.2020.9378115

[XGF96] Xevi, E. ; Gilley, J. ; Feyen, J.: Comparative study of two crop yield simulation models. In: *Agricultural Water Management* 30 (1996), apr, Nr. 2, pp. 155–173. http://dx.doi.org/10.1016/0378-3774(95)01218-4. – DOI 10.1016/0378–3774(95)01218–4

[XKW03] Xie, Y. ; Kiniry, J. R. ; Williams, J. R.: The ALMANAC model's sensitivity to input variables. In: *Agricultural Systems*

78 (2003), oct, Nr. 1, pp. 1–16. http://dx.doi.org/10.1016/s0308-521x(03)00002-7. – DOI 10.1016/s0308–521x(03)00002–7

[XMJL17] Xu, M. ; Ma, L. ; Jia, Y. ; Liu, M.: Integrating the effects of latitude and altitude on the spatial differentiation of plant community diversity in a mountainous ecosystem in China. In: *PLOS ONE* 12 (2017), mar, Nr. 3, pp. e0174231. http://dx.doi.org/10.1371/journal.pone.0174231. – DOI 10.1371/journal.pone.0174231

[XQH+20] Xu, C. ; Qu, J. J. ; Hao, X. ; Cosh, M. H. ; Zhu, Z. ; Gutenberg, L.: Monitoring crop water content for corn and soybean fields through data fusion of MODIS and Landsat measurements in Iowa. In: *Agricultural Water Management* 227 (2020), jan, pp. 105844. http://dx.doi.org/10.1016/j.agwat.2019.105844. – DOI 10.1016/j.agwat.2019.105844

[XWS+21] Xing, W. ; Wang, W. ; Shao, Q. ; Song, L. ; Cao, M.: Estimation of Evapotranspiration and Its Components across China Based on a Modified Priestley–Taylor Algorithm Using Monthly Multi-Layer Soil Moisture Data. In: *Remote Sensing* 13 (2021), aug, Nr. 16, pp. 3118. http://dx.doi.org/10.3390/rs13163118. – DOI 10.3390/rs13163118

[YDL+04] Yang, H. S. ; Dobermann, A. ; Lindquist, J. L. ; Walters, D. T. ; Arkebauer, T. J. ; Cassman, K. G.: Hybrid-maize—a maize simulation model that combines two crop modeling approaches. In: *Field Crops Research* 87 (2004), may, Nr. 2-3, pp. 131–154. http://dx.doi.org/10.1016/j.fcr.2003.10.003. – DOI 10.1016/j.fcr.2003.10.003

[YMJ+11] Yin, X. ; McClure, M. A. ; Jaja, N. ; Tyler, D. D. ; Hayes, R. M.: In-Season Prediction of Corn Yield Using Plant Height under Major Production Systems. In: *Agronomy Journal* 103 (2011), may, Nr. 3, pp. 923–929. http://dx.doi.org/10.2134/agronj2010.0450. – DOI 10.2134/agronj2010.0450

[ZBZ+22] Zheng, B. ; Brown, H. ; Zhao, Z. ; Wang, E. ; Huth, N. ; Dillon, S. ; Hyles, J. ; Rathjen, T. ; Bloomfield, M. ; Celestina, C. ; Hunt, J. ; Trevaskis, B.: Prediction of wheat leaf appearance through integration of single nucleotide polymorphisms (SNPs) with a crop model. In: *Proceedings of the 20th Agronomy Australia Conference*. Toowomba, Australia, 2022

[ZCK74] Zadoks, J. C. ; Chang, T. T. ; Konzak, C. F.: A decimal code for the growth stages of cereals. In: *Weed Research* 14 (1974), dec, Nr. 6, pp. 415–421. http://dx.doi.org/10.1111/j.1365-3180.1974.tb01084.x. – DOI 10.1111/j.1365–3180.1974.tb01084.x

[Zhe19] Zheng, Y.: Predicting Remaining Useful Life Based on Hilbert-Huang Entropy with Degradation Model. In: *Journal of Electrical and Computer Engineering* 2019 (2019), feb, pp. 1–11. http://dx.doi.org/10.1155/2019/3203959. – DOI 10.1155/2019/3203959

[ZHNL19] Zhang, Y. ; Han, W. ; Niu, X. ; Li, G.: Maize Crop Coefficient Estimated from UAV-Measured Multispectral Vegetation Indices. In: *Sensors* 19 (2019), nov, Nr. 23, pp. 5250. http://dx.doi.org/10.3390/s19235250. – DOI 10.3390/s19235250

[ZKL+18] Zhao, P. ; Kang, S. ; Li, S. ; Ding, R. ; Tong, L. ; Du, T.: Seasonal variations in vineyard ET partitioning and dual crop coefficients correlate with canopy development and surface soil moisture. In: *Agricultural Water Management* 197 (2018), jan, pp. 19–33. http://dx.doi.org/10.1016/j.agwat.2017.11.004. – DOI 10.1016/j.agwat.2017.11.004

[ZSC+20] Zhang, B. ; Sajjad, S. ; Chen, K. ; Zhou, L. ; Zhang, Y. ; Yong, K. K. ; Sun, Y.: Predicting Tree Height-Diameter Relationship from Relative Competition Levels Using Quantile Regression Models for Chinese Fir (Cunninghamia lanceolata) in Fujian Province, China. In: *Forests* 11 (2020), feb, Nr. 2, pp. 183. http://dx.doi.org/10.3390/f11020183. – DOI 10.3390/f11020183

[ZSG11] Zhou, R. R. ; Serban, N. ; Gebraeel, N.: Degradation Modeling applied to Residual Lifetime Prediction using Functional Data Analysis. In: *The Annals of Applied Statistics* 5 (2011), Nr. 2B, pp. 1586–1610. http://dx.doi.org/10.124/10-AOAS448. – DOI 10.124/10–AOAS448

This thesis is based on the results and development steps presented in the following previous publications:

Journal articles

[OS22b] Owino, L.; Söffker, D.: How much is enough in watering plants? State-of-the-art in irrigation control: advances, challenges, and opportunities with respect to precision irrigation In: *Frontiers in Control Engineering*, 2022. http://dx.doi.org/10.3389/fcteg.2022.982463

[OHKS19] Owino, L.; Hilkens, M.; Kögler, F.; Söffker, D.: Automated measurement and control of germination paper water content. In: *MDPI Sensors, Special Issue: Sensors in Agriculture* 19(10), 2232. http://dx.doi.org/10.3390/s19102232

Conference papers

[OS19a] Owino, L. ; Söffker, D.: Deficit irrigation-based control of leaf appearance in early vegetative stages of maize growth. *Gesellschaft fur Pflanzenbauwissenschaften e.V*, 62.e Jahrestagung, Berlin (2019), pp. 63-64

[OS19b] Owino, L. ; Söffker, D.: Development and test of predictive model for maize leaf appearance during vegetative phase. *IFAC Agricontrol Conference*, Sydney (2019), pp. 126-131. https://doi.org/10.1016/j.ifacol.2019.12.509

[SKO19] Söffker, D.; Kögler, F. ; Owino, L.: Crop growth modeling- a new data driven approach. *IFAC Agricontrol Conference*, Sydney (2019), pp. 132-136. https://doi.org/10.1016/j.ifacol.2019.12.510

[OS22c] Owino, L. ; Söffker, D.: Modeling and prediction of corn growth during vegetative phase. *AgEng 2021*, Évora (2021), pp. 433-440.

[OS21b] Owino, L. ; Söffker, D.: State machine-based model for estimation and prediction of above ground biomass in corn during vegetative stage. *AgEng 2021*, Évora (2021), pp. 426-432.

[OS21c] Owino, L. ; Söffker, D.: Predictive precision irrigation-based control of maize leaf growth under laboratory conditions. *Gesellschaft fur Pflanzenbauwissenschaften e.V*, 63.e Jahrestagung, Rostock (2021), pp. 261-262.

[OS22a] Owino, L. ; Söffker, D.: Deficit irrigation-based growth control of maize plants using hybrid model predictive / trellis decoding algorithm. *IFAC PapersOnline*, Vol 55 (32) 2022, pp 183-187, Presented at *IFAC Agricontrol Conference*, Munich (2022).http://dx.doi.org/10.1016/j.ifacol.2022.11.136

[OS23] Owino, L. ; Söffker, D.: Dynamic water stress threshold determination for precision irrigation control using clustering and regression algorithms.*IFAC PapersOnline*, Vol 56 (2) 2023, pp 5287-5292 ,Presented at *IFAC World Congress*, Yokohama (2023).https://doi.org/10.1016/j.ifacol.2023.10.170

In the context of research projects at the Chair of Dynamics and Control, the following student thesis has been supervised by Lina Owino and Univ.-Prof. Dr.-Ing. Dirk Söffker. Development steps and results of the research projects and the student theses are integrated with each other and hence are integrated into this dissertation.

[Heb19] Hebner I., Performance eines neuen Zustandsautomatenmodells: Vergleich mit analytischen/numerischen Beschreibungen unter Nutzung experimenteller Daten, Bachelor Thesis, September 2019.

[Oue20] Oueslati A., Predictive modeling and analysis of plant growth parameters under deficit irrigation conditions based on experimental data, Bachelor Thesis, January 2020.

[Set20] Sethi E., Conception and research of a digital field assistant: A review of plant growth modelling approaches, Bachelor Thesis, September 2020.

[Tan20] Tan W., Automated IR-camera based surface temperature measurement of non-stationary objects applied to greenhouse plants, Bachelor Thesis, December 2020.

[Alj20] Aljurdi H., Automatic image-based determination of plant growth for irrigation control applications, Bachelor Thesis, April 2022.

[Man22] Manjouneh M., Automatisierung und Weiterentwicklung des Greenhaus Versuchsstandes zur pflanzenphysiologischen Datenerhebung sowie experimentelle Bestimmung des Wasserstresses der Pflanzen, Master Thesis, January 2022.

DOI: 10.17185/duepublico/81431
URN: urn:nbn:de:hbz:465-20240126-112123-5